THESIS

SYNTHESIS AND CHARACTERIZATION OF LITHIUM-ION CATHODE MATERIALS IN THE SYSTEM $(1-x-y)LiNi_{1/3}Mn_{1/3}Co_{1/3}O_2 \cdot xLi_2MnO_3 \cdot yLiCoO_2$

Submitted by

Rushendra Paravasthu

Department of Mechanical Engineering

In partial fulfillment of the requirements

For the Degree of Master of Science

Colorado State University

Fort Collins, Colorado

Spring 2012

Master's Committee:

Advisor: Susan P. James

Amy Prieto
Mingzhong Wu

ABSTRACT

SYNTHESIS AND CHARACTERIZATION OF LITHIUM-ION CAHTODE MATERIALS IN THE SYSTEM (1-x-y)$LiNi_{1/3}Mn_{1/3}Co_{1/3}O_2$·x$Li_2MnO_3$·y$LiCoO_2$

Considering various technologies for storing energy the usage of lithium (Li) – ion batteries still stands as one of the most promising options, especially for the on-going huge demand for electric and plug-in hybrid vehicles. The main limiting factor in the performance of a Li-ion battery is the cathode material. The current cathode material that is being used in the present market is $LiCoO_2$ cathode which is effective but is expensive and toxic. The objective of this thesis is to find a cathode material which is advantageous and a probable replacement for $LiCoO_2$.

Based on the previously studied work on ternary solid solutions and its advantages, this system (1-x-y)$LiNi_{1/3}Mn_{1/3}Co_{1/3}O_2$·x$Li_2MnO_3$·y$LiCoO_2$ was chosen. This was made using a ternary composition diagram which is a combination of $LiNi_{1/3}Mn_{1/3}Co_{1/3}O_2$, Li_2MnO_3 and $LiCoO_2$ materials. Points inside the ternary diagram were chosen in an arrangement conducive to mathematical modeling and compositions of the cathodes were processed accordingly. All the 28 samples in the system were synthesized using the sol-gel method, each sample was characterized using X-ray diffraction (XRD) scans and electrochemical testing was performed by using an Arbin BT2000 battery testing system with MITS Pro Arbin software.

The XRD results showed that all the samples established a α-$NaFeO_2$ structure and a space group of R3m with varying degrees of purity in the crystal structure. The compounds in this system showed fairly consistent charge/ discharge curves during the electrochemical testing

with initial discharge capacities varying from 122mAh/g to 240mAh/g and high capacity compositions were found in the region of high Li_2MnO_3 content. The highest capacity found was $Li_{1.222}Mn_{0.5}Ni_{.056}Co_{0.222}O_2$ composition with a discharge capacity of 242mAh/gin the voltage range 4.6 – 2V at a C/15 rate.

A statistical based analysis was carried out using JMP version 7.0.1 with the design of experiments (DOE) procedure for a mixture design to find variations in capacity and cyclability trends over the composition triangle. Inductively couple plasma (ICP) analysis was carried out on 4 samples which were found to be most promising basing on the statistical analysis. ICP results confirmed the formation of optimum compositions for the specified synthesis conditions.

All these 4 samples were synthesized and tested again to confirm consistent performance across repeat samples. XPS (X-ray photoelectron spectroscopy) was conducted for these samples to determine the chemical environment of transition metals. The composition with the highest capacity was found to be $Li_{1.222}Mn_{0.5}Ni_{0.056}Co_{0.222}O_2$ electrode. Its high capacity is attributed to the Ni^{+2}/Ni^{+4} and Co^{+3}/Co^{+4} red-ox couple and the Li-ion extraction form Li_2MnO_3 at a voltage >4.5V which results in an extended discharge profile. This cathode composition is very promising because it shows high capacity and good cyclability, and would be much cheaper than conventional $LiCoO_2$ cathodes since it has more manganese which is less expensive than cobalt.

ACKNOWLEDGEMENTS

I want to thank my advisor, Dr. Susan P. James for being the one to support my research work in the first place and for giving me invaluable guidance over the last year. I would also like to thank Dr. Amy Prieto and Dr. Mingzhong Wu for agreeing to serve on my committee. Additionally, I would like to thank Dr. Sandeep kohli and Dr. Pat Mccurdy from the department of chemistry for helping me with different characterization techniques. My colleagues Brandon Kelly, Anish Yerramilli, Madhu Channabasappa, Josh Garrett, Bhavin Patel, Mike Yeager and Siddharth Paravasthu all have played an important role in my research work and were always helpful. Finally, I would like to thank my family and friends for always being there for me and for supporting me in whatever I do.

TABLE OF CONTENTS

List of Tables……x

List of Figures……xi

Chapter 1 Introduction……1

1.1 Aim and Purpose……..……..1

1.2 History of Li-ion batteries……..……3

1.3 Working Principal……..……5

1.4 Cell design and Configuration……..…7

1.5 Battery Specifications……..12

1.5.1 Capacity and Rate capability……13

1.5.2 Cyclability……....14

1.5.3 Safety……15

1.5.4 Cost……..…….15

1.6 Recent Developments……...……16

Chapter 2 Cathode Materials……..……18

2.1 Layered Metal Oxides……...…18

2.1.1 $LiCoO_2$……19

2.1.2 $LiMn_yNi_{1-y}O_2$……...…21

2.1.3 $LiNi_{1/3}Mn_{1/3}Co_{1/3}O_2$……22

2.1.4 $LiMnO_2$ (layered)/$LiMn_2O_4$ (Spinel)……..……23

2.1.5 Li_2MnO_3……..……25

2.2 Binary and Ternary Solid solutions containing Li_2MnO_3…….……26

2.2.1 $Li[Li_{x/3}Co_{1-x}Mn_{2x/3}]O_2$…….……26

2.2.2 Li_2MnO_3-$LiNi_{1/3}Co_{1/3}Mn_{1/3}O_2$- $LiNiO_2$…….…….27

2.2.3 $Li[Li_{(1-x)/3}Mn_{(2-x)/3}Ni_{x/3}Co_{x/3}]O_2$……...28

2.2.4 $Li[Ni_xLi_{(1/3-2x/3)}Mn_{(2/3-x/3)}]O_2$……..….28

2.2.5 $(1-x-y)LiNi_{1/2}Mn_{1/2}O_2 \cdot xLi[Li_{1/3}Mn_{2/3}]O_2 \cdot yLiCoO_2$…….....29

Chapter 3 System Analysis……30

3.1 Research Statement……...……30

3.2 Objective……...…30

3.3 Approach……...…30

Chapter 4 Experimental Methods……..…….……34

4.1 Synthesis……...…34

4.2 Material Characterization……..…35

4.2.1 X-ray Diffraction (XRD)……36

4.2.3 Inductively Coupled Plasma (ICP)…….…37

4.2.4 X-ray Photoelectron Spectroscopy (XPS)……..…37

4.2.5 Statistical Analysis……..…38

4.3 Cathode Preparation…….....39

4.4 T-cell Assembly……...…40

4.5 Electrochemical Testing……...41

Chapter 5 Results and Discussion……42

5.1 (1-x-y)$LiNi_{1/3}Mn_{1/3}Co_{1/3}O_2$·x$Li_2MnO_3$·y$LiCoO_2$……..…….42

5.1.1 System Overview……..……42

5.1.2 XRD……..……45

5.1.3 Battery Testing……...……...…49

5.2 Statistical Analysis……..……..…….……57

5.2.1 Optimization…….……57

5.2.2 Repetition……..……61

5.2.3 ICP……63

5.2.4 XRD……..……64

5.2.5 XPS……...……66

5.2.6 Battery Testing…….……69

5.3 Results and Discussion……71

Chapter 6

Conclusions……..……..……...…76

References……..…….…...……78

LIST OF TABLES

1. Material compositions of all the 28 samples in the system……...…44
2. Results for the 28 samples in the system after testing……..56
3. Input data for regression analysis……...…58
4. Material compositions of selected samples for repetition…….…….61
5. ICP data analysis……...…….63
6. Results from ICP calculations……..……..64
7. Results analysis for 4 repeated samples…….…72
8. Comparison between capacities of original and repeated samples……..…..73

LIST OF FIGURES

1. Comparison of various battery technologies in terms of energy density…….....2

2. Dendrite formation on lithium anode…….…..3

3. Structure of graphite intercalated with lithium……...…….4

4. Diagram of Li-ion cell during charging and discharging…….....6

5. Electrode and cell reactions in a lithium ion battery……....6

6. Battery configurations cylindrical, coin, prismatic and thin/flat polymer……...7

7. Coated foil layout for Sony 18650 $LiCoO_2$ battery…….8

8. Typical small-scaled coating machine…….9

9. Calendaring machine…….10

10. Winding machine……...10

11. Battery manufacturing process flow chart…….…11

12. Capacity plot (Voltage v. Capacity)……..13

13. Comparison of the rate capability at constant current for 18650 batteries……14

14. Voltage v. capacity for positive and negative electrodes for next generation Li-cells….17

15. Layered structured transition metal oxides……....19

16. Layered structure of $LiCoO_2$……..20

17. Unit cell of $LiMn_yNi_{1-y}O_2$ showing li-filled and Ni, Mn-filled layers……...21

18. Comparison between layered $LiMnO_2$ and spinel $LiMn_2O_4$ structure……...…24

19. The rock salt structure of Li_2MnO_3……....25

20. Ternary composition triangle proposed by Zhang et al…….31

21. Ternary composition triangle proposed by Madhu et al……32

22. Ternary composition triangle for $(1-x-y)LiNi_{1/3}Mn_{1/3}Co_{1/3}O_2 \cdot xLi_2MnO_3 \cdot yLiCoO_2$…….33

23. Sample XRD plot……..….36

24. Schematic diagram of X-ray photoelectron spectroscopy……..…38

25. T-cell configuration……...…41

26. Ternary composition triangle…….……43

27. XRD scans for the 28 samples in the system……...…..48

28. Capacity plots for the 28 samples in the system……54

29. Regression analysis in terms of capacity……...….59

30. Regression analysis in terms of cyclability……...….60

31. Selected region in the composition triangle for repetitions……...…62

32. XRD scans for the selected samples……...…65

33. Individual XPS plots for sample #17……..…66

34. XPS plots for all the selected samples……...68

35. Capacity plots for the selected samples……70

36. Comparison between charge and discharge profiles for repeated samples……71

37. Initial charge/discharge profile of sample #17……..74

38. Plot between cycle number v. discharge capacity for sample #17……75

Chapter 1 Introduction

1.1 Aim and purpose

Energy and environmental based issues have become the major areas of concern in the 21st century as these factors are directly linked to technological development; therefore, the search for alternative sources of energy continues. Presently the energy economy, which is predominantly based on fossil fuels, is at risk due to the decrease in non-renewable resources and the continuously increasing demand for energy. Furthermore, CO_2 emissions associated with the use of fossil fuels are one of the main causes of global warming, which is becoming an important issue in global energy politics [1].

Accordingly, investments for the exploitation of renewable energy resources are increasing worldwide, with particular attention to solar, wind and battery power systems. Batteries have many advantages as an alternative source of energy storage mechanism. Currently the conventional battery technologies, such as lead-acid and nickel cadmium, are slowly being replaced by lithium-ion (Li-ion) batteries, fuel-cell technologies and nickel metal hydride batteries. Li-ion battery technology stands as a forerunner and market leader when compared to the other possible energy systems.

The main motivation for using this Li ion battery technology is the fact that lithium is the lightest and most electropositive metallic element, and therefore facilitates very high energy density[2](Figure 1). Li-ion batteries have been found to be stable over 500 cycles, can be fabricated in different sizes and also require very little maintenance compared to the other battery

technologies. Researchers continue to work on many different aspects of this technology such as decreasing the cost, improving the cycling life and increasing the safety. This technology is already being used in high-end electronics, has recently been introduced to the power tool markets and is entering the hybrid electric-vehicle market making it a serious contender to power the electric cars of the future.

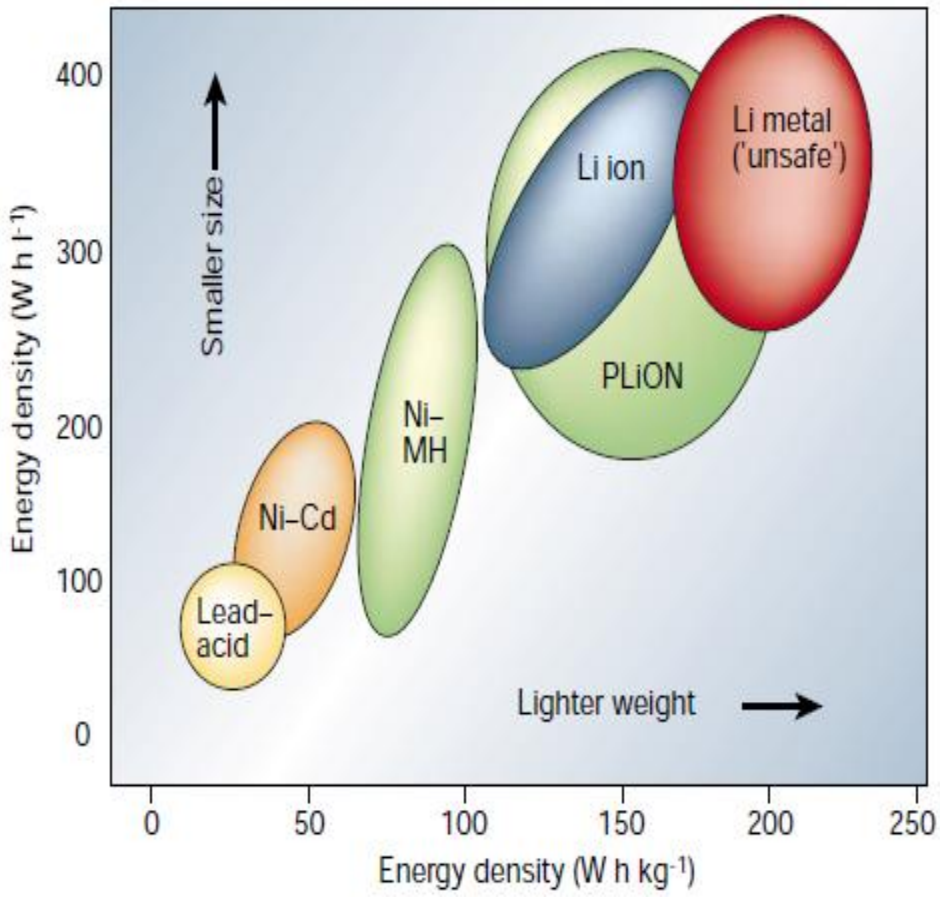

Figure 1: Comparison of various battery technologies in terms of energy density[2].

The goal of this thesis is to discover new Li-based cathode material compositions comprised of lithium and other elements that can exhibit high capacities and possibly replace conventional $LiCoO_2$ cathodes, which are effective but are also expensive and toxic.

1.2 History of Lithium-Ion batteries

Lithium is the lightest of all metals, has the greatest electrochemical potential and provides the largest energy content of the metals. The first step in tapping the actual potential of Li-ion began in the year 1912 by G.N Lewis who was the dean of the department of chemistry at the University of California Berkeley[3]. It was not until the early 1970's that the first lithium-ion non-rechargeable batteries were made commercially available, this was proposed by M.S.Whittingham at Exxon[4]. These batteries were made with TiS_2 as cathode and Li metal as the anode, while the positive cathode worked well, the lithium metal anode was shown to have uneven dendrite growth during cycling (Figure 2).

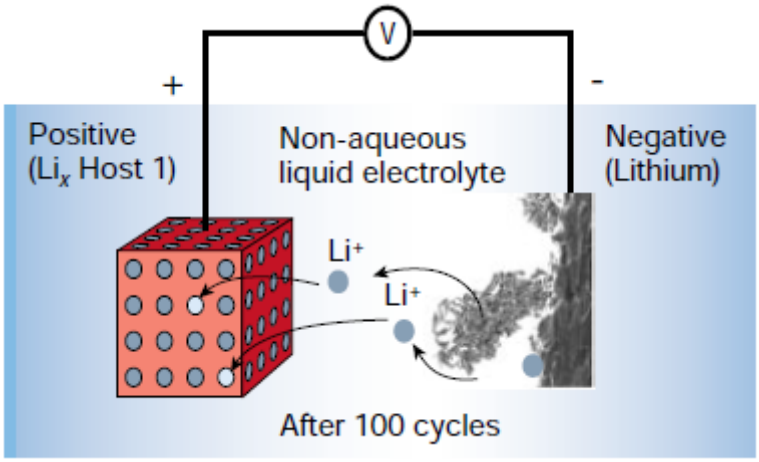

Figure 2: Dendrite formation on lithium anode[2].

Attempts to develop rechargeable lithium batteries followed in the 1980's, and it was found that rechargeable batteries using lithium metal anode are capable of providing both high voltage and excellent capacity. These characteristics led to an extraordinarily high energy density, but failed due to safety concerns because of the violent chemical reactions that were

taking place due to the temperature changes. Therefore, research was shifted to non-metallic lithium battery using lithium-ions which was comparatively safe then lithium metal.

A significant advancement in the development of lithium batteries came with the discovery of intercalation materials where lithium was used as an insertion material for rechargeable batteries. In 1986 electrochemical properties of lithium intercalation in graphite was shown by Rachid Yazami et al[5].

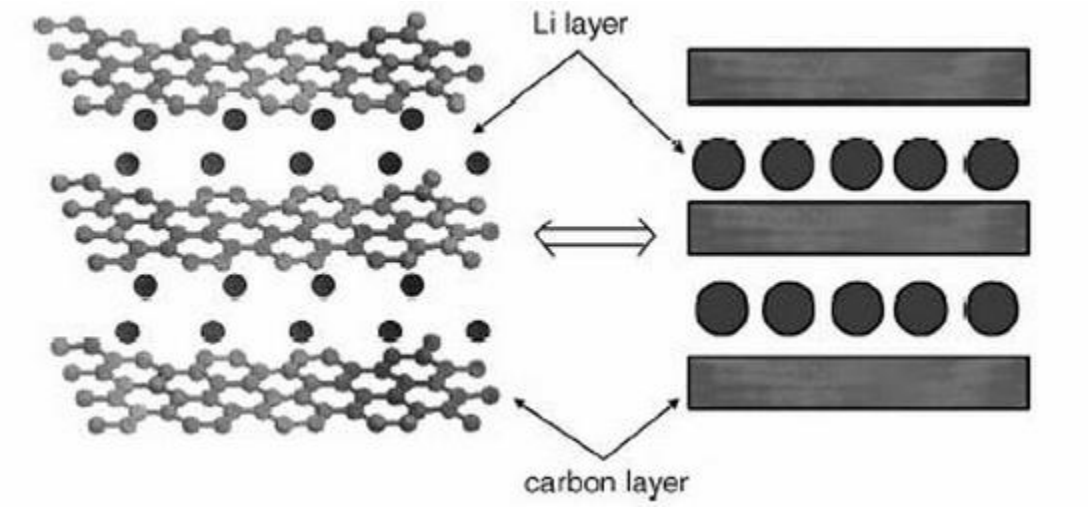

Figure 3: Structure of graphite intercalated with lithium[6].

Intercalation is a process where metal ions are reversibly removed or inserted into a host without a significant structural change to the host. Yazami et al showed the reversible intercalation of lithium into graphite in a lithium/polymer electrolyte/graphite half-cell. A few years later, Dr.J.Goodenough proposed the materials under the family $LixMO_2$ (M = Co, Mn or Ni) as a cathode material[7], and also research was being done to find a replacement for Li metal anodes. Eventually, based on research by John Goodenough's team the first commercial lithium ion battery was released by Sony in 1991[8, 9].

1.3 Working Principal

An electrical battery is one or more electrochemical cells that convert stored chemical energy into electrical energy. There are two major types of batteries: primary and secondary. Primary batteries are those which cannot be recharged because the chemical reaction inside the battery cannot be reversed and once used it must be discarded. Secondary batteries can be recharged and can be reused multiple times. A Li-ion battery usually refers to a secondary battery in which energy is stored chemically through red-ox reactions that employ lithium intercalation between the positive (cathode) and the negative (anode) electrodes i.e. as a battery is charged and discharged the lithium ions move back and forth between the cathode and the anode because of this they are also referred as "Rocking-chair" batteries[10]. Basically there are four primary components of a lithium-ion battery: the anode, cathode, separator and electrolyte for which a variety of materials may be used. The cathode acts as a positive electrode which accepts the electrons while reducing and the anode acts as a negative electrode which donates the electrons and oxidizes during the discharge cycles. The electrodes do not touch each other but are electrically connected by the electrolyte while the separator prevents the mixing between them but allows ions to flow.

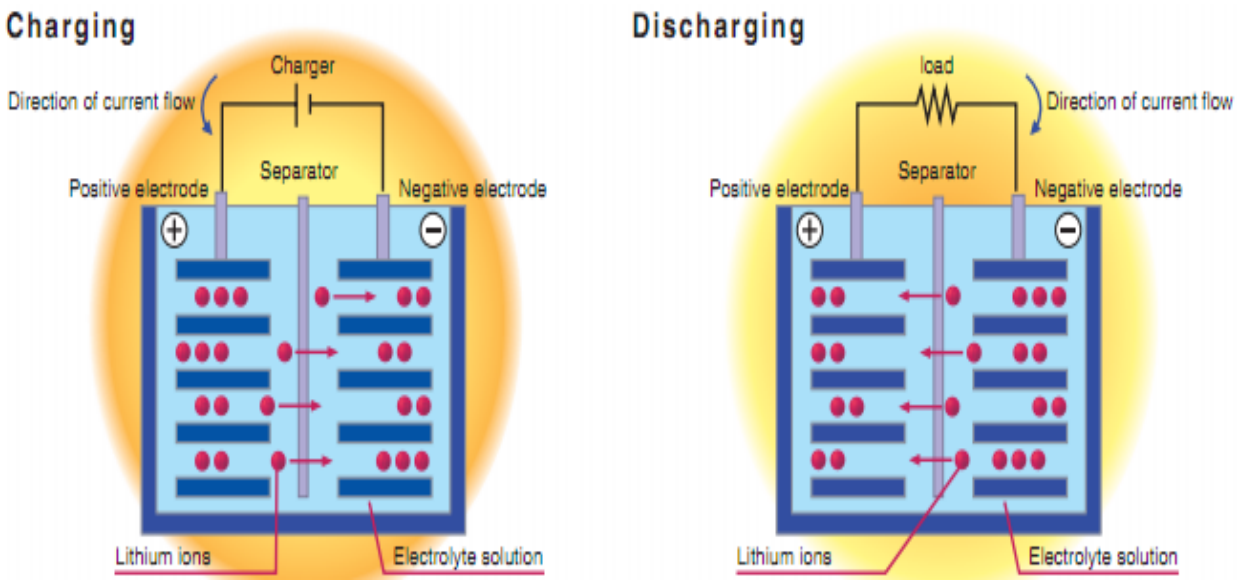

Figure 4: Diagram of Li-ion cell during charging and discharging[11].

To understand this process briefly we can consider the example of a standard $LiCoO_2$ battery in which $LiCoO_2$ acts as a cathode. During charging, lithium ions move from cathode to anode and electrons are removed from cathode by an external field and then are transferred to anode. During discharge, anode supplies the ions to electrolyte and electrons to the external circuit where the ions intercalate into cathode and electrons from the external circuit for charge compensation. This red-ox reaction is shown below.

$$\text{Positive:} \quad LiMO_2 \underset{\text{discharge}}{\overset{\text{charge}}{\rightleftharpoons}} Li_{1-x}MO_2 + xLi^+ + xe^-$$

$$\text{Negative:} \quad C + xLi^+ + xe^- \underset{\text{discharge}}{\overset{\text{charge}}{\rightleftharpoons}} Li_xC$$

$$\text{Overall:} \quad LiMO_2 + C \underset{\text{discharge}}{\overset{\text{charge}}{\rightleftharpoons}} Li_xC + Li_{1-x}MO_2$$

Figure 5: Electrode and cell reactions in a Lithium Ion battery [9].

1.4 Cell design and configuration

The basic configuration of almost all lithium-ion batteries consists of four main parts: 1) The cathode material usually $LiCoO_2$ which is coated onto an aluminum foil, 2) Layered mesocarbon micro beads carbon (MCMB) as the anode material which is coated onto a copper foil, 3) An ionically good conducting electrolyte usually liquid type which is made from a solution of lithium salts in organic solvents typically carbonates and 4) An insulating separator made with layers composed of polyethylene and polypropylene which is placed between the anode and cathode to avoid shorting.

There are four different configurations of lithium ion batteries that can be found in the current market i.e. cylindrical, thin and flat polymer, coin and prismatic battery configurations.

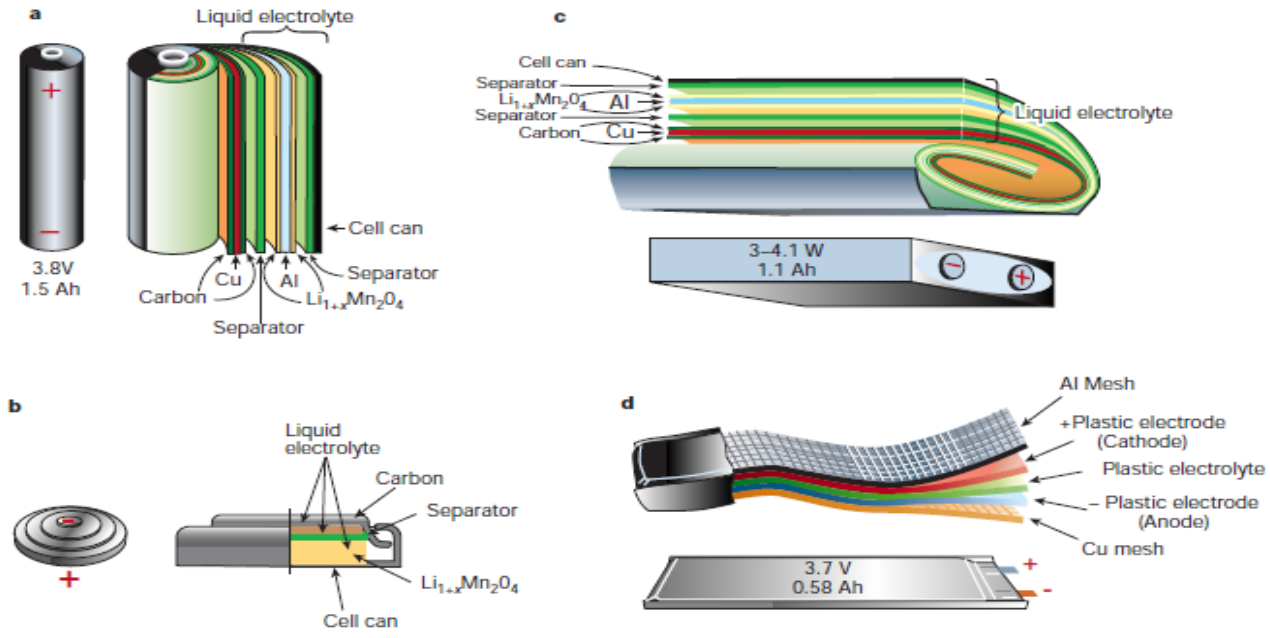

Figure 6: Battery configurations a, Cylindrical b, Coin c, Prismatic and d, Thin and Flat polymer[2].

Among these battery configurations the most commonly used is the cylindrical 18650 i.e. (18 x 65 mm) type. Figure 7 shows the electrodes from inside a Li-ion 18650 Sony battery. These can be commonly found in laptops and also in electric cars while the batteries found in cell-phone are of prismatic configuration. The positive electrode is fabricated from a slurry which is made from the mixture of active material ($LiCoO_2$), acetylene black and polymer binder PVDF (polyvinylidene fluoride) and is coated on both sides of an aluminum substrate. The negative electrode is made up of a copper substrate which is coated with a mixture of carbon active material (MCMB) and polymer binder on both sides. Figure 8 represents a lab scaled coating machine. Before the coating procedure the slurry of both the positive and negative electrodes must be thoroughly mixed in order to have a uniform mixture and also these coatings must be maintained at a certain thickness.

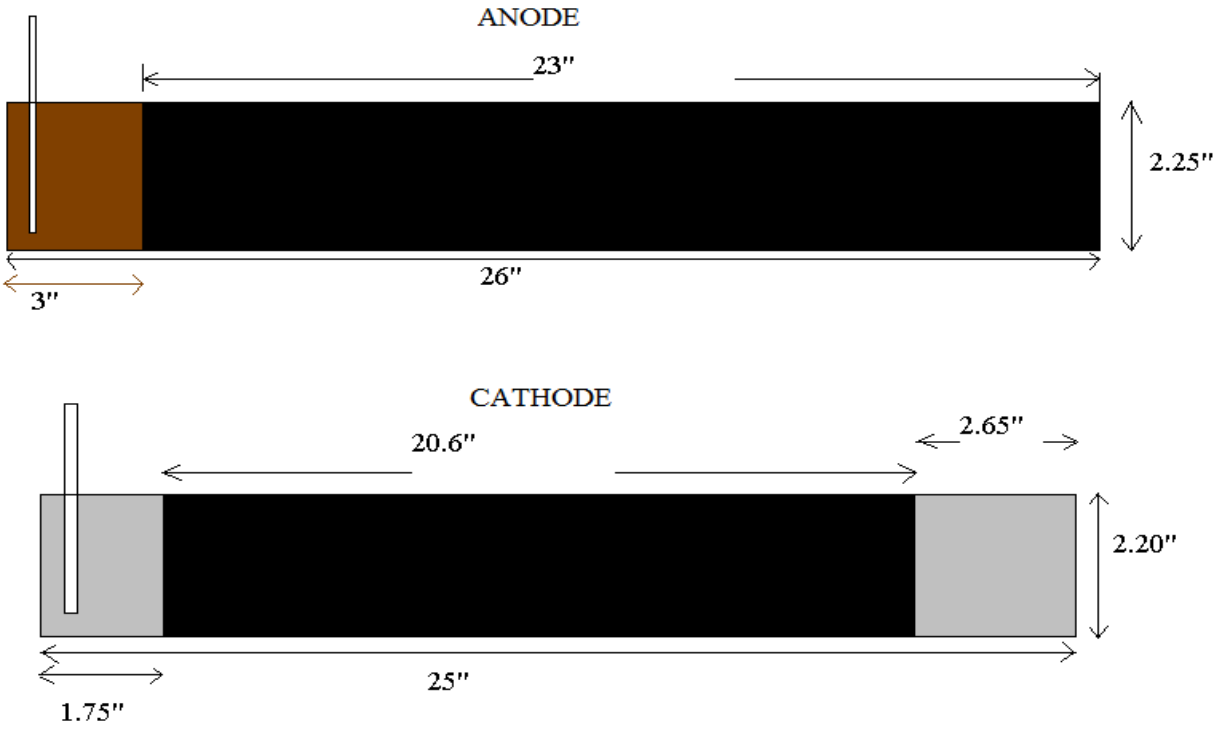

Figure 7: Coated foil layout for Sony 18650 $LiCoO_2$ battery.

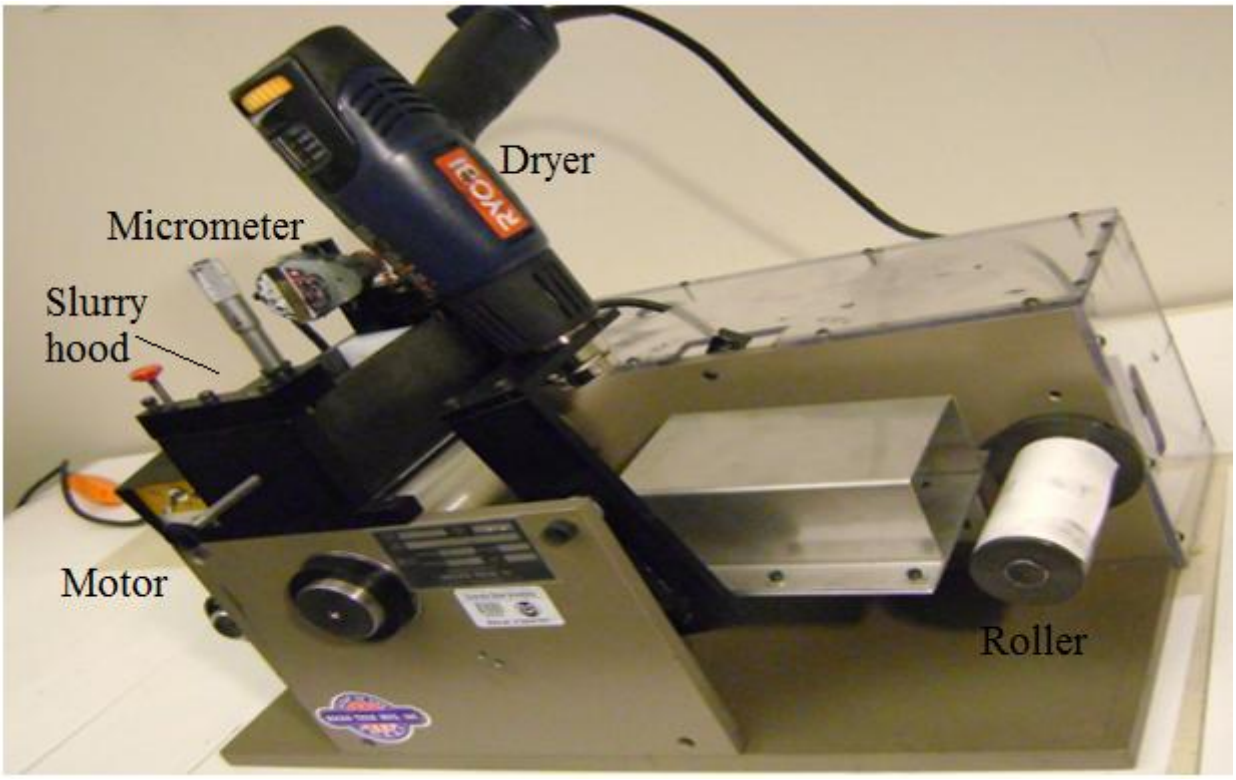

Figure 8: Typical small-scale coating machine.

Once the coatings are ready and dried, the foils are cut to the required dimensions. These foils are then calendared by passing them several times through the calendaring machine (Figure 9). Calendaring basically involves pressing the foils in between two rollers such that a uniform thickness is achieved and also to make sure the slurry sticks onto the foils.

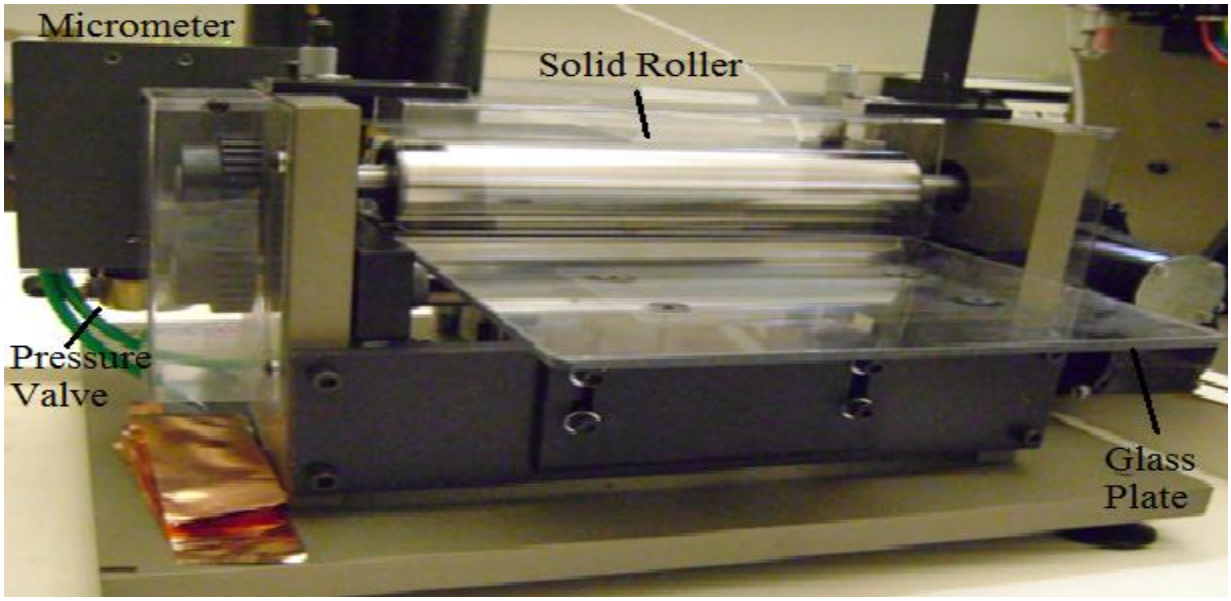

Figure 9: Calendaring Machine

Finally the fabrication process of this 18650 cell involves in rolling the anode and cathode coated foils along with the separator with the help of a winding machine (Figure 10) and then placing it in a cylinder of diameter 18mm and length 65.0mm.

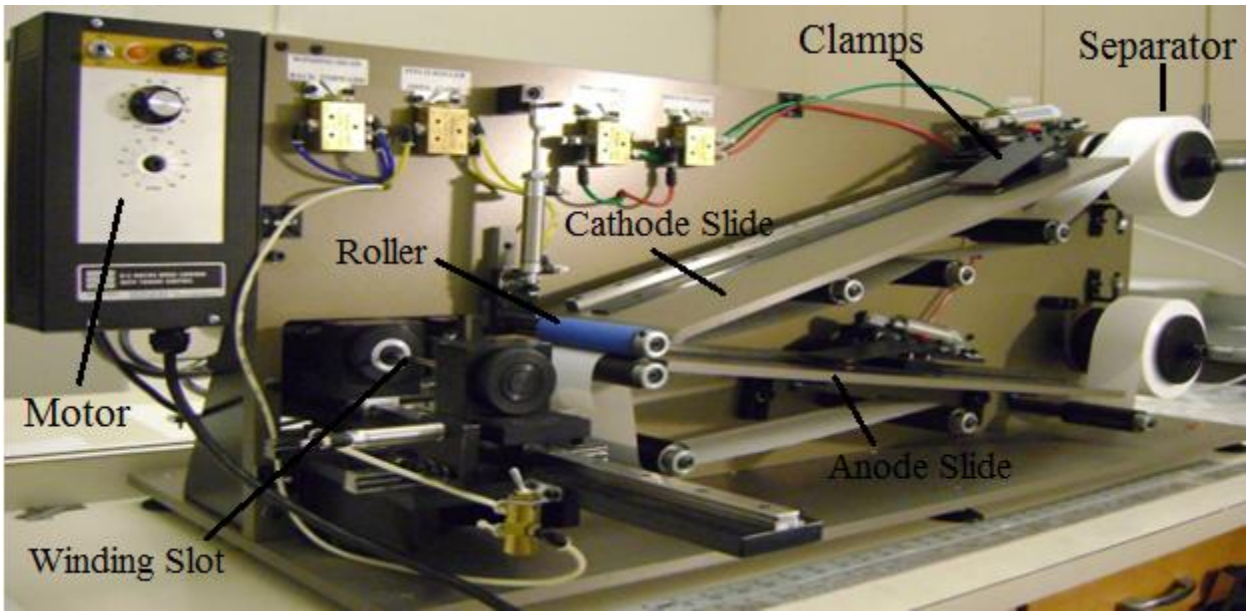

Figure 10: Winding Machine.

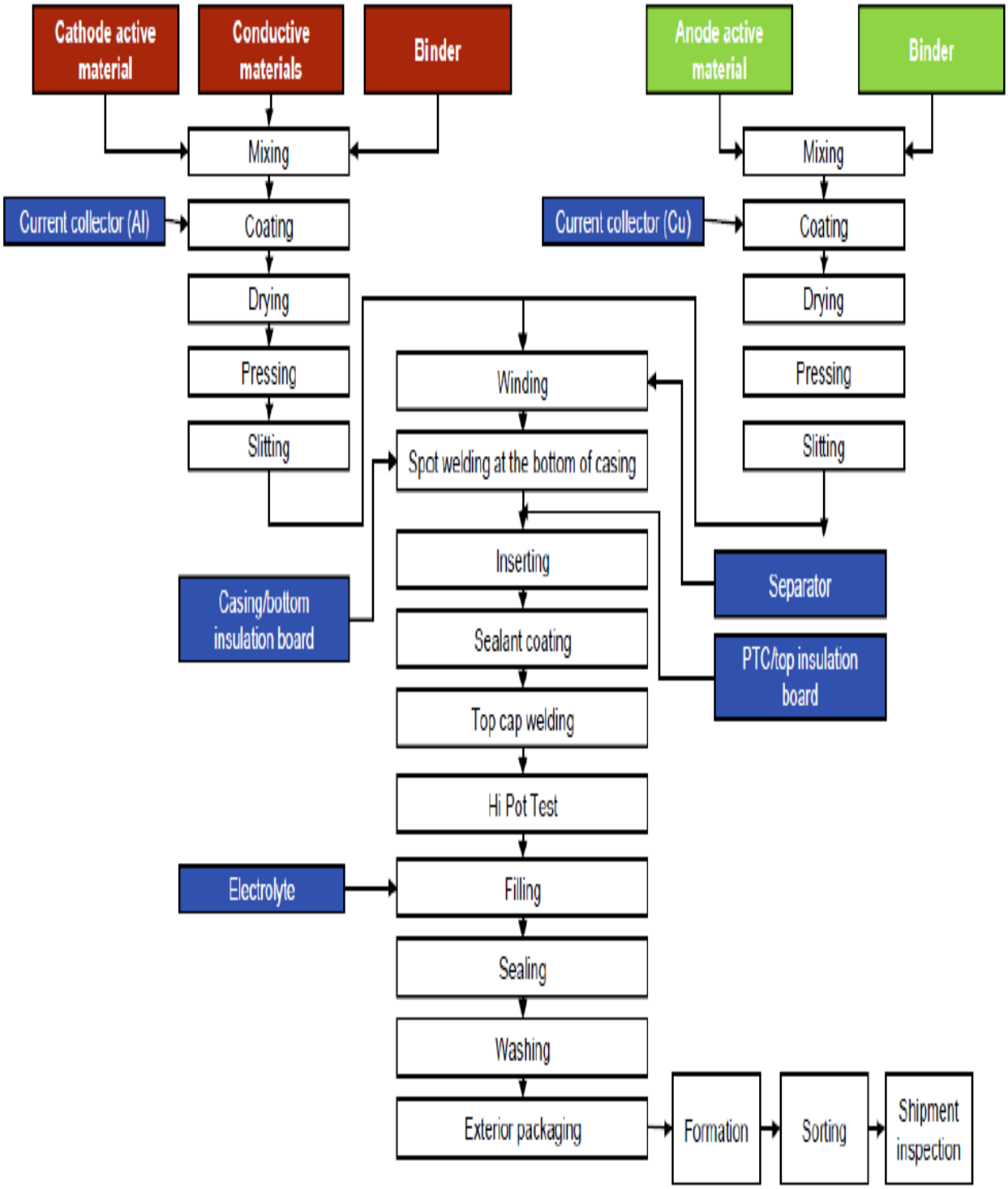

Figure 11: Process flow chart for battery manufacturing.

1.5 Battery Specifications

Typically the performance of a battery is based on the properties of the anode, cathode and the electrolyte. Cathode is often the area in which there is more scope of research since it has a high free energy of reaction with the lithium[10]. Also one of the reasons is that the anode material usually used i.e. MCMB has a capacity twice that compared to $LiCoO_2$ with no concern about the safety and it is relatively inexpensive.

One of the important factors for material selection of a cathode is to see whether it is structurally stable or not, mainly because a cell needs to incorporate large amounts of lithium reversibly without any structural changes associated with it. Additionally, the cathode materials need to be electrically conductive, ionically diffusive and finally must be inexpensive. Even for considering various materials for anode selection the desired characteristics are same as that for a cathode.

The electrolyte used commonly is a mixture of a lithium salt dissolved in an organic solvent. An electrolyte needs to be ionically conductive rather than being electrically conductive and must also support ion transportation between the anode and cathode. Additionally, it should not reduce or oxidize at different voltage ranges. The most important characteristic of an electrolyte is that it must not react with either the anode or cathode and even other components of a cell. To understand the performance characteristics of a battery there are several terms that need to be understood such as specific capacity and rate capability, cyclability, safety and cost.

1.5.1 Capacity and Rate Capability

Specific capacity is defined as the amount of energy that can be store in a given amount of volume or mass and is measured in terms of Amp-hour (Ah), while the rate capability of a battery can be defined as the rate at which the cell is being charged. The C-rate is the capacity of the battery divided by the hourly charging rate. For example, when a 4 Ah battery is being charged at 2A then it is said to be being charged at a rate of C/2. The rate capability and capacity of Li-ion batteries are dependent on their design, and varies considerably between different manufactures. A typical discharge capacity curve for 18650-type C/$LiCoO_2$ Sony battery is shown in the following figure.

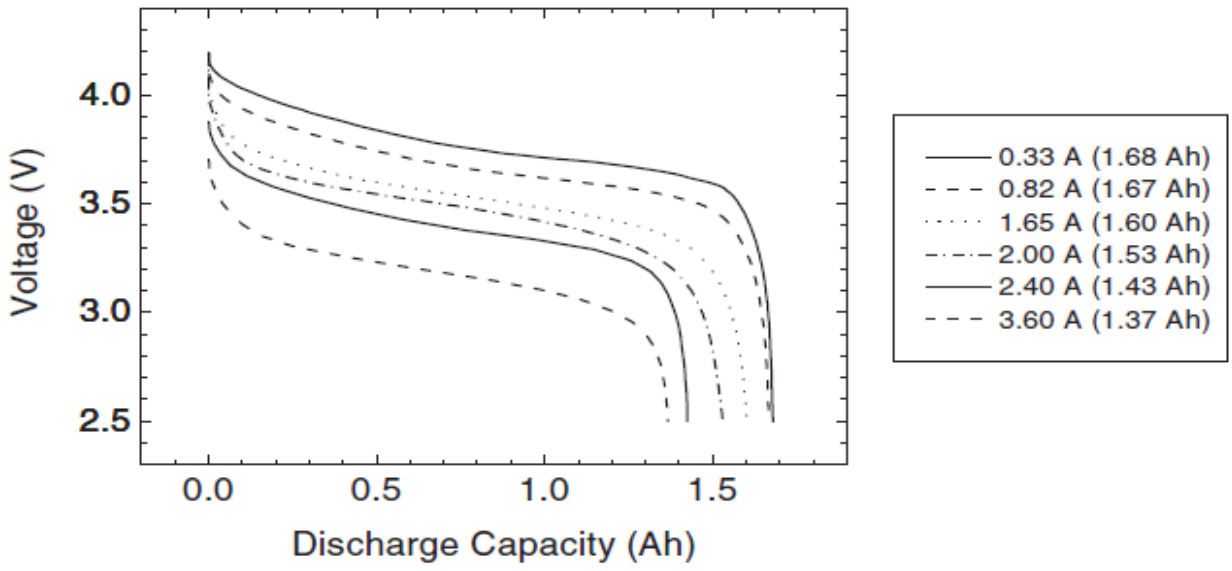

Figure 12: Capacity plots (voltage Vs Capacity)[10].

A typical graph representing the rate capability of an 18650 type C/$LiCoO_2$ can be shown in the following figure.

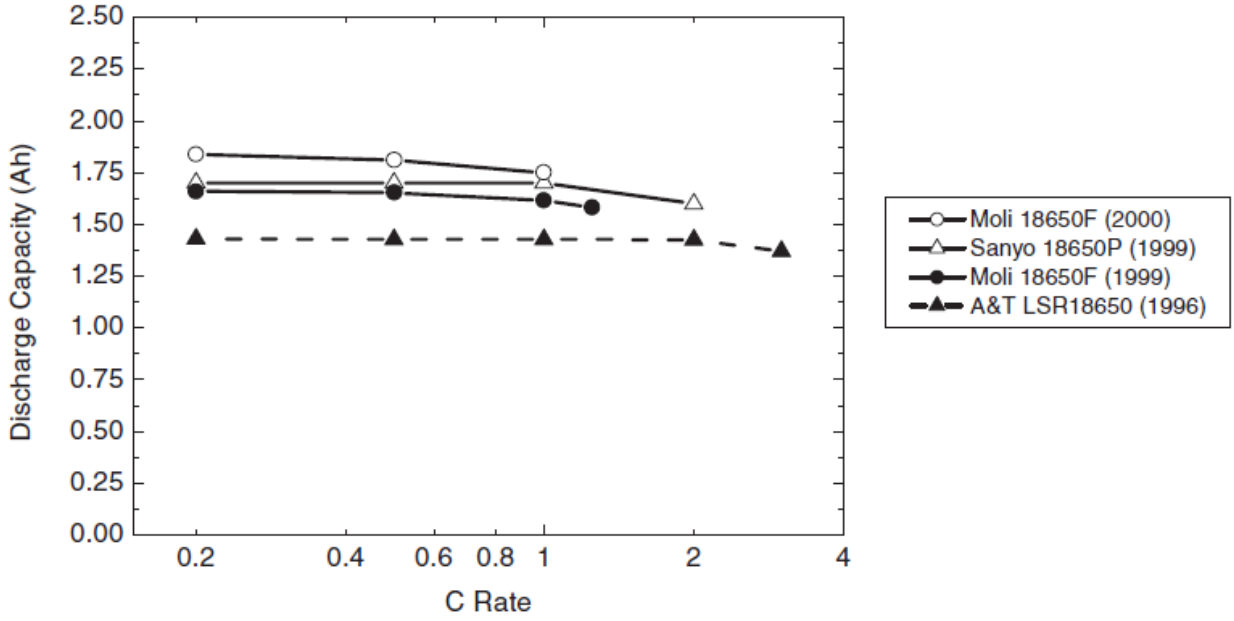

Figure 13: Comparison of the rate capability at constant current for C/$LiCoO_2$ 18650 batteries[10].

1.5.2 Cyclability

One of the best advantages of lithium-ion batteries is their long cycle life and their ability to perform at continuously varying temperatures. For example, lithium-ion batteries were found to be stable even after 500 cycles which is very high when compared to its counter-parts such as nickel cadmium and nickel metal hydride batteries. In simple terms cyclability can be defined as life cycle or the number of charging cycles a battery can undergo in its lifetime. Not only the capacity but even the cyclability is a very important term that must be taken into consideration. High end electronics such as laptops and power tools and also electric vehicles are mostly required to run over a long period of time and this is where cyclability comes into picture.

Cyclability, capacity and C-rate are inter-related to each other since C-rate has a direct effect on the cyclability of a battery. For example, if current is discharge at a higher C-rate then

the cyclability of the battery decreases substantially compared to batteries discharge at a lower C-rate. Similarly, the discharge capacity of a battery continuously decreases with the increase in the number of cycles. This results from structural changes in the cathode material during the charging cycle all the lithium that moves toward the anodic side of the battery does not all make it back to the cathode side during the discharge cycle. Apart from this, when the numbers of cycles increase it also increases the impedance, resulting in reduced voltage and lower delivered energy.

1.5.3 Safety

The main safety concern associated with lithium-ion batteries has been over heating or overcharging which causes thermal runaway and cell rupture. This has been the major drawbacks of this technology and is considered to be the main disadvantage when compared to other battery technologies[1]. There have been many cases involving exploding of laptops and cell phones which have caused major injuries. Approximately 80% of the all research publications on Li-ion batteries in the recent past has focused on various safety issues such as internal shorting, overcharging and on the effects of operating the battery at different temperatures[1].

1.5.4 Cost

One of the most important factors for a commercial product is cost. Though Li-ion batteries are the most cost-effective rechargeable battery technology currently on the market, they are still high priced and reducing their cost will enhance their use in hybrid and electric vehicles. The cobalt element which is present in the conventional $LiCoO_2$ cathode batteries is very rare and expensive. Therefore considerable research is being done to either replace this

element with other elements which have the oxidation states of +3 such as vanadium, chromium, manganese, iron and nickel or to reduce the amount of cobalt used in various battery chemistries.

1.6 Recent developments:

The ever-increasing demand for portable electronic devices and electric vehicles has been a driving force for technological advancements in Li-ion battery technology. Ever since the discovery of $LiCoO_2$ battery in 1991 by Sony Corporation, researchers have been seeking a new combination of anode-electrolyte-cathode with better performance in terms of energy output, safety, cost and better material availability. Whatever the battery technology, the measures of its performance such as capacity, energy density and cyclability are directly related to the proprieties of the material that form the electrodes and electrolyte.

Initially there was considerable research on materials with layered structure similar to that of $LiCoO_2$ such as $LiNiO_2$. This material displayed favorable specific capacity compared to $LiCoO_2$, but safety reasons and structural instability prevented further development. Similar layered structures such as $LiFeO_2$ and $LiMnO_2$ were considered to take the advantage of Fe^{4+}/Fe^{3+} and Mn^{4+}/Mn^{3+} redox couples. Research was limited for $LiFeO_2$ since it was not possible to prepare electrochemically active $LiFeO_2$ phases. $LiMnO_2$, though easy to prepare had issues concerning the structural instability because of the layered phase reversing to spinel $LiMn_2O_4$ during cycling. Recently it has been found that this can be diminished by cationic substitution of chromium[10].

Cathode research has shifted to materials with different structures, such as olivine (magnesium iron silicate) or the NaSICON (family of Na super-ionic conductors) which are built from corner sharing MO_6 octahedra (where M is Fe, Ti, V or Nb) and XO_4 tetrahedral anions

(where X is S, P, As or Mo) because they offer interesting results[2]. For example, $LiFePO_4$ can be used at 90% of its theoretical capacity of about 165mAh/g with decent rate capabilities and is presently being considered as a candidate cathode material for next generation Li-ion cells.

Figure 14 shows a graph of voltage versus capacity and summarizes the various anode and cathode materials under serious consideration for next generation batteries.

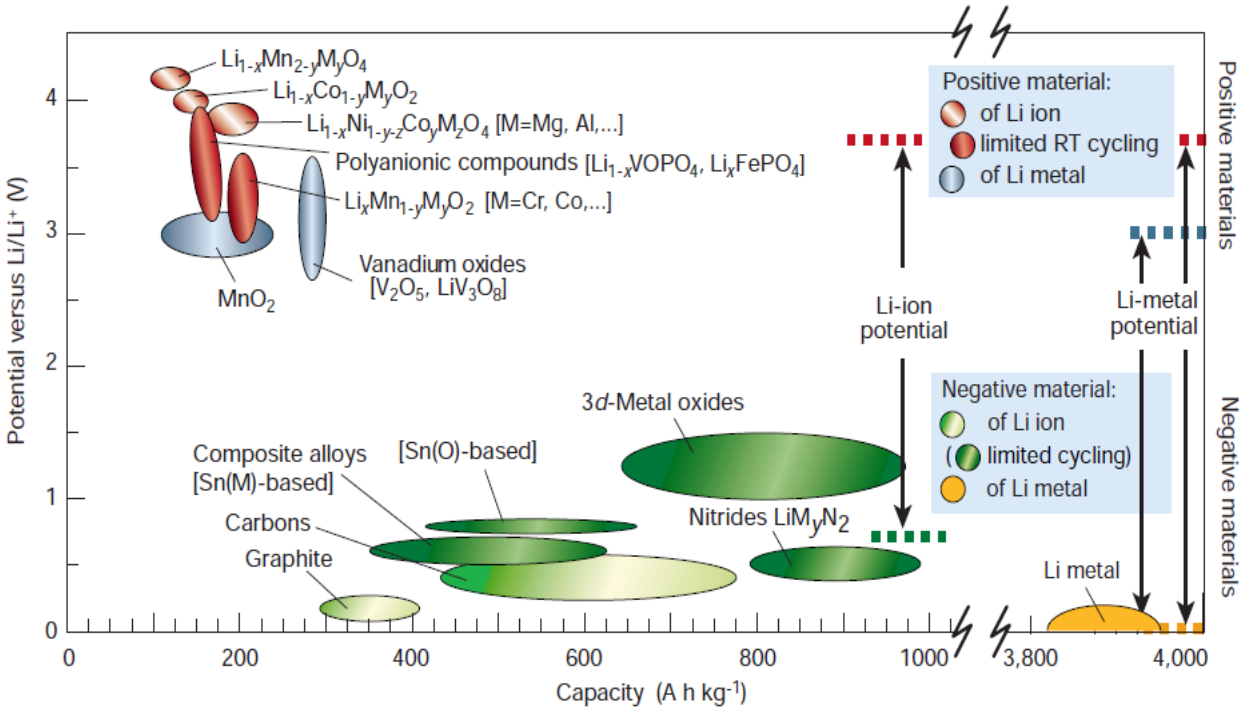

Figure 14: Voltage v. capacity for positive and negative electrode materials under consideration for the next generation of rechargeable Li-based cells[2].

Chapter 2 Cathode Materials

Over the last two decades there has been intensive research in improving the overall performance of Li - ion batteries. Among the different components of the battery mechanism one of the main foci has been alternative cathode materials. The graphite anode currently used in Li-ion rechargeable batteries have a theoretical capacity of 370mAh/g, which is twice the theoretical capacity of the formerly used layered $LiCoO_2$ cathodes, and avoids the use of expensive and toxic cobalt.

Varieties of positive materials have been developed and are available commercially. Cathode materials can primarily be categorized based on structure types. $LiCoO_2$, $LiNiO_2$, Li_2MnO_3, $LiNi_{1-x}Co_xO_2$, $LiNi_{1/3}Mn_{1/3}Co_{1/3}O_2$ etc. have layered structures where as $LiFePO_4$ based materials have the olivine structure, and $LiMn_2O_4$ and spinel materials have a three-dimensional framework structure.

2.1 Layered Structure Metal Oxides

These materials usually have layered α-$NaFeO_2$ structure, which is a distorted rock-salt structure where the cations order in alternating (1 1 1) planes[12]. This ordering results in a trigonal structure also known as R3m space group. In these structures the oxygen atoms are arranged in a face centered cubic close-packed arrangement with the transition metal oxides present within the oxygen octahedral and the lithium atoms would reside in the space between the oxygen layers. This structure supports the intercalation process where the lithium ions are inserted and removed from the structures during charge and discharge cycles[13].

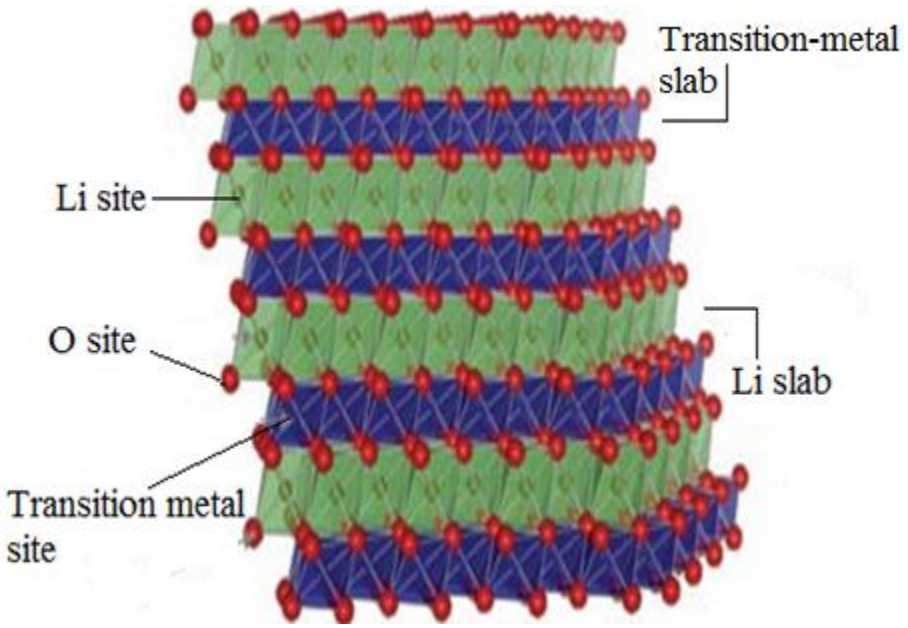

Figure 15: Layered structured transition metal oxides.

2.1.1 $LiCoO_2$

Presently the lithium ion battery industry is dominated by the $LiCoO_2$ cathodes and carbon anodes first introduced by Sony in 1991. This material was first reported by John Goodenough who recognized that this material had layered structure and that lithium could be removed electrochemically, thus making it a promising cathode material.

$LiCoO_2$ has α-$NaFeO_2$ structure with O atoms present in a cubic closely-packed FCC arrangement, when lithium is completely removed; the oxygen layers rearrange themselves to give hexagonal close packing in form of CoO_2. The following figure represents the layered structure $LiCoO_2$.

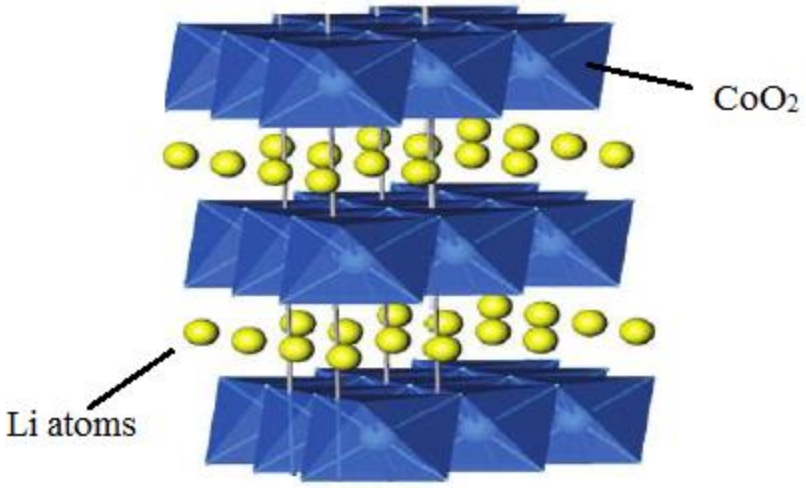

Figure 16: Layered structure of $LiCoO_2$ [14].

This material shows an initial discharge capacity of 140mAh/g at an average voltage of 3.7V. Cho et al showed that the capacity can be improved by coating a metal oxide or phosphate on the surface of the $LiCoO_2$ particles. They found that the capacity could be increased from 140mAh/g to 170mAh/g when cycled between 2.75 and 4.4V without capacity fade over 70 cycles. Also improvement was shown in the cyclability for this material when coated with metal oxides such as Al_2O_3.

Though $LiCoO_2$ cathode material is leading the lithium-ion battery market, there is limited availability of cobalt, thereby making it an expensive material. A lot of research is being done to find a probable replacement for Co with materials that are abundant and that are environmental friendly such as Ni, Mn, Fe and Cr etc. Also, since $LiCoO_2$ provides good rate capability various materials are being researched which form solid solution with $LiCoO_2$ such as $LiNiO_2$-Li_2MnO_3-$LiCoO_2$[14], $LiCoO_2$-Li_2MnO_3[15], $LiNi_{1/2}Mn_{1/2}O_2$-Li_2MnO_3-$LiCoO_2$[16, 17], $LiNiO_2$-$LiCoO_2$[18].

2.1.2 $LiNi_{1-y}Mn_yO_2$

Lithium nickel manganese oxides have been of great interest among researchers for advanced lithium-ion batteries and as a possible replacement for $LiCoO_2$ [17, 19-27]. Material compounds of this type were first reported by Dahn et al in 1992[21]. They reported a solid solution for $y \leq 0.5$ but a deterioration of the electrochemical behavior with increasing manganese content.

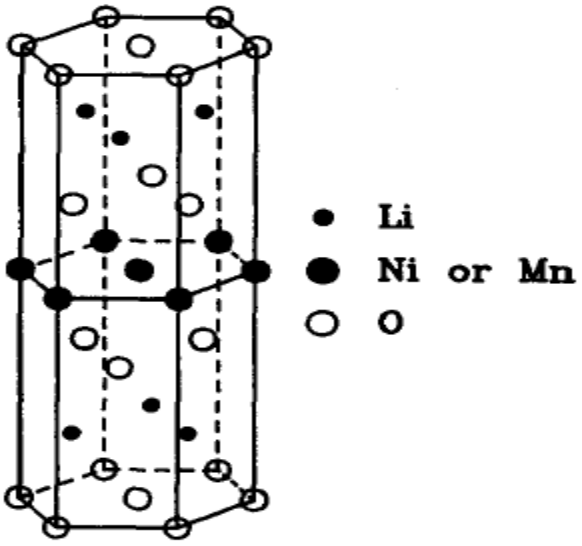

Figure 17: Unit cell of $LiMn_yNi_{1-y}O_2$ showing li-filled and Ni, Mn-filled layers[21].

The main advantage of this material is the fact that there is no Co content which is very expensive and a toxic compound compared to Ni and Mn. The most successful material of this group has been $LiNi_{1/2}Mn_{1/2}O_2$. Saphr et al [22]repeated the work of Dahn and showed maximum solubility of 0.5Mn, he was the first one to report the electrochemical behavior on $LiNi_{1/2}Mn_{1/2}O_2$ material. They showed that the Ni and Mn were present in +2 and +4 oxidation states rather the +3 and + 3 respectively through XPS and magnetic data and also that this material showed a capacity of 150mAh/g falling to 125mAh/g after 25 cycles and to 75mAh/g

after 50 cycles when prepared at 700C.The active element in this material is Ni, which cycles between the +2 and +4 valences states, while manganese remains as +4, thereby leaving with no concern for Jahn-Teller distortion associated with the Mn^{+3} ion. This material is commonly referred as "550" material (0.5Ni, 0.5 Mn, 0 Co) was rediscovered by Ohzuku in 2001[20]. Ohzuku reported an initial discharge capacity of 150mAh/g for 30 cycles using top-up charging at 4.3V when prepared at 1000C. Recently, Ohzuku reported the cycle tests of lithium cells with $LiNi_{1/2}Mn_{1/2}O_2$ operated in voltages of 2.5-4.5V of about 200mAh/g of rechargeable capacity for 30 cycles[19].

2.1.3 $LiNi_{1/3}Mn_{1/3}Co_{1/3}O_2$

Mixing proper levels of these three transition metals to get the advantageous qualities of each led to the discovery of this material. This material is derived from $LiNi_{1-y-z}Mn_yCo_zO_2$ family group (where y = z = 1/3) which were first published in 1999 by Liu et al[28] and in 2000 by Yoshio et al[29]. Yoshio hypothesized that the addition of cobalt to $LiMn_{1-y}Ni_yO_2$ would stabilize the structure in a strictly two-dimensional fashion by blocking the nickel atoms from entering the lithium layer while Mn and Ni content would provide increased structural stability and high capacities respectively. Mixing these three cations at optimum levels is very important since too much of Co would lead to decrease in capacity, too much of Ni will result in cation mixing and too much of Mn can lead to a transformation to the spinel structure.

This $LiNi_{1/3}Mn_{1/3}Co_{1/3}O_2$ layered compound was first proposed by T.Ozhuku in 2001[30] and ever since its introduction this material has been of great interest and has been extensively researched. This material shows a reversible discharge capacity of about 200mAh/g in the range of 2.5– 4.6V as well as an excellent rate capability and good thermal stability [12, 30, 31].

Also commonly referred as the "333" material can also be considered as a special case of Co substitution in $Li(Ni_{1/2}Mn_{1/2})O_2$ as reported by Lu et al and McNeil et al. with the formula $Li(Ni_xCo_{1-2x}Mn_x)O_2$, x = 1/3. For proper stoichiometry in these materials the average oxidation state must be +3 thereby it is assumed that the valence states are Ni^{+2}, Co^{+3} and Mn^{+4} for the metal ions and it was shown that the electrochemical process in the range 2.5-4.4V versus Li involves the two electron transfer reaction as Ni^{+2}/ Ni^{+4} in addition to Co^{+3}/Co^{+4}[32, 33]. Studies from the DSC measurement have also shown that this material has better thermal stability when compared to the conventional $Li(Ni_{0.8}Co_{0.2})O_2$ and $LiNi_{0.8}Co_{0.15}Al_{0.05}O_2$ cathodes [34, 35]. Some of the disadvantages of this material are that its rate capability is worse than that of $LiCoO_2$, but is better than that of $LiNi_{1/2}Mn_{1/2}O_2$ and also this material is structurally instable at voltages >4.6V since it shows a capacity retention below 80% in 50 cycles when charges at 4.7V[36]

2.1.4 $LiMnO_2$ (layered)/$LiMn_2O_4$ (spinel)

Along with its counterparts such as $LiNiO_2$ and $LiCoO_2$, this material has also been researched a lot over the last decade mainly for its prospects of providing not only a low-cost but also an environmentally benign cathode material[37, 38]. However, in spite of these advantages $LiMnO_2$ was never a viable cathode mainly because this material is unstable at elevated temperatures and cannot be synthesized by the same methods as used for materials like $NaMnO_2$. One of the successful attempts for synthesis was accomplished by Na+ ion exchange [38]and by low temperature methods such as hydrothermal synthesis[37].

Even when $LiMnO_2$ is synthesized, it tends to revert itself to form a more stable spinel structure $LiMn_2O_4$. Though initially was not desired, $LiMn_2O_4$ has proven to be a viable cathode material mainly because of the three-dimensional framework which adds stability to the structure

during delithiation. Additionally, unlike $LiNiO_2$ and $LiCoO_2$, this material does not react exothermically with the electrolyte making it potentially safer than $LiNiO_2$ and $LiCoO_2$. The following figure shows a comparison between $LiMnO_2$/LiMn2O_4 structures.

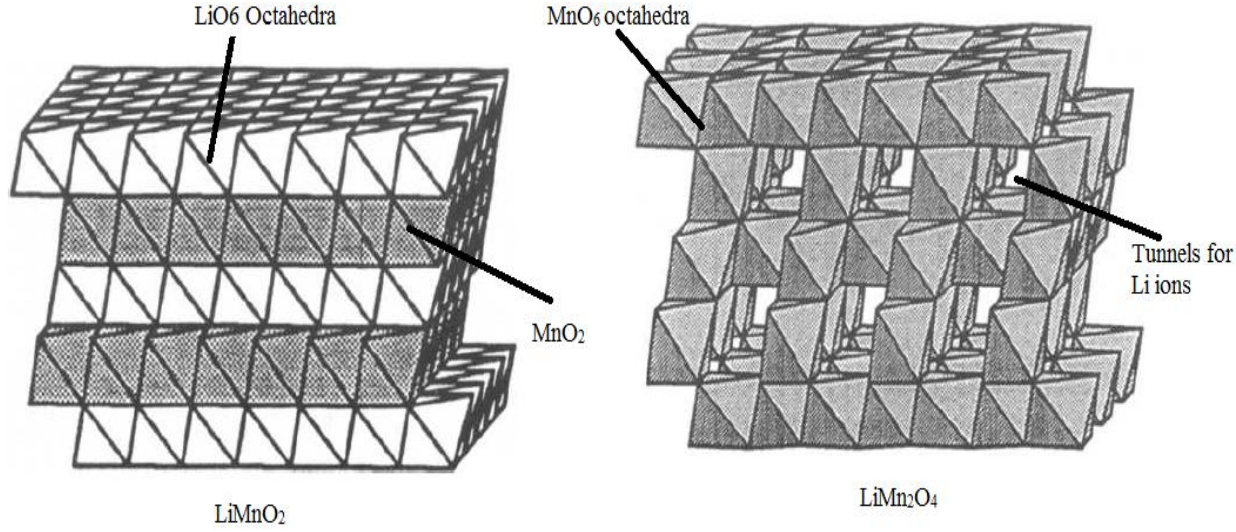

Figure 18: Comparison between layered $LiMnO_2$ structure and Spinel $LiMn_2O_4$ structure[39].

The tunnel like structure for $LiMn_2O_4$ allows lithium to move out of the structure without collapse even under high charge/discharge rates. However, the main drawback of this material is the nature of its discharge which can be divided into 2 regions: one at 4V and the other at 3V range with a capacity of 150mAh/g. After the 4V plateau, it is possible for one or more lithium ions to be present because the reaction is not in equilibrium leading to Jahn-Teller distortion which is associated with the phase transition from cubic to a tetragonal crystal structure. Additionally this material also tends to self discharge at elevated temperature [40]. There have been several attempts in improving the capacity fade by coating the material with different oxides [41-43] and also techniques like cation substitution and surface treatments have been employed to address the problem with self discharging.

2.1.5 Li_2MnO_3

This material has garnered much interest over the past few years mainly because, composite cathodes utilizing Li_2MnO_3 and other $LiMO_2$ phases (M = transition metals) have been found to have higher capacities and better safety systems [16, 44-51]. Additionally manganese oxides based compounds are less toxic and are relatively inexpensive than $LiCoO_2$. Li_2MnO_3 has a layered rock salt like structure that is comprised of Mn and Li ions in alternating layers in 2:1 ratio respectively, these layers are separated by closely-packed cubic oxygen layers. It is similar to the layered structure of $LiCoO_2$ and $LiNiO_2$ with a R3m space group, this leads to the notation of $Li[Li_{1/3}Mn_{2/3}]O_2$[52].

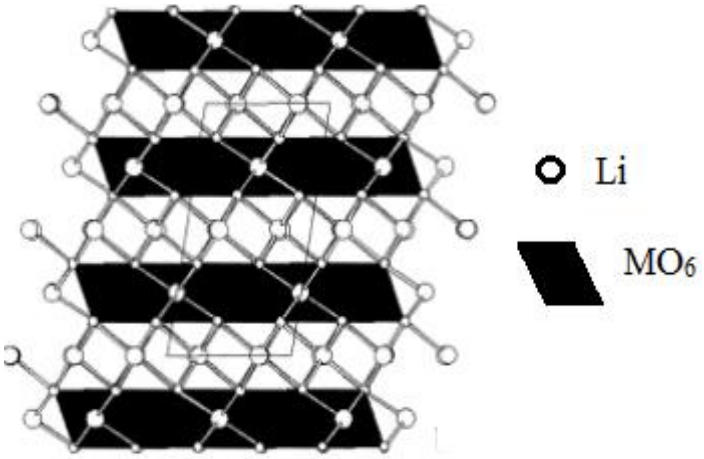

Figure 19: The rock salt structure of Li_2MnO_3[53].

Li_2MnO_3 is considered to be electrochemically inactive since Mn is present in +4 oxidation state and it cannot be further oxidized under low voltages, but when this material is charged to higher voltages i.e. >4.5V it tends extract Li+ ion in the form of Li_2O leaving behind MnO_2 component. However, this process is not reversible and only one Li+ ion can return on discharge to form $LiMnO_2$ which is an active material.

The extra Li atom which gets extracted during charging adds to the higher capacities, but also contributes to irreversible capacity loss. The concept of integrating composites cathodes with Li_2MnO_3 is attractive since it not only facilitates the intercalation process but also provides overall structural stability during the intercalation process [27, 52].

2.2 Binary and ternary solid solutions containing Li_2MnO_3

Solid solutions were primarily considered in order to obtain a material composition with excellent overall performance in terms of capacity, cyclability and structural stability while keeping costs low. These complicated compounds have been found to retain the advantages of its single transition-metal species and overcome their shortcomings, which has extended the research fields of the cathode materials for lithium-ion batteries. Recently, many solid solutions both binary and ternary systems have been widely studied such as $LiNiO_2$-Li_2MnO_3-$LiCoO_2$[14, 54], $LiNiO_2$-Li_2MnO_3[24, 49, 55, 56], $LiCoO_2$-Li_2MnO_3[15, 57], $LiNi_{1/2}Mn_{1/2}O_2$-Li_2MnO_3[27], $LiNi_{1/2}Mn_{1/2}O_2$-Li_2TiO_3[58, 59], $LiCrO_2$-Li_2TiO_3[60, 61], $LiNiO_2$-Li_2TiO_3[62, 63], $LiFeO_2$-Li_2MnO_3[64, 65]. Solid solutions containing Li_2MnO_3 as one of its component were found to be of great interest for two main reasons: 1) the extraction of two Li+ ions when charged at voltages >4.5V gives the extra amount of initial charge capacity and 2) the MnO_2 component which on removal of lithium gives good structural stability to the whole composition. Following are some of the most important solid solution compositions containing Li_2MnO_3 component.

2.2.1 $Li[Li_{x/3}Co_{1-x}Mn_{2x/3}]O_2$

$Li[Li_{x/3}Co_{1-x}Mn_{2x/3}]O_2$ is a solid solution between $LiCoO_2$ and Li_2MnO_3. This material was first proposed by Numata et al[57] in 1999. An excess amount of lithium carbonate was used

into the mixture on calcinations at 900 – 1000C to obtain the solid solution. They reported that the discharge capacity decreased with the increase of x value in the solution.

In 2006 Sun et al developed the same solid solution containing $LiCoO_2$ and Li_2MnO_3 but used spray drying method between 750C and 950C for synthesis [15]. It was found that the oxidation states of Co and Mn were at +3 and +4 respectively by using redox titration and XPS testing. Their measurements showed that the discharge capacity of the samples reduced gradually with the increase in Li_2MnO_3 content and that when charged to 4.5V the samples showed excellent electrochemical cycling performance.

2.2.2 $Li2MnO_3$ - $LiNi1_{/3}Co_{1/3}Mn_{1/3}O_2$ - $LiNiO_2$

As the name indicates the samples synthesized from this group are from solid solution mixture of Li_2MnO_3, $LiCoO_2$ and $LiNi_{1/3}Mn_{1/3}Co_{1/3}O_2$. This material was first developed by Sun et al in 2009[66]. Compositions in this system were synthesized using metal oxide precursor by adopting co-precipitation method. Results showed that the maximum initial discharge capacity was found to be at 243.8mAh/g for $Li[Li_{0.20}Ni_{0.133}Co_{0.133}Mn_{0.534}]O_2$ material composition when charged between 2-4.6V.

However, this material showed a low capacity retention 50mA/g forming one of the bases for the research proposed in this thesis. In this research work one of the end components $LiNiO_2$ has been replaced by $LiCoO_2$, since adding $LiCoO_2$ would not only increase the capacity but also would help in capacity retention.

2.2.3 $Li[Li_{(1-x)/3}Mn_{(2-x)/3}Ni_{x/3}Co_{x/3}]O_2$

$Li[Li_{(1-x)/3}Mn_{(2-x)/3}Ni_{x/3}Co_{x/3}]O_2$ is a solid solution between (1-x)Li_2MnO_3 and $xLiNi_{1/3}Mn_{1/3}Co_{1/3}O_2$, that was first reported by Wu and Manthiram in 2006[67]. Materials of this type were found to be of great interest mainly because of their high capacities and also since theses material had low cobalt content making them cost effective. Results showed that the materials produced initial discharge capacities of 227mAh/g for x= 0.7 and 253mAh/g for x = 0.4 when charged between 2 – 4.8V at a rate of C/20. Initially these materials showed a irreversible capacity loss (ICL) of 63 and 75 mAh/g for x = 0.7 and 0.4, respectively.

However, they showed that when these particles were coated with metal oxides like Al_2O_3, ICL got reduced to 38 and 41mAh/g[67]. Another recent development has been in modifying the surface of the active material by 2 wt.%Al_2O_3, 2 wt%.RuO_2 and 1 wt.% Al_2O_3+1 wt.% RuO_2[68]. The sample which was surface modified with 1 wt.% Al_2O_3+1 wt.% RuO_2 delivered a capacity of 280mAh/g at C/20 rate with a capacity retention of 94.3% in 30 cycles.

2.2.4 $Li[Ni_xLi_{(1/3-2x/3)}Mn_{(2/3-x/3)}]O_2$

$Li[Ni_xLi_{(1/3-2x/3)}Mn_{(2/3-x/3)}]O_2$ is a solid solution between $xLiNi_{1/2}Mn_{1/2}O_2$ and (1-x) Li_2MnO_3. This material was first reported by Lu et al in 2001[24]. This material showed an initial discharge capacity of 220mAh/g with x= 1/3at 55C between 2 and 4.6V using a current density of 30mAh/g. They also showed that the oxidation states of Ni and Mn were +2 and +4, respectively instead of +3 and +3 through a series of XPS testing. Since its introduction this material has been very popular because of its high capacities and low cost.

In 2004 Yoon et al developed $Li[Ni_{0.17}Li_{0.22}Mn_{0.61}]O_2$ and $Li[Ni_{0.25}Li_{0.17}Mn_{0.58}]O_2$ material compounds from the same solid solution as that of Lu et al[47]. These compounds showed high discharge capacities of over 245mAh/g and a stable cycle performance in the voltage range 2 – 4.8V. Also around the same time, Thackeray et al studied the electrochemical behavior of $0.3Li_2MnO_3 \cdot 0.7\ LiMn_{1/2}Ni_{1/2}O_2$ when charged to potentials ≥ 4.5V [27, 44]. They showed that electrodes from this material delivered capacity >250mAh/g when cycled between 2 -5V. They were the first to report that Li_2MnO_3 was responsible for the extra voltage plateau beyond 4.5V since Li_2MnO_3 becomes active when charged to voltage >4.5V by the subsequent removal of Li_2O which cause the extra capacity. This work has also been one of the foundations bases for the research proposed in the current thesis.

2.2.5 $(1-x-y)LiNi_{1/2}Mn_{1/2}O_2 \cdot xLi[Li_{1/3}Mn_{2/3}]O_2 \cdot yLiCoO_2$

This is a system is made from a ternary solid solution comprising of Li_2MnO_3, $LiCoO_2$ and $LiNi_{1/2}Mn_{1/2}O_2$ which was first developed by Zhang et al[69]. Their work was aimed at improving the electrochemical performance of $xLiNi_{1/2}Mn_{1/2}O2 \cdot (1-x)Li_2MnO_3$ by adding Co content in order to suppress the release of oxygen at higher voltages.

Samples were synthesized using simple solid state reaction and XRD results showed good structural compatibility between three layered compounds Li_2MnO_3, $LiNi_{1/2}Mn_{1/2}O_2$ and $LiCoO_2$. Zhang basically worked on two regions mainly $0 \leq x = y \leq 0.3$ and $x + y = 0.5$. The best results were shown in the region $0.3 \leq x+y \leq 0.6$ which delivered capacities around 200mAh/g. They also demonstrated the effect of integrating Li_2MnO_3 and $LiCoO_2$ components into $LiNi_{1/2}Mn_{1/2}O_2$ since the region which showed the best results had high content of Li_2MnO_3.

Chapter 3 System Analysis

3.1 Research Statement

The overall goal of this thesis is to discover material compositions present within the (1-x-y)$LiNi1_{/3}Mn_{1/3}Co_{1/3}O_2$· xLi_2MnO_3·$yLiCoO_2$ system with high initial discharge capacity and excellent cyclability compared to current lithium-ion cathode materials.

3.2 Objectives

The objective in this research work was to find new lithium-ion based cathode materials within the (1-x-y) $LiNi1_{/3}Mn_{1/3}Co_{1/3}O_2$·$xLi_2MnO_3$·$yLiCoO_2$ system which are advantageous over $LiCoO_2$ in terms of initial discharge capacity, cyclability and cost. Therefore, various points were taken within the compositional triangle of the system and samples were synthesized, characterized and tested accordingly. Results were analyzed to determine the best combination of initial discharge capacity, cost and cyclability. Since the samples in this system are low in cobalt content, we already have an advantage over $LiCoO_2$ in terms of cost. A $LiCoO_2$ cathode has an initial discharge capacity of 140mAh/g, therefore any material in this system with initial capacity of more than 140mAh/g and good cyclability can be considered as a possible replacement for $LiCoO_2$.

3.3 Approach

Motivation for working on the system (1-x-y) $LiNi1_{/3}Mn_{1/3}Co_{1/3}O_2$·$xLi_2MnO_3$·$yLiCoO_2$ came from prior work on binary and ternary solid solutions which showed that structural

compatibility between Li_2MnO_3 and other layered structured $LiMO_2$ components (M= transition metals) such as $LiCoO_2$ –Li_2MnO_3[15, 57], $xLiNi_{1/2}Mn_{1/2}O_2 \cdot (1\text{-}x)Li_2MnO_3$[44, 45, 47], $LiNi_{1/3}Mn_{1/3}Co_{1/3}O_2$-$Li_2MnO_3$[36, 67, 68], $LiNiO_2$-$LiNi_{1/3}Mn_{1/3}Co_{1/3}O_2$-$Li_2MnO_3$[66], $LiNi_{1/2}Mn_{1/2}O_2$-Li_2MnO_3-$LiCoO_2$[16, 69], $LiNiO_2$-Li_2MnO_3-$LiCoO_2$[14].

The process for choosing material compositions in this research for testing is similar to that used by Zhang et al who synthesized compositions within (1-x-y) $LiNi_{1/2}Mn_{1/2}O_2$-xLi_2MnO_3-$yLiCoO_2$system[69] and Madhu et al for $LiNiO_2$-Li_2MnO_3-$LiCoO_2$ system[14].

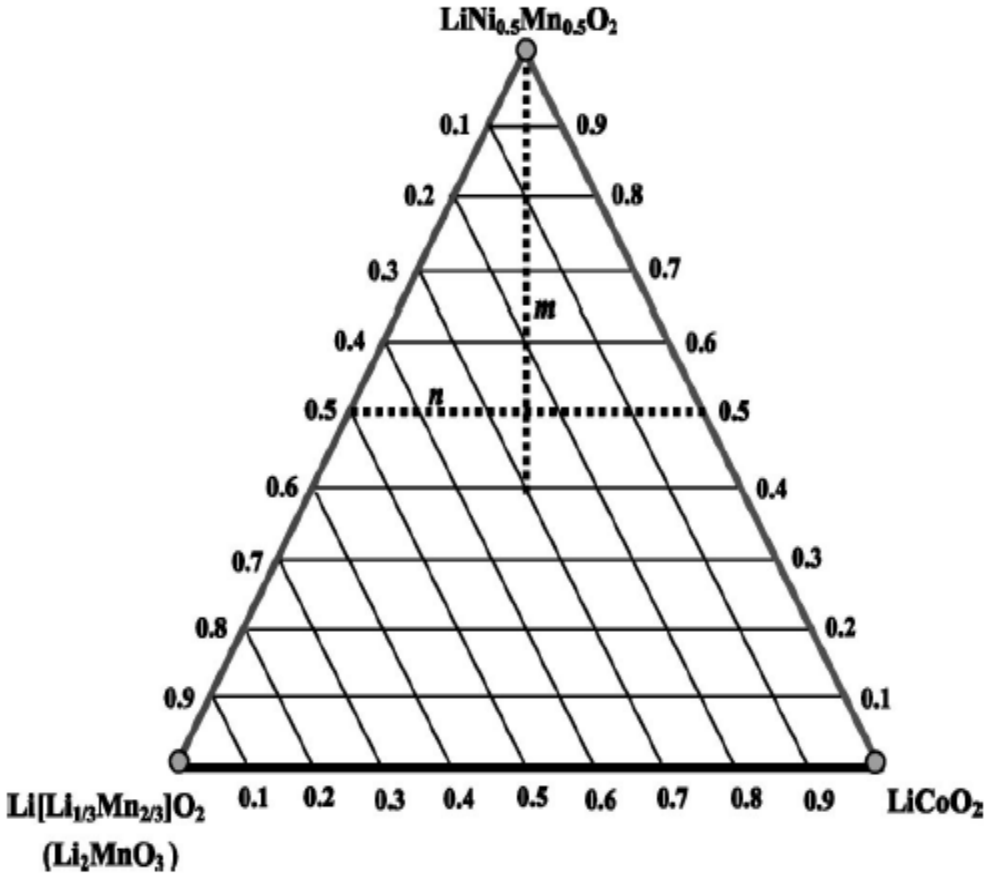

Figure 20: Ternary composition triangle proposed by Zhang et al for the system (1-x-y) $LiNi_{1/2}Mn_{1/2}O_2$-xLi_2MnO_3-$yLiCoO_2$. Where m and n represent lines that were investigated for work[69].

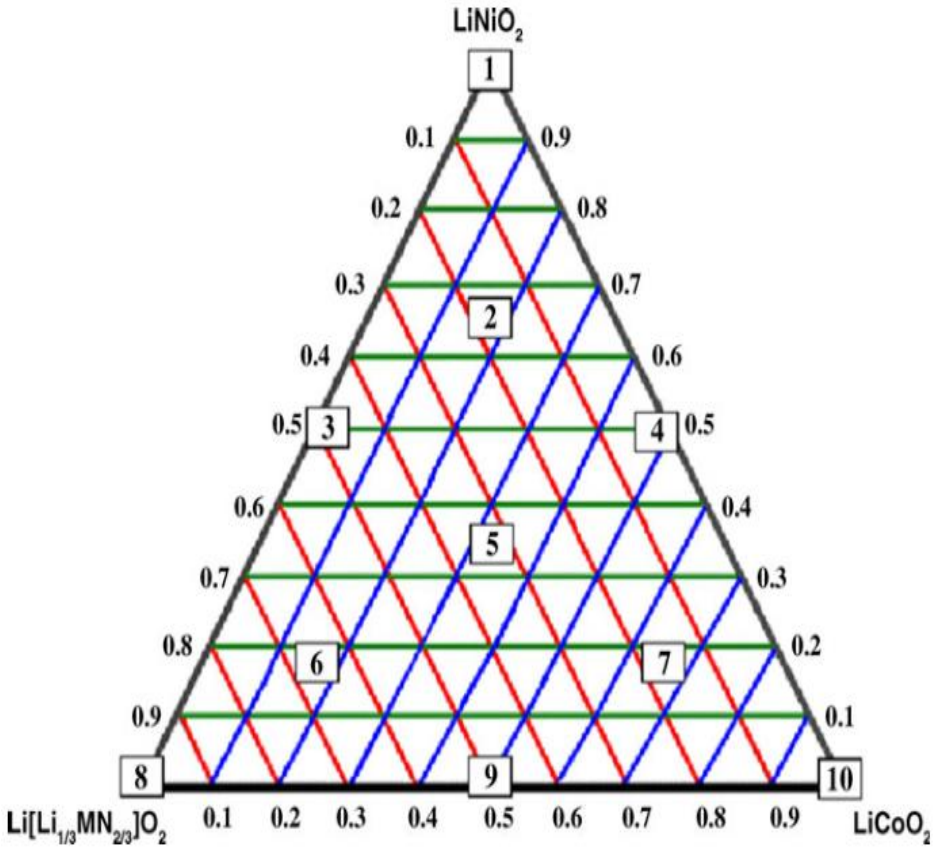

Figure 21: Ternary composition triangle proposed by Madhu et al for the system (1-x-y) $LiNiO_2$-xLi_2MnO_3-$yLiCoO_2$[14].

The current system (1-x-y) $LiNi_{1/3}Mn_{1/3}Co_{1/3}O_2$-$xLi_2MnO_3$-$yLiCoO_2$ is a ternary solid solution with $LiNi_{1/3}Mn_{1/3}Co_{1/3}O_2$, Li_2MnO_3 and $LiCoO_2$ forming the end components. This is similar to that proposed by Zhang et al and Madhu et al with the only difference that one of the end components i.e. $LiNi_{1/2}Mn_{1/2}O_2$ and $LiNiO_2$ respectively has been replaced by $LiNi_{1/3}Mn_{1/3}Co_{1/3}O_2$. Mainly, because of the higher capacities that are delivered by $LiNi_{1/3}Mn_{1/3}Co_{1/3}O_2$ when compared to $LiNi_{1/2}Mn_{1/2}O_2$ and $LiNiO_2$. Also the other two end components, Li_2MnO_3 and $LiCoO_2$, would offer good structural stability and rate capability, respectively, to the whole system.

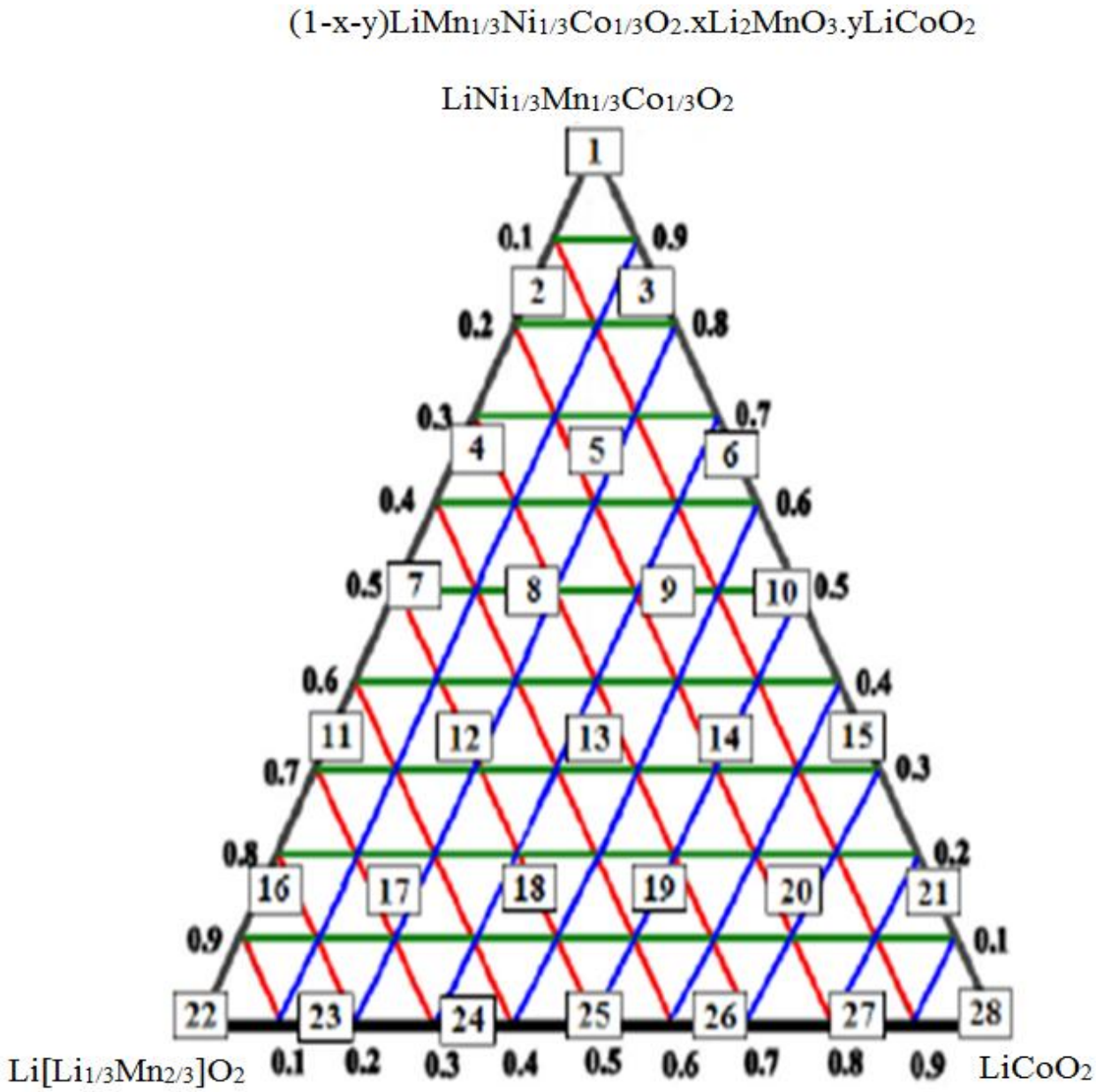

Figure 22: Ternary composition triangle for (1-x-y)$LiNi_{1/3}Mn_{1/3}Co_{1/3}O_2 \cdot xLi_2MnO_3 \cdot yLiCoO_2$ and the 28 points chosen for testing.

Twenty-eight different composition points were chosen in order to find an optimized material with good electrochemical performance.

Chapter 4 Experimental Methods

Material synthesis, characterization, cathode assembly, cell assembly and electrochemical testing form the sequence of steps in which an electrochemical cell is processed and tested. Samples from the proposed (1-x-y)$LiNi_{1/3}Mn_{1/3}Co_{1/3}O_2$·$xLi_2MnO_3$·$yLiCoO_2$ system which demonstrated the best results were created again in triplicate to confirm consistency and repeatability, and also to enable statistical comparison between samples with different compositions.

4.1 Synthesis

All the 28 samples in the system were synthesized using the sol-gel synthesis method. This synthesis method was mainly used because the chemical reaction is easy, requires only a low reaction temperature and has a high degree of homogeneity compared to the conventional solid-state synthesis.

Stoichiometric weights of the acetates Li-$(COOCH_3)_2$·$2H_20$, Mn-$(COOCH_3)_2$·$4H_20$, Ni-$(COOCH_3)_2$·$4H_2O$, and Co-$(COOCH_3)_2$·$4H_2O$ which were used as precursor agents for the proposed system were measured out so as to have a standard batch size of five grams. This mixture of precursors was first dissolved in 50ml of DI H_2O and then equi-molar weights (approx~ 3.5 grams) of citric acid was added. This solution was continuously stirred for about 20mins for the formation of a homogeneous mixture of gel and then is kept under a hot-plate for 10-12hrs at 100 ºC so that all the distilled water gets evaporated.

Acetates basically require two heating stages for the formation of a proper phase for end material. The temperatures for the synthesis must be selected taking into consideration that all the acetates get decomposed and a proper phase is formed rather the resulting in an undesired decomposition. The beaker containing the gel is then kept in a furnace and is heated to 350 ºC for 3 hrs; the first heating is at a low temperature. Basically what happens during this stage is that all the acetates present would get burned off, but the desired phase is not formed. After the 1st heating the material from the beaker is scrapped out, grounded until a fine powder is obtained and is kept in a crucible for the 2nd heating stage which is at 800 ºC for 12 hours. The 2nd heating is done at higher temperatures because of the wide range of materials present in the composition and also more importantly to ensure the formation of a proper phase for the crystalline structure. Finally, the material collected from the furnace is grounded and is stored at a dry place until it is made into a cathode.

4.2 Material Characterization

X-ray diffraction was performed on all the 28 samples proposed in the system and also the samples which were repeated, to determine whether the proper phase was achieved or not. X-ray photoelectron spectroscopy (XPS) and inductively coupled plasma atomic emission spectroscopy (ICP-AES) characterization techniques were only performed on the samples which showed promising results and were repeated. While XPS was done to have an in-depth idea about the percentage amount and the oxidations states of the elements present in the composition, ICP was performed for the detection of any trace elements and also to verify the exact composition of the sample.

4.2.1 X-Ray Diffraction (XRD)

X-Ray diffraction is a characterization technique that reveals information about the crystallographic structure, lattice parameters, planar spacing, crystallite size etc. This technique works on the principle of Bragg's law, where the material is bombarded with X-rays at different angles and the intensity of the beam is measured.

X-ray diffraction was conducted on all the sample using a Scintag X_2 powder X-ray diffraction system that utilized Cu K_α radiation with λ= 1.54A. Samples were in powder form, and scans were run from 2Θ values of 15º to 70º at a rate of 3º per minute. The graph obtained is a plot between intensity vs. angle, an example is shown in the following figure.

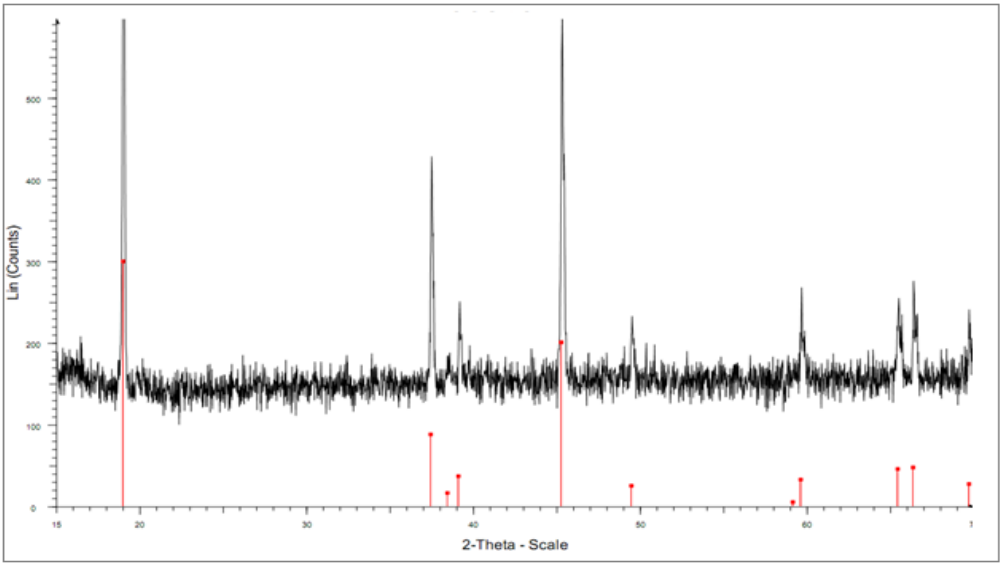

Figure 23: XRD plot of sample #28 from the current system.

If the Θ value satisfies the Bragg's law the X-rays will be in phase with the material and sharp peaks are observed, these peaks are used for analyzing the structure of the material, lattice parameters and to determine the formation of a pure phase and also most importantly it is used to

identify the presence of any unknown substances by comparing the observed diffraction data against a database maintained by the International Centre for Diffraction Data

4.2.3 Inductively Coupled Plasma (ICP-AES)

Inductively coupled plasma atomic emission spectroscopy (ICP-AES) is a technique that is used for the detection of trace metals in a given material composition. This technique uses inductively coupled plasma to produce atoms and ions that emit radiation at wavelengths of a particular element. The concentration of the element is directly related to the intensity of the emission.

ICP analysis was conducted on the samples that showed the best possible results from the statistical data analysis. The instrument that was used for the testing is a PerkinElmer Optima 7300 DV with a Cetac ASX- 520 auto sampler, Mein hard concentric nebulizer and a cyclonic spray chamber with baffle.

4.2.4 X-ray Photoelectron Spectroscopy (XPS)

X-ray photoelectron spectroscopy is an analytical technique that measures the valence states, elemental composition and the empirical formula of the elements that are present within a material. XPS spectra are obtained by bombarding a material with a beam of X-rays while simultaneously measuring the kinetic energy and the number of electrons that escape from the material.

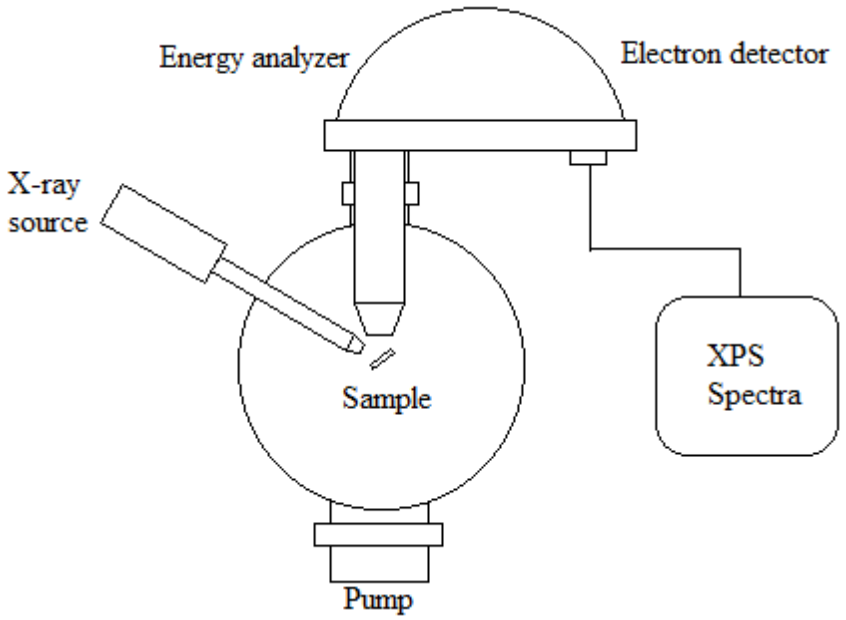

Figure 25: Schematic diagram of X-ray photoelectron spectroscopy.

XPS experiments were performed on a Physical Electronics PHI 5800 ESCA system. This system has a monochromatic Al K_α X-ray source (h_α = 1,486.6 eV), hemispherical analyzer and a multichannel detector. A low energy (30eV) electron gun was used for the charge neutralization on the non-conducting samples. The binding energies for the samples were referenced to the C1s peak at 284.8 eV. The spectra were collected at room-temperature. Multipak version 6.1 peak fitting software was used to divide individual peak components.

4.2.5 Statistical Analysis

A statistical based analysis was conducted on the system to find the most promising materials and to discover the trends in the capacity and cyclability range over the composition triangle.

Response surface regression was estimated using the JMP version 7.0.1 with the design of experiments (DOE) procedure for a Mixture Design. The model included effect for each variable $LiNi_{1/3}Mn_{1/3}Co_{1/3}O_2$, Li_2MnO_3 and $LiCoO_2$ and the two way interactions.

4.3 Cathode Preparation

After the 2nd heating, XRD was performed to verify the formation of the desired phase before these samples were again ground and sieved to a particle size of 45 microns. Controlling the particles size is very important for the performance of a battery. After sieving the sample were made for cathode preparation by a solid rolling, which is commonly used in lab testing. Accordingly, 75% active material and 20% of acetylene black were weighed and ball milled for 20 minutes, then a polymer binder polytetrafluoroethylene (PTFE) was added as the remaining 5% of the composition and dried overnight in an oven.

Acetylene black is added to improve the electrical conductivity and PTFE is added mainly to hold the mixture together. Once dry, this mixture was mixed together and rolled into thin sheets and a ½ inch diameter punch used to form disc-shaped electrodes. It was verified that none of the electrodes showed visible imperfections such as cracks present on the surface of the electrode and that they were all of uniform thickness (verified gravimetrically). Some electrodes rolled and punched several times till the target weight was achieved. The synthesis condition for all the samples were the same.

4.4 T-cell Assembly:

In order to be tested the electrodes were assembled in a T-shaped casing. The punched out cathode was placed on a solid aluminum cylinder over which a microfiber filter and a sheet of separator material are set and this is inserted into the T-shaped casing with a plastic nut fastened on the end to have it sealed. The filter is used to hold the electrolyte and the separator used was a Cell guard 2400 polymer (porous polypropylene) type separator. This stack was dried in an oven and later moved into an argon chamber (i.e., inert atmosphere).

Lithium foil was used as the anode material which is punched out in a method similar to that used for the cathode. It is then pressed on a short stainless steel cylinder, a porous polypropylene separator is placed on top of it, and it is then inserted into the other half of the T-shaped casing. A longer stainless steel cylinder is attached to the short one by placing a spring in between and is inserted until both the electrodes are tightly in contact with each other at around the center of the T-shaped casing. $LiPF_6$ electrolyte in a 1:1 ratio of ethylene carbonate and dimethyl carbonate (EC/DMC) was added using a pipette until the separators get soaked and a small amount is left over at the top for absorbing over time. An air-tight seal casing is made by fastening plastic screws at all ends of the T-shaped casing and also to ensure that the electrolyte does not leak. The t-cell is kept to rest over a period of 24 hours. While testing, the anode and cathode collectors from the t-cells are connected to the testing machine by using alligator clips.

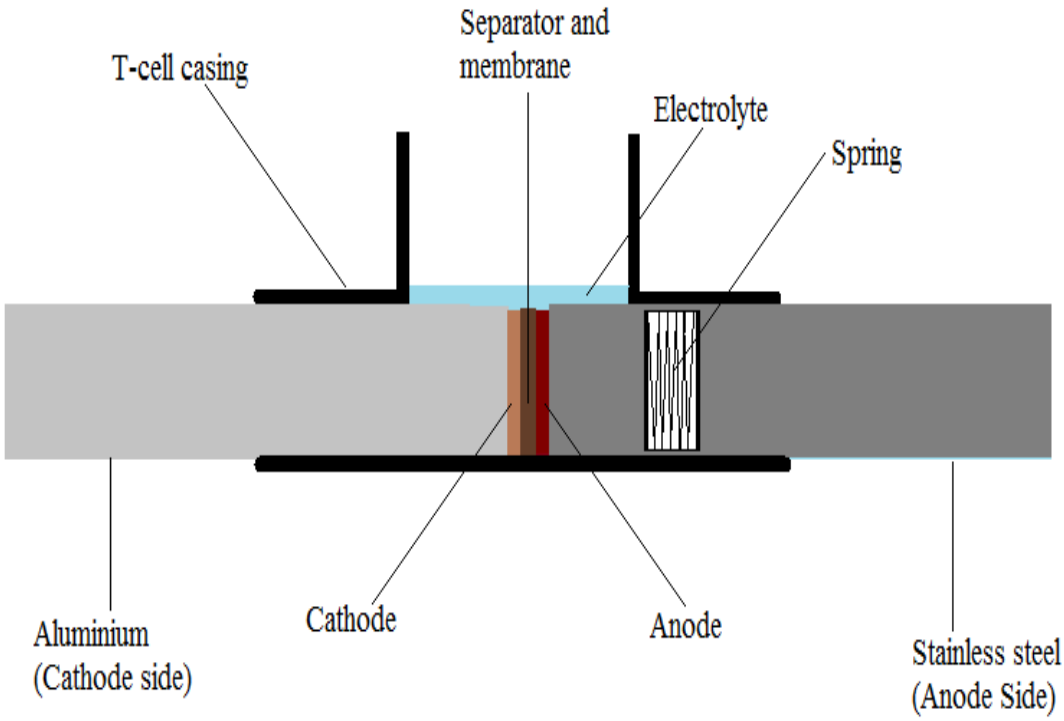

Figure 26: T-Cell configuration.

4.5 Electrochemical testing

All the cells were tested using Arbin BT2000 battery testing system and a MITS Pro Arbin software. These tests were carried out at room temperature and the cells were cycled between 2V and 4.6V at a C-rate of C/15 by applying a constant current of 300μA. All the samples were tested for 5 charge and discharge cycles. The samples which were found to be most promising were tested for 10 charge and discharge cycles.

Chapter 5 Results and Discussion

5.1 (1-x-y)$LiNi_{1/3}Mn_{1/3}Co_{1/3}O_2 \cdot xLi_2MnO_3 \cdot yLiCoO_2$

5.1.1 System Overview

In the whole ternary diagram, 28 specific points were chosen to find promising regions and trends in capacity and cyclability. The ternary diagram is shown in the following figure 27.

The perpendicular lines for each end point indicate the percentage of material present. For example, for $LiCoO_2$ the blue line indicates how much of it is present it decreases form 1 to 0 as the line moves away from $LiCoO_2$ towards the other corners of the diagram.

The lever rule can be applied to determine the compositions of the material at any chosen point. Table 1 shows the theoretical material compositions of all the 28 samples.

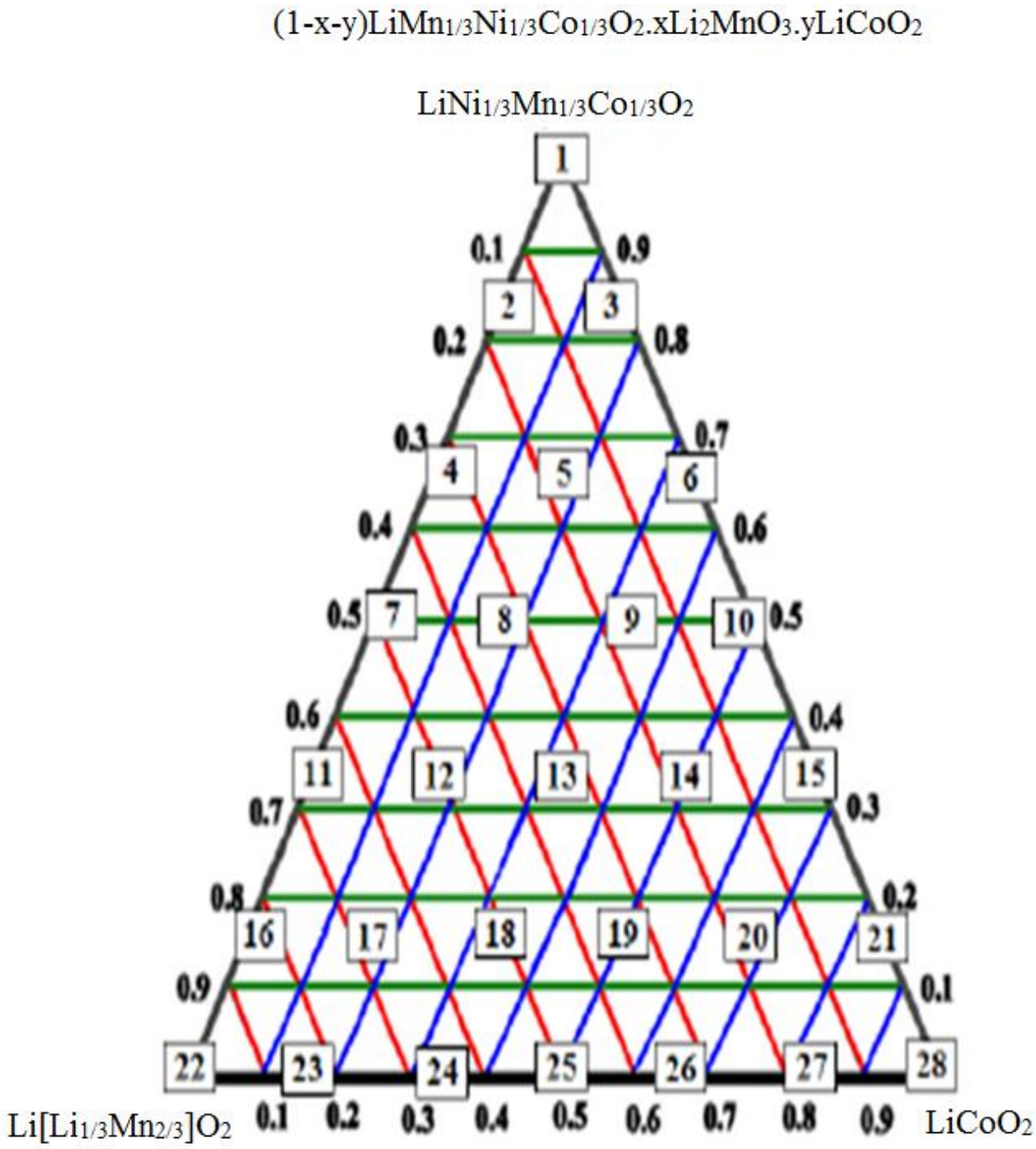

Figure 27: Ternary composition triangle for the system

$(1\text{-}x\text{-}y)LiNi_{1/3}Mn_{1/3}Co_{1/3}O_2 \cdot xLi_2MnO_3 \cdot yLiCoO_2$.

Location	Composition
1	$LiMn_{.333}Ni_{.333}Co_{.333}O_2$
2	$Li_{1.056}Mn_{.389}Ni_{.278}Co_{0.278}O_2$
3	$LiMn_{.278}Ni_{.278}Co_{.444}O_2$
4	$Li_{1.111}Mn_{.444}Ni_{.222}Co_{.222}O_2$
5	$Li_{1.056}Mn_{.333}Ni_{.222}Co_{.389}O_2$
6	$LiMn_{.222}Ni_{.222}Co_{.556}O_2$
7	$Li_{1.167}Mn_{.5}Ni_{.167}Co_{.167}O_2$
8	$Li_{1.111}Mn_{.389}Ni_{.167}Co_{.333}O_2$
9	$Li_{1.056}Mn_{.278}Ni_{.167}Co_{.5}O_2$
10	$LiMn_{.167}Ni_{.167}Co_{.667}O_2$
11	$Li_{1.222}Mn_{.556}Ni_{.111}Co_{.111}O_2$
12	$Li_{1.167}Mn_{.444}Ni_{.111}Co_{.278}O_2$
13	$Li_{1.111}Mn_{.333}Ni_{.111}Co_{.444}O_2$
14	$Li_{1.056}Mn_{.222}Ni_{.111}Co_{.611}O_2$
15	$LiMn_{.111}Ni_{.111}Co_{.778}O_2$
16	$Li_{1.278}Mn_{.611}Ni_{.056}Co_{.056}O_2$
17	$Li_{1.222}Mn_{.5}Ni_{.056}Co_{.222}O_2$
18	$Li_{1.167}Mn_{.389}Ni_{.056}Co_{.389}O_2$
19	$Li_{1.111}Mn_{.278}Ni_{.056}Co_{.556}O_2$
20	$Li_{1.056}Mn_{.167}Ni_{.056}Co_{.722}O_2$
21	$LiMn_{.056}Ni_{.056}Co_{.889}O_2$
22	$Li_{1.333}Mn_{.667}O_2$
23	$Li_{1.278}Mn_{.556}Co_{.167}O_2$
24	$Li_{1.222}Mn_{.444}Co_{.333}O_2$
25	$Li_{1.167}Mn_{.333}Co_{.5}O_2$
26	$Li_{1.111}Mn_{.222}Co_{.667}O_2$
27	$Li_{1.056}Mn_{.111}Co_{.833}O_2$
28	$LiCoO_2$

5.1.2 XRD

X-ray diffraction was conducted on all the 28 samples in the system $(1-x-y)LiNi_{1/3}Mn_{1/3}Co_{1/3}O_2 \cdot xLi_2MnO_3 \cdot yLiCoO_2$. The following figure shows the XRD spectra.

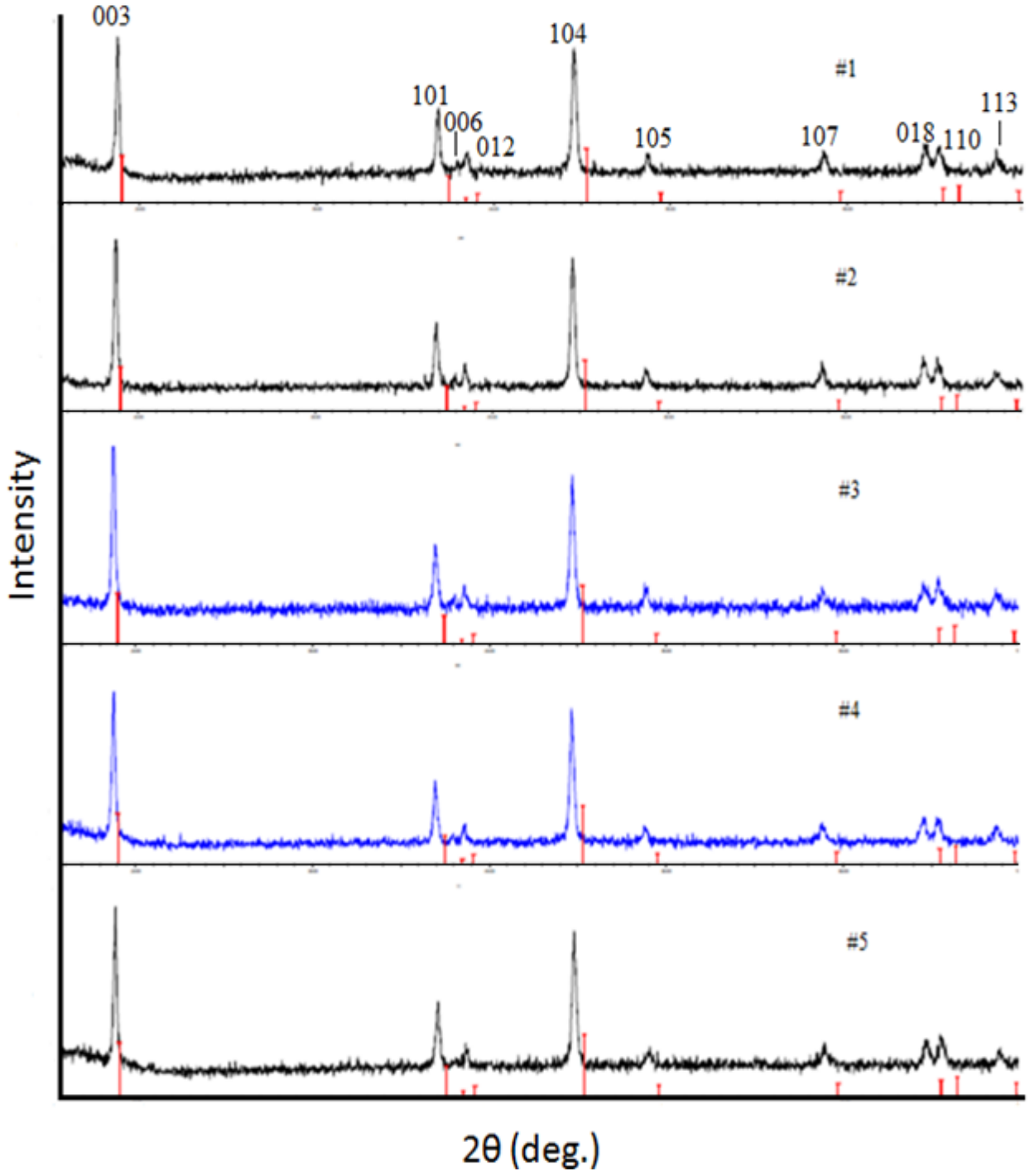

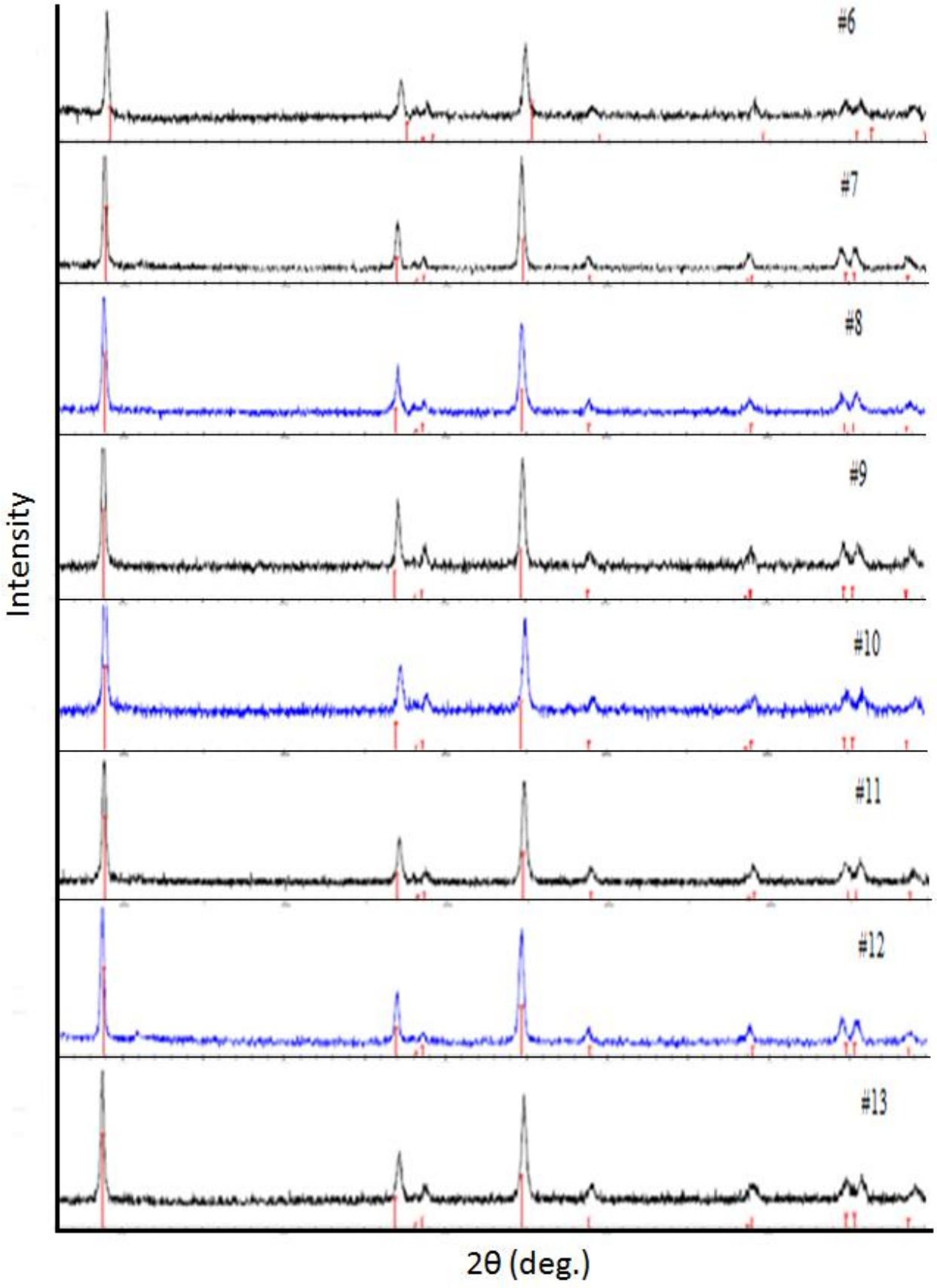
#6
#7
#8
#9
#10
#11
#12
#13
Intensity
2θ (deg.)

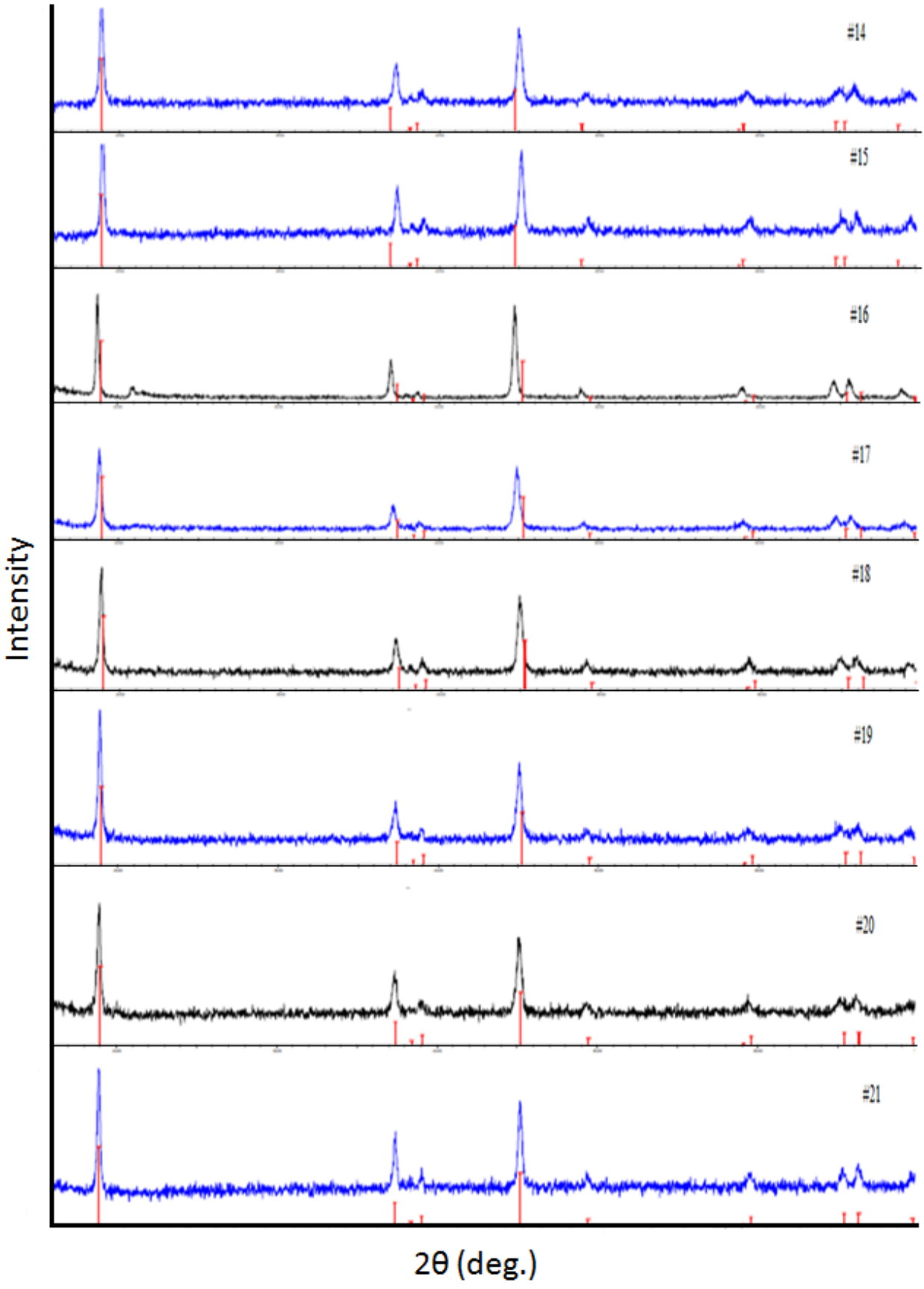
#14
#15
#16
#17
#18
#19
#20
#21
Intensity
2θ (deg.)

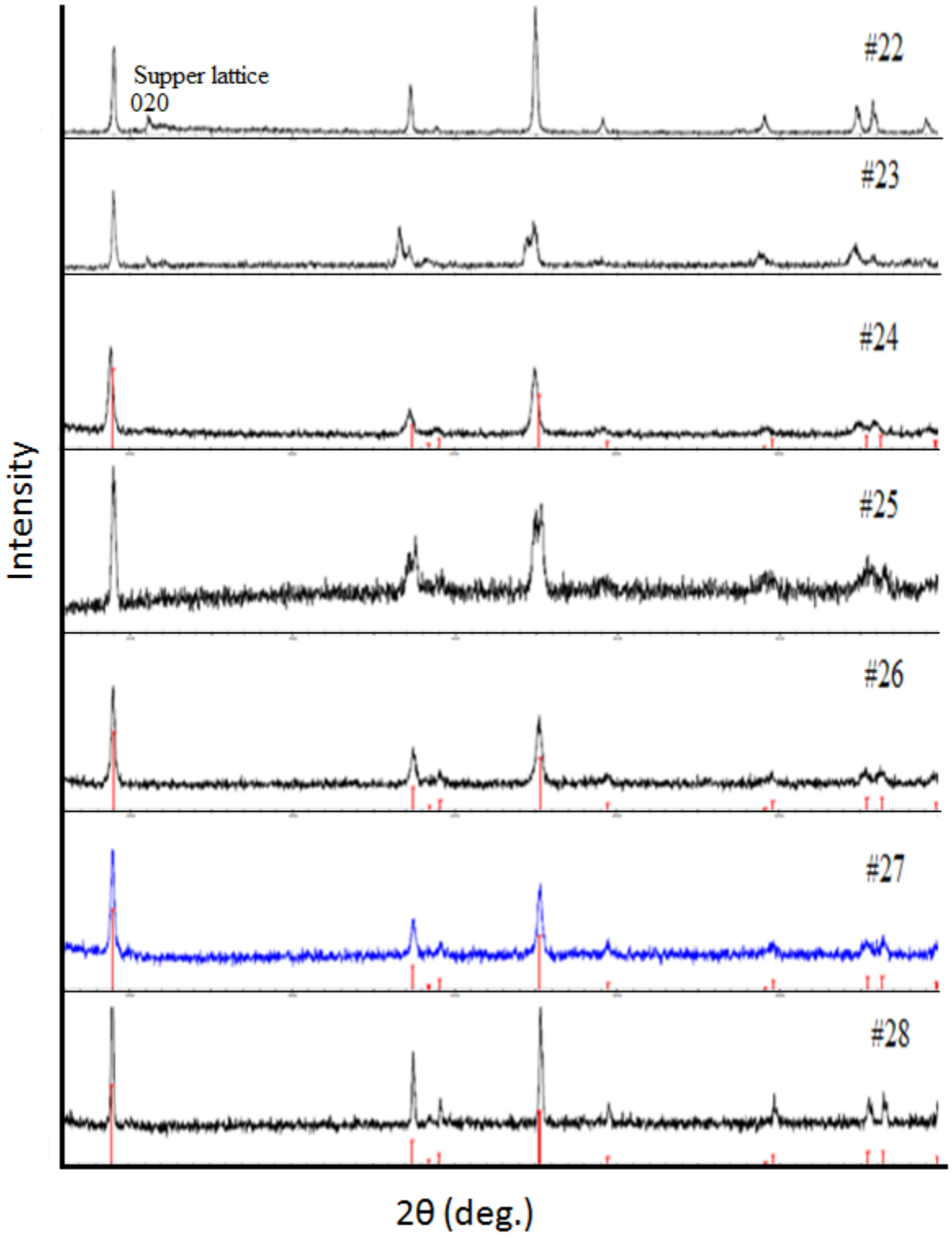

Figure 28: XRD scans for all the 28 samples.

All the prepared material compounds were identified as α-$NaFeO_2$ with a space group of R3m. This was determined by the fact that all of the XRD patterns accorded well with a typical hexagonal pattern and showed a clear split between (108) and (110) peaks. XRD also showed that, in addition to the Bragg reflections, weak reflections corresponding to super lattice peaks were observed in the 2Θ range of 20-25º, intensity of which largely increased with the increasing content of Li_2MnO_3 (large x values). Li_2MnO_3 or $Li[Li_{1/3}Mn_{2/3}]O_2$ is a layered structure consisting of Li only layer, mixed layers of 1/3Li and 2/3Mn, and pure O_2 layers which separate the Li and the transition-metal layers. Since the atomic ratio is Li/Mn = 1:2 in the transition-metal layers, there is a super lattice ordering of Li and Mn which reduces the symmetry from R-3m to C 2/m[49]. Overall, the intensities and the peak location for all the samples were found to be correct and there were no signs of impurities or unknown peaks in any samples.

5.1.3 Battery Testing

All the samples were electrochemically tested by using an Arbin BT2000 battery testing system and MITS Pro Arbin software. Cell testing was carried out at room temperature and all the T cells were cycled between 2-4.6V at a constant C-rate of C/15. Initially all the cells were tested for 5 charge and discharge cycles. Figure 29 shows the charge-discharge curves (capacity v/s voltage plots).

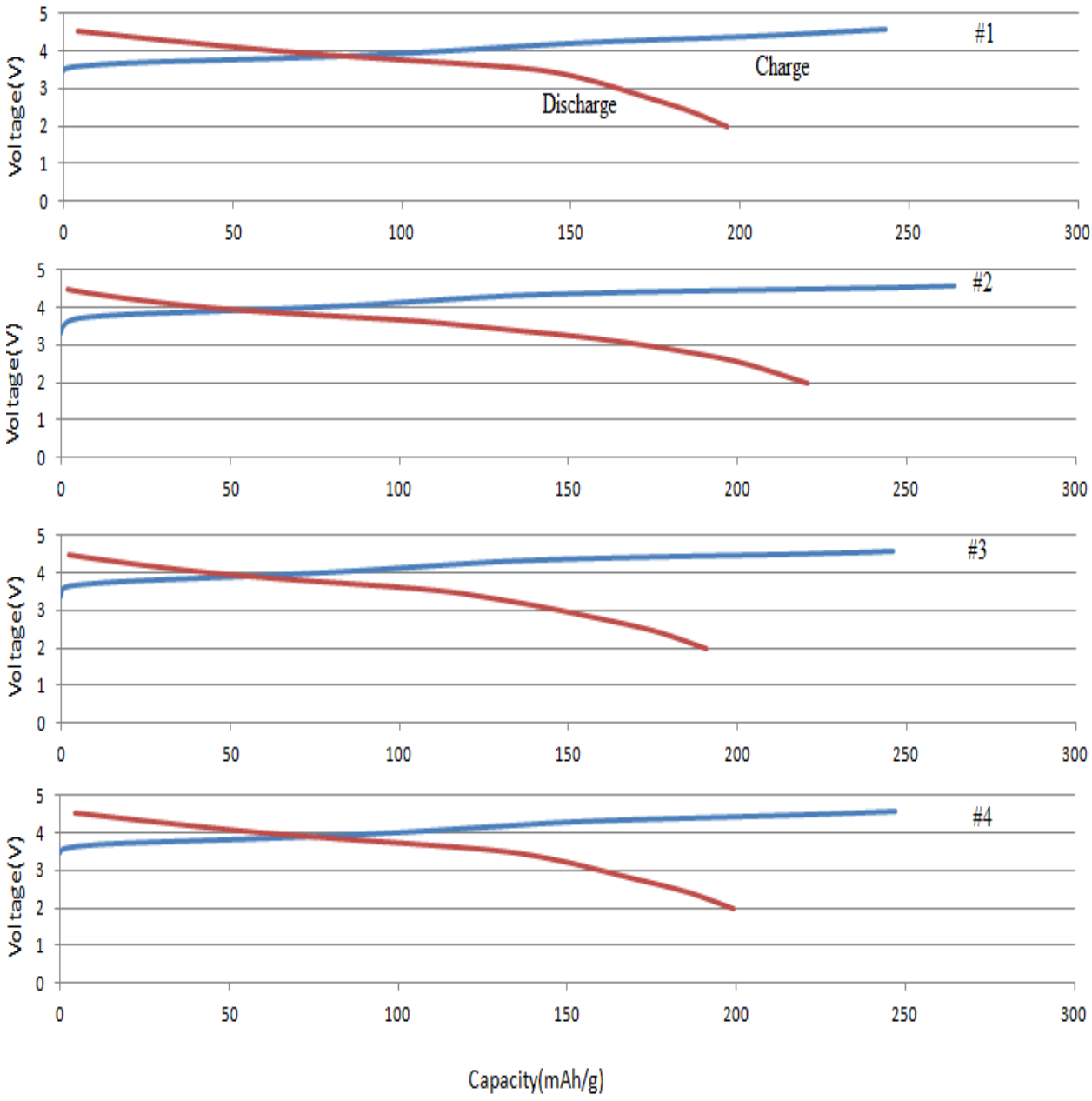
#1
Charge
Discharge
#2
#3
#4
Voltage(V)
Capacity(mAh/g)
0
1
2
3
4
5
0
50
100
150
200
250
300

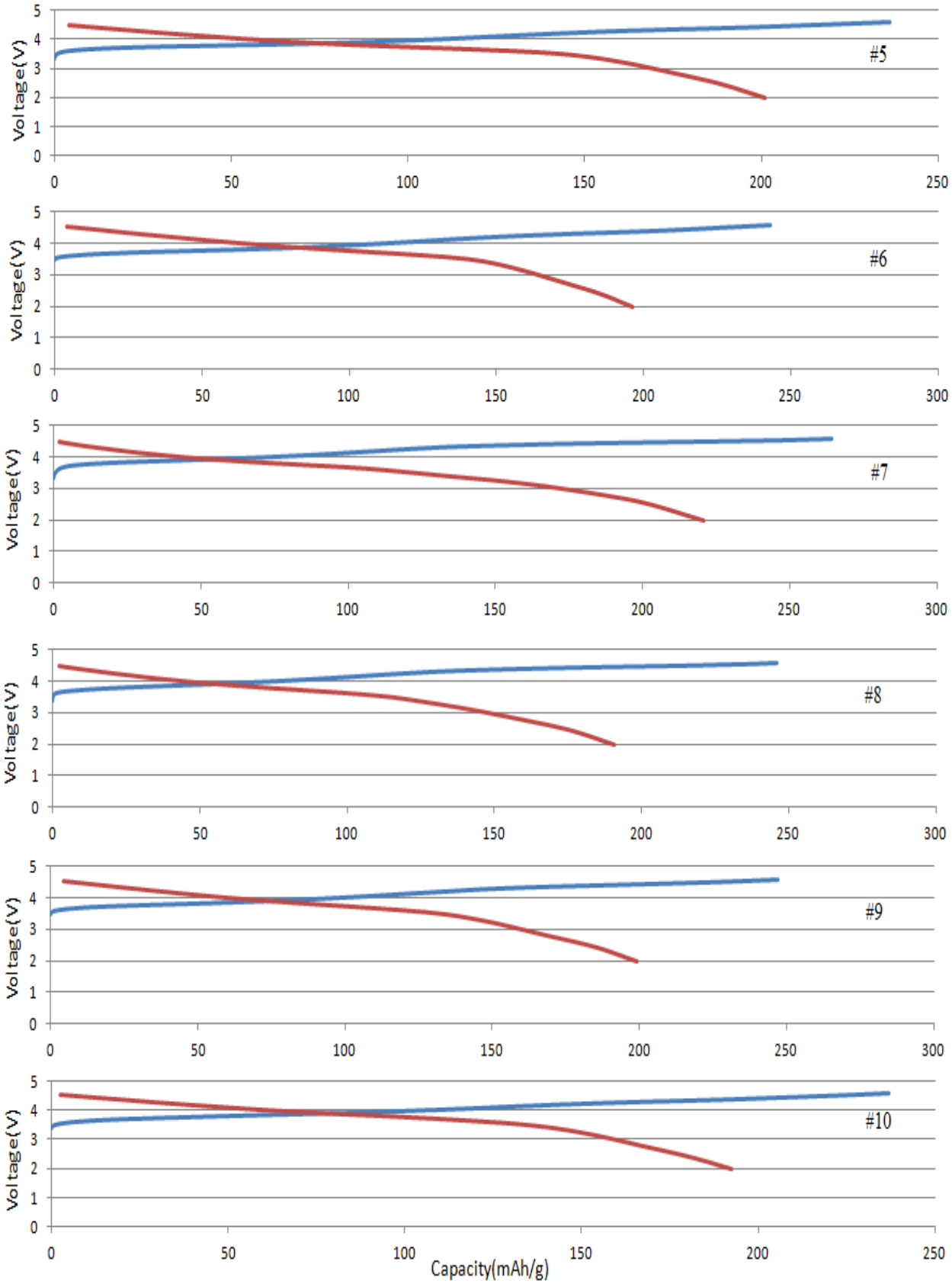
Voltage(V)
#5
#6
#7
#8
#9
#10
Capacity(mAh/g)

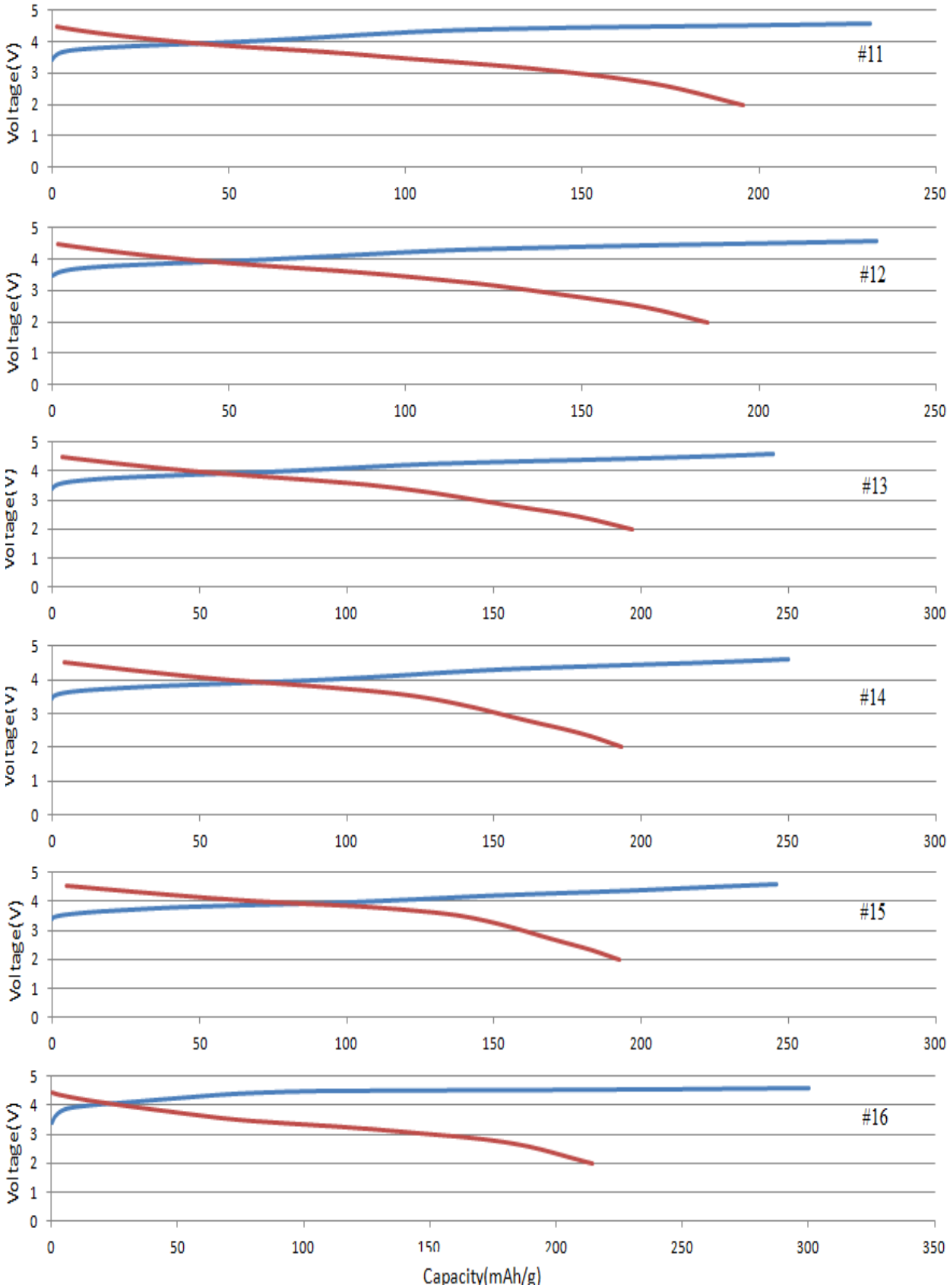
Voltage(V)
#11
#12
#13
#14
#15
#16
Capacity(mAh/g)

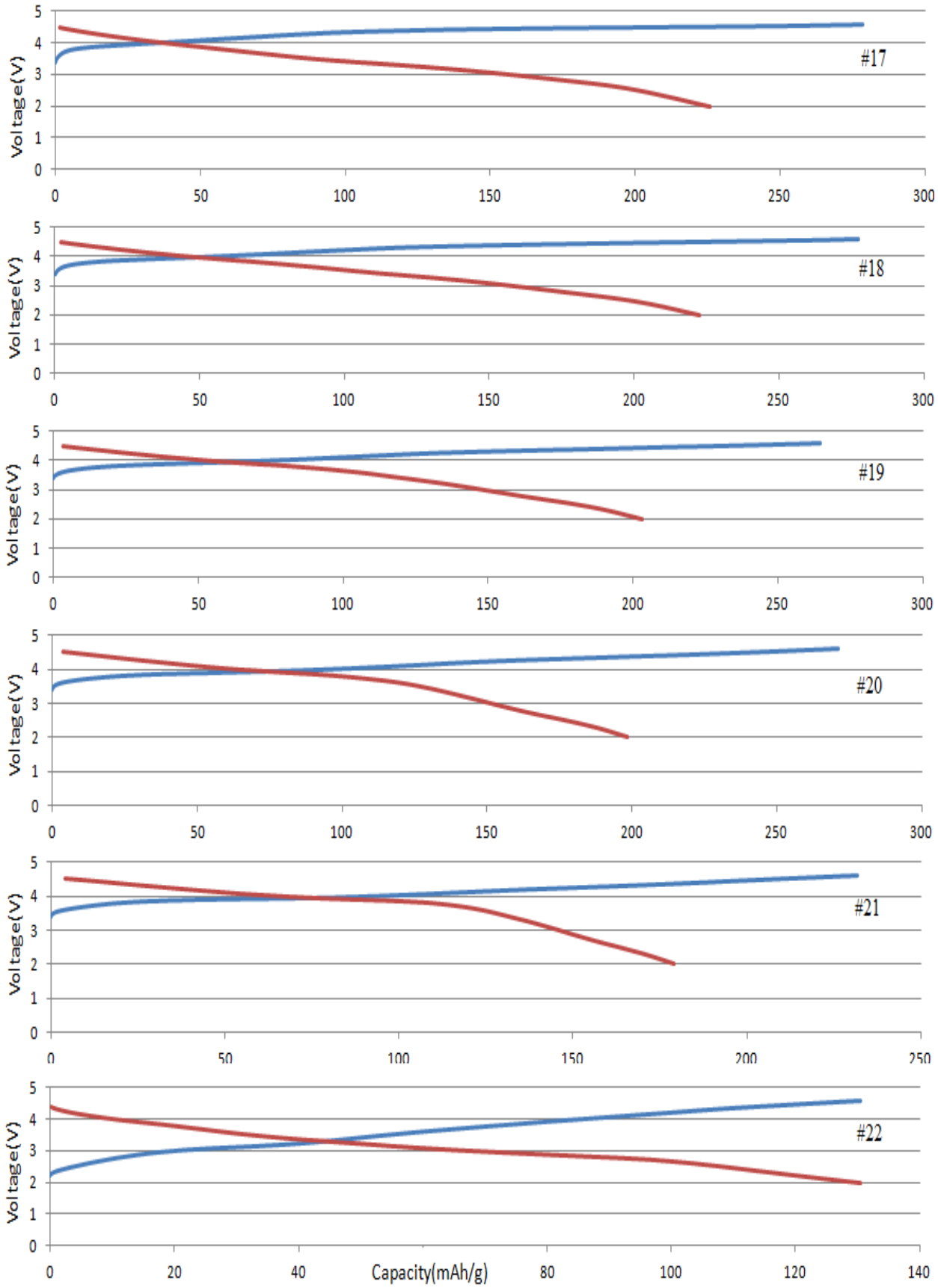
Voltage(V)
#17
#18
#19
#20
#21
#22
Capacity(mAh/g)

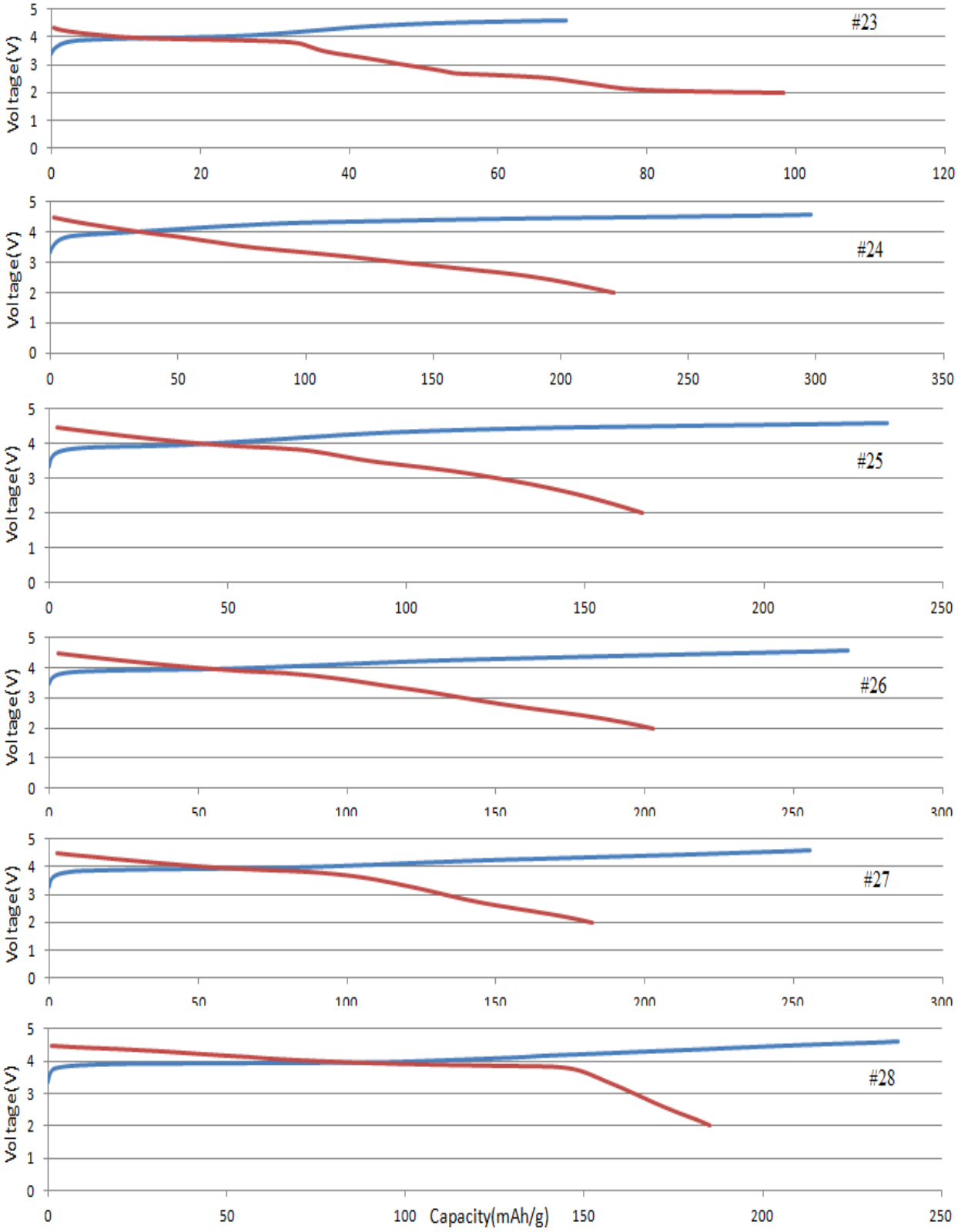

Figure 29: Capacity plots for all the 28 samples.

Cells were tested in the voltage range of 4.6 to 2V based on Thackeray's paper[27]. Li_2MnO_3 is basically inactive and gets electrochemically active by removing Li_2O from the structure, which happens when Li/Li_2MnO_3 cells are charged to a high potential, typically >4.5V. It is also a known fact that on the initial charge to 4.5V, only 20 mAh/g could be extracted from the Li_2MnO_3 electrode, but when charged to 5V a capacity of 383mAh/g (83% of theoretical capacity) was obtained. Complete removal of Li_2O from the Li_2MnO_3 structure leaves Mn_2O and it must also be noted that on discharge it is possible to reinsert only one Li-ion before the rocksalt $LiMnO_2$ stoichiometry is reached. Table 2 shows the results obtained from testing.

From figure 29, we can see that most of the samples in this system showed fairly consistent charge/discharge curves throughout the composition range with the discharge capacities varying between the range of 122mAh/g to 230mAh/g. Discharge curves are mainly expected to show an S-shaped profile and should become linear as the composition moves down the diagram.

Table 2 summarizes the initial charge /discharge capacities with the percentage retention for all the samples in the system $(1-x-y)LiNi_{1/3}Mn_{1/3}Co_{1/3}O_2 \cdot xLi_2MnO_3 \cdot yLiCoO_2$. Out of the 28 samples, 12 samples showed discharge capacities of more than 200mAh/g in which Sample #17 showed the highest capacity and 100% retention in the 4.6-2V range. It is worthy to note that samples having large Mn content showed good results in comparison to Co and Ni based materials, therefore giving the possibility of cost advantages.

No.	SAMPLE COMPOSITION	Charge capacity (mAh/g)	Discharge capacity (mAh/g)	Retention (%)
1	$LiMn_{.333}Ni_{.333}Co_{.333}O_2$	243.80	202.70	83
2	$Li_{1.056}Mn_{.389}Ni_{.278}Co_{0.278}O_2$	246.50	208.37	91
3	$LiMn_{.278}Ni_{.278}Co_{.444}O_2$	225.30	186.58	85
4	$Li_{1.111}Mn_{.444}Ni_{.222}Co_{.222}O_2$	248.30	205.43	96
5	$Li_{1.056}Mn_{.333}Ni_{.222}Co_{.389}O_2$	236.33	201.16	89
6	$LiMn_{.222}Ni_{.222}Co_{.556}O_2$	243.13	196.41	79
7	$Li_{1.167}Mn_{.5}Ni_{.167}Co_{.167}O_2$	264.40	226.00	100
8	$Li_{1.111}Mn_{.389}Ni_{.167}Co_{.333}O_2$	246.10	190.70	95
9	$Li_{1.056}Mn_{.278}Ni_{.167}Co_{.5}O_2$	246.95	199.27	92
10	$LiMn_{.167}Ni_{.167}Co_{.667}O_2$	238.17	192.41	82
11	$Li_{1.222}Mn_{.556}Ni_{.111}Co_{.111}O_2$	231.42	206.00	105
12	$Li_{1.167}Mn_{.444}Ni_{.111}Co_{.278}O_2$	233.28	189.71	101
13	$Li_{1.111}Mn_{.333}Ni_{.111}Co_{.444}O_2$	245.00	197.06	94
14	$Li_{1.056}Mn_{.222}Ni_{.111}Co_{.611}O_2$	250.60	193.25	90
15	$LiMn_{.111}Ni_{.111}Co_{.778}O_2$	246.12	192.53	79
16	$Li_{1.278}Mn_{.611}Ni_{.056}Co_{.056}O_2$	300.04	219.00	100
17	$Li_{1.222}Mn_{.5}Ni_{.056}Co_{.222}O_2$	278.45	230.00	100
18	$Li_{1.167}Mn_{.389}Ni_{.056}Co_{.389}O_2$	277.63	227.00	95
19	$Li_{1.111}Mn_{.278}Ni_{.056}Co_{.556}O_2$	264.72	203.10	91
20	$Li_{1.056}Mn_{.167}Ni_{.056}Co_{.722}O_2$	271.10	198.43	85
21	$LiMn_{.056}Ni_{.056}Co_{.889}O_2$	231.86	179.01	74
22	$Li_{1.333}Mn_{.667}O_2$	130.46	130.48	141
23	$Li_{1.278}Mn_{.556}Co_{.167}O_2$	120.78	121.71	109
24	$Li_{1.222}Mn_{.444}Co_{.333}O_2$	298.21	225.15	85
25	$Li_{1.167}Mn_{.333}Co_{.5}O_2$	236.75	168.00	95
26	$Li_{1.111}Mn_{.222}Co_{.667}O_2$	268.36	202.70	90
27	$Li_{1.056}Mn_{.111}Co_{.833}O_2$	255.50	182.40	86
28	$LiCoO_2$	238.04	185.25	80

5.2 Statistical Analysis

5.2.1 Optimization

In this model X1, X2 and X3 are taken as the point of the ternary diagram.

Where,

$X1 = Li_2MnO_3$

$X2 = LiCoO_2$

$X3 = LiNi_{1/3}Mn_{1/3}Co_{1/3}O_2$

While the responses to these locations are considered as Y1 and Y2.

Where,

Y1 = Capacity (mAh/g)

Y2 = Cyclability

The following table 3 shows an interpretation of all the input variables for the regression analysis.

RUN	BLEND	X1	X2	X3	Y1	Y2
1	Pure	0	0	1	202.7	83
2	Binary	0.167	0	0.833	208.37	91
3	Binary	0	0.167	0.833	186.58	85
4	Binary	0.333	0	0.667	205.43	96
5	All components	0.167	0.167	0.667	201.16	89
6	Binary	0	0.333	0.667	196.41	79
7	Binary	0.5	0	0.5	226	100
8	All components	0.333	0.167	0.5	190.7	95
9	All components	0.167	0.333	0.5	199.27	92
10	Binary	0	0.5	0.5	192.41	82
11	Binary	0.667	0	0.333	206	105
12	All components	0.5	0.167	0.333	189.71	101
13	All components	0.333	0.333	0.333	197.06	94
14	All components	0.167	0.5	0.333	193.25	90
15	Binary	0	0.667	0.333	192.53	79
16	Binary	0.833	0	0.167	219	100
17	All components	0.667	0.167	0.167	230	100
18	All components	0.5	0.333	0.167	227	95
19	All components	0.333	0.5	0.167	203.1	91
20	All components	0.167	0.667	0.167	198.43	85
21	Binary	0	0.833	0.167	179.01	74
22	Pure	1	0	0	130.48	141
23	Binary	0.833	0.167	0	121.71	109
24	Binary	0.667	0.333	0	225.15	85
25	Binary	0.5	0.5	0	168	95
26	Binary	0.333	0.667	0	202.7	90
27	Binary	0.167	0.833	0	182.4	86
28	Pure	0	1	0	185.25	80

The following figure shows the results from the regression analysis and the variation in terms of capacity on the composition triangle.

Effect	Estimate	Std Error	t Ratio	P Value
X1	148.35	15.786	9.3971	<.0001
X2	181.83	15.787	11.518	<.0001
X3	190.15	15.789	12.043	<.0001
X1*X2	111.72	64.906	1.7213	0.0992
X1*X3	195.54	64.906	3.0127	0.0064
X2*X3	2.972	64.908	0.045788	0.9639

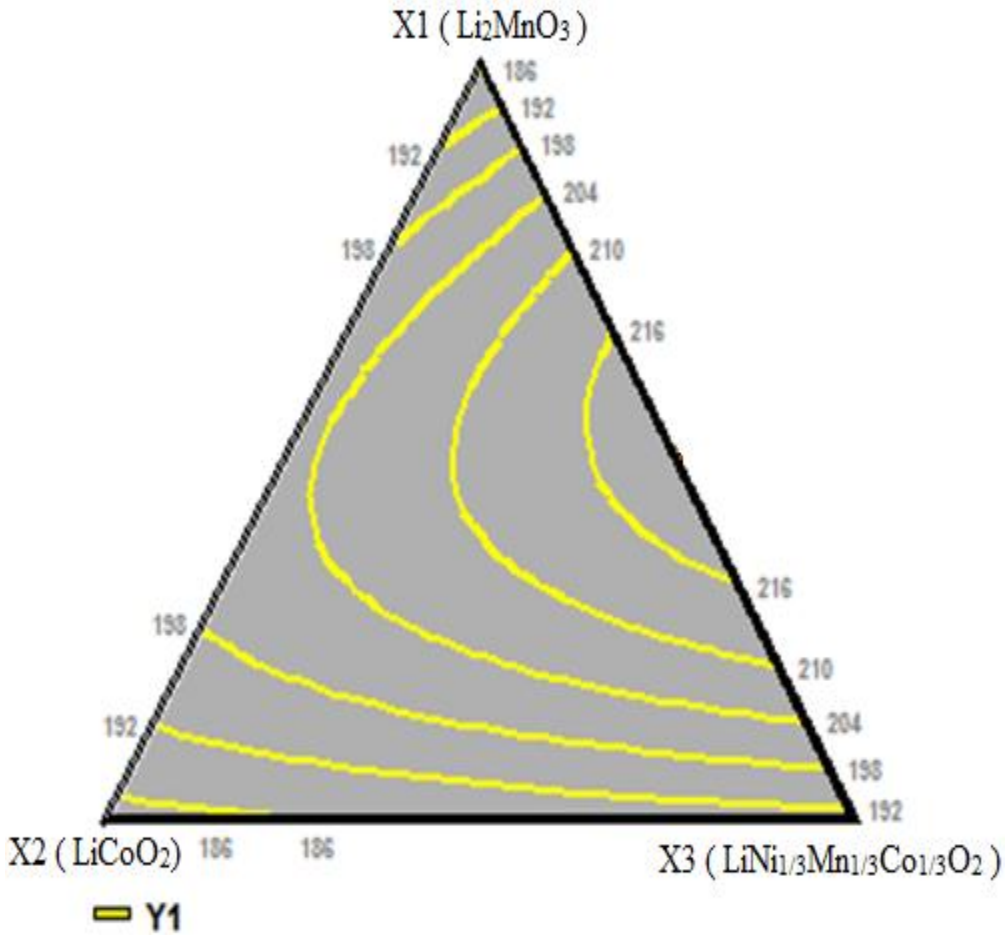

Figure 30: Regression analysis in terms of capacity.

The following figure shows the results from the regression analysis and the variation in terms of cyclability on the composition triangle.

Effect	Estimate	Std Error	t Ratio	P Value
X1	123.33	5.0369	24.486	<.0001
X2	79.927	5.037	15.868	<.0001
X3	85.299	5.0378	16.932	<.0001
X1*X2	-36.944	20.709	-1.7839	0.0882
X1*X3	-16.371	20.709	-0.79052	0.4377
X2*X3	1.2274	20.71	0.059267	0.9533

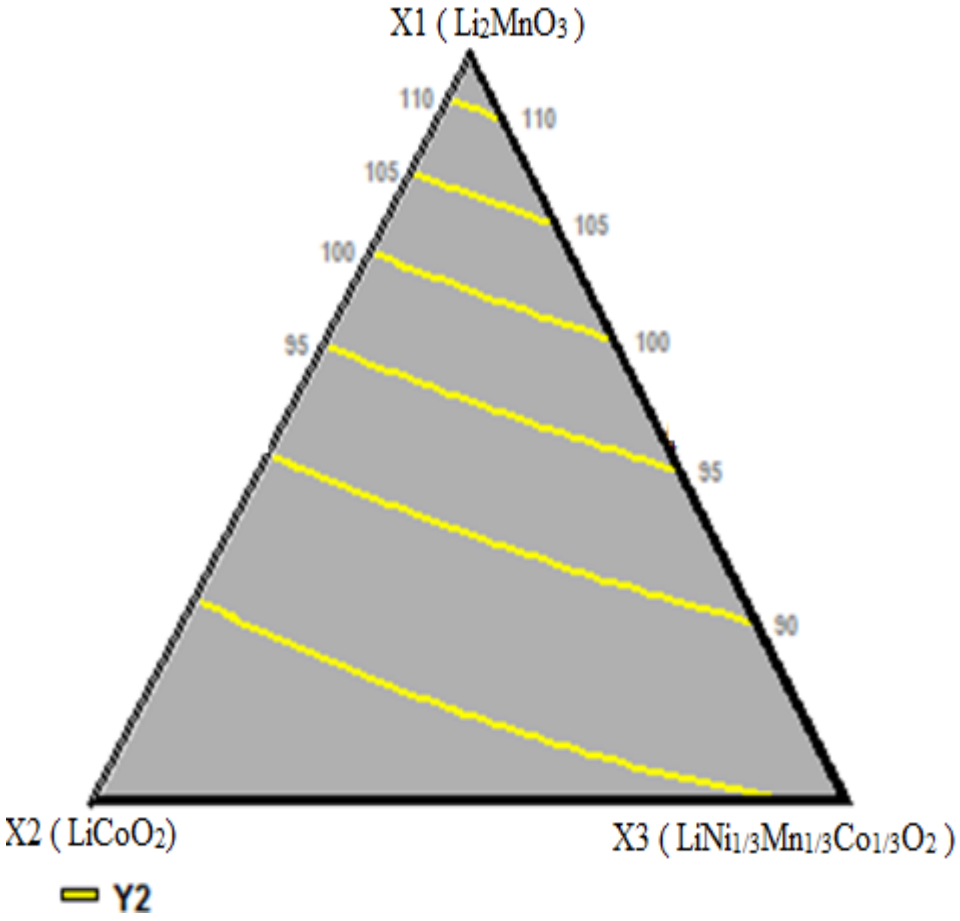

Figure 31: Regression analysis in terms of cyclability.

The statistical analysis report showed that, for capacity the end points X1, X2, X3 and the two-way interaction X1*X3 were found to be having a significant effect on the overall system. For cyclability trends, only the end points X1, X2, X3 have been found to be statistically significant.

As we can see from figures, the model shows various general capacity and cyclability trends with defined areas of maximum capacity and good cyclability. If we take capacity into consideration, maximum capacities were found in regions closer to and between X1 and X3 while in terms of cyclability it is clearly visible that regions close to X1 are found to be the ones having good cyclability.

5.2.2 Repetitions

In order to have a region in the system which has characteristics of both maximum capacity as well as good cyclability these two models were overlapped and an area was selected which has optimum levels of capacity and cyclability.

Table 4: Material composition of the selected samples

Location	**Composition**
7	$Li_{1.167}Mn_{.5}Ni_{.167}Co_{.167}O_2$
16	$Li_{1.278}Mn_{.611}Ni_{.056}Co_{.056}O_2$
17	$Li_{1.222}Mn_{.5}Ni_{.056}Co_{.222}O_2$
18	$Li_{1.167}Mn_{.389}Ni_{.056}Co_{.389}O_2$

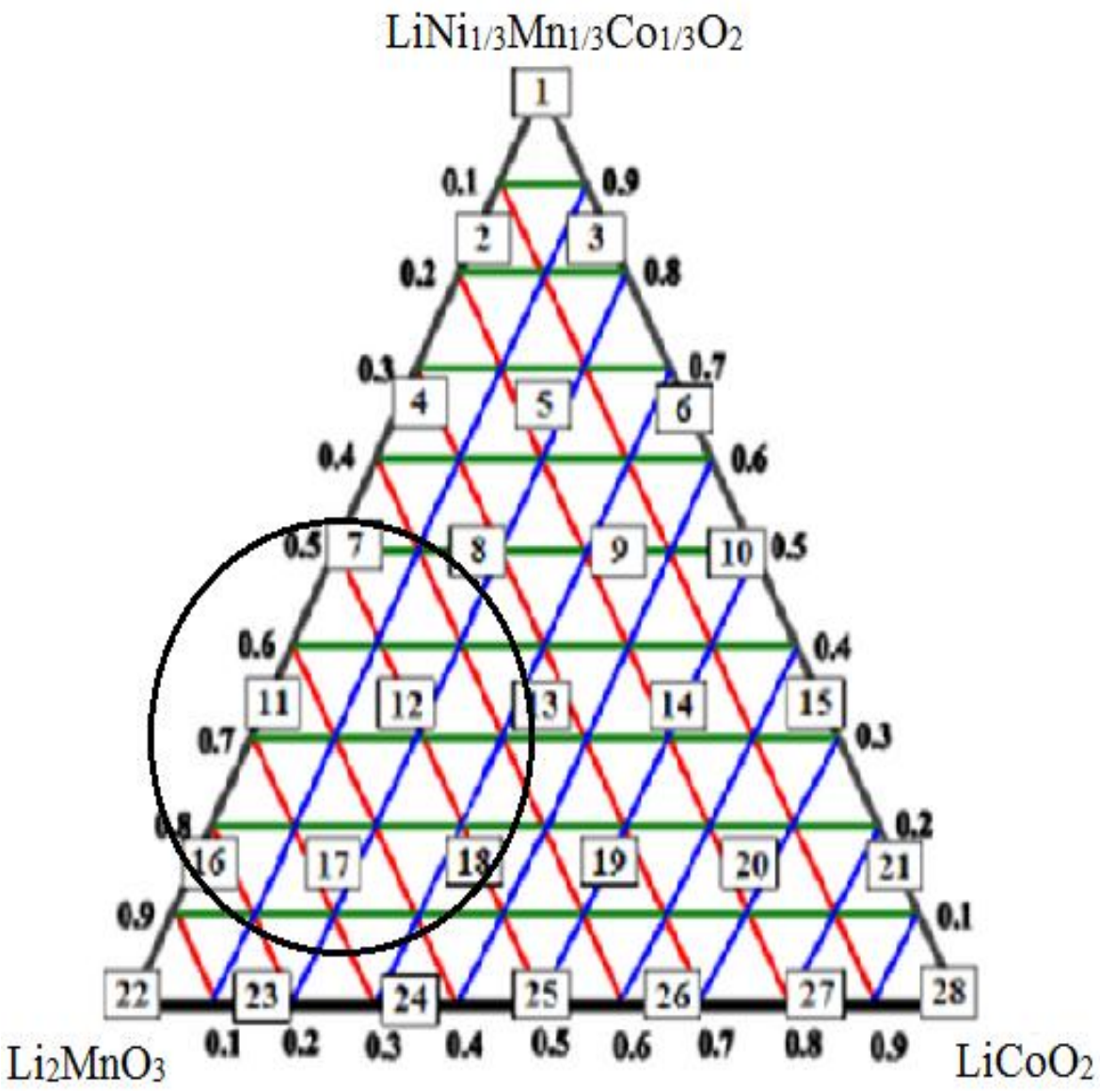

Figure 32: Selected region for testing.

From the circled region 4 samples were selected, taking into consideration the previous initial testing results. These samples were again processed, characterized and tested under the same initial conditions. These repetitions were carried out to justify the results obtained during the preliminary initial testing. Table 4 represents the material compositions of the selected samples for repetitions.

5.2.3 ICP

ICP analysis was conducted on the 4 samples that were taken into consideration from the statistical analysis. The material that was left over after testing these samples was used for the analysis. Following table summarizes the results from the ICP analysis.

Table 5: Results from the ICP analysis

Sample ID	Prep wt (grams)	Prep Vol (mL)	Prep DF	Co mg/kg	Li mg/kg	Mn mg/kg	Ni Mg/kg
MDL				0.005	0.01	0.002	0.002
7	0.21	20.6982	98.5628	1,11,321.657	88,384.579	2,88,192.61	1,07,895.73
16	0.198	20.5462	103.768	39,760.885	1,00,111.010	3,50,462.17	36,572.870
17	0.205	20.7826	101.379	1,49,293.557	97,247.639	2,92,670.55	36,619.695
18	0.188	20.6353	109.762	2,57,534.814	91,751.749	2,33,052.30	36,565.270

The results from the above table represent the amount of each element present in the material composition it is given in terms of mg/kg for example 88,384.579mg/kg lithium means 88,384.579 grams of lithium present in kg sample. This value must be converted to molar fraction, therefore it must be first converted to g/kg and then must be divided by the molecular weight of that element and then needs to be fractioned out by the total value. Following table 6 shows the difference between the original molecular compositions to the calculated samples.

Table 6: Results from ICP calculations

Sample	Calculated (ICP) composition	Original composition
7	$Li_{1.171}Mn_{0.482}Ni_{0.169}Co_{0.173}O_2$	$Li_{1.167}Mn_{.5}Ni_{.167}Co_{.167}O_2$
16	$Li_{1.30}Mn_{0.58}Ni_{0.056}Co_{0.061}O_2$	$Li_{1.278}Mn_{.611}Ni_{.056}Co_{.056}O_2$
17	$Li_{1.240}Mn_{0.474}Ni_{0.056}Co_{0.225}O_2$	$Li_{1.222}Mn_{.5}Ni_{.056}Co_{.222}O_2$
18	$Li_{1.177}Mn_{0.378}Ni_{0.056}Co_{0.389}O_2$	$Li_{1.167}Mn_{.389}Ni_{.056}Co_{.389}O_2$

5.2.4 XRD

X-ray diffraction technique was conducted on the 4 samples that were chosen from the above discussion in the system. The following figure shows the scans of XRD.

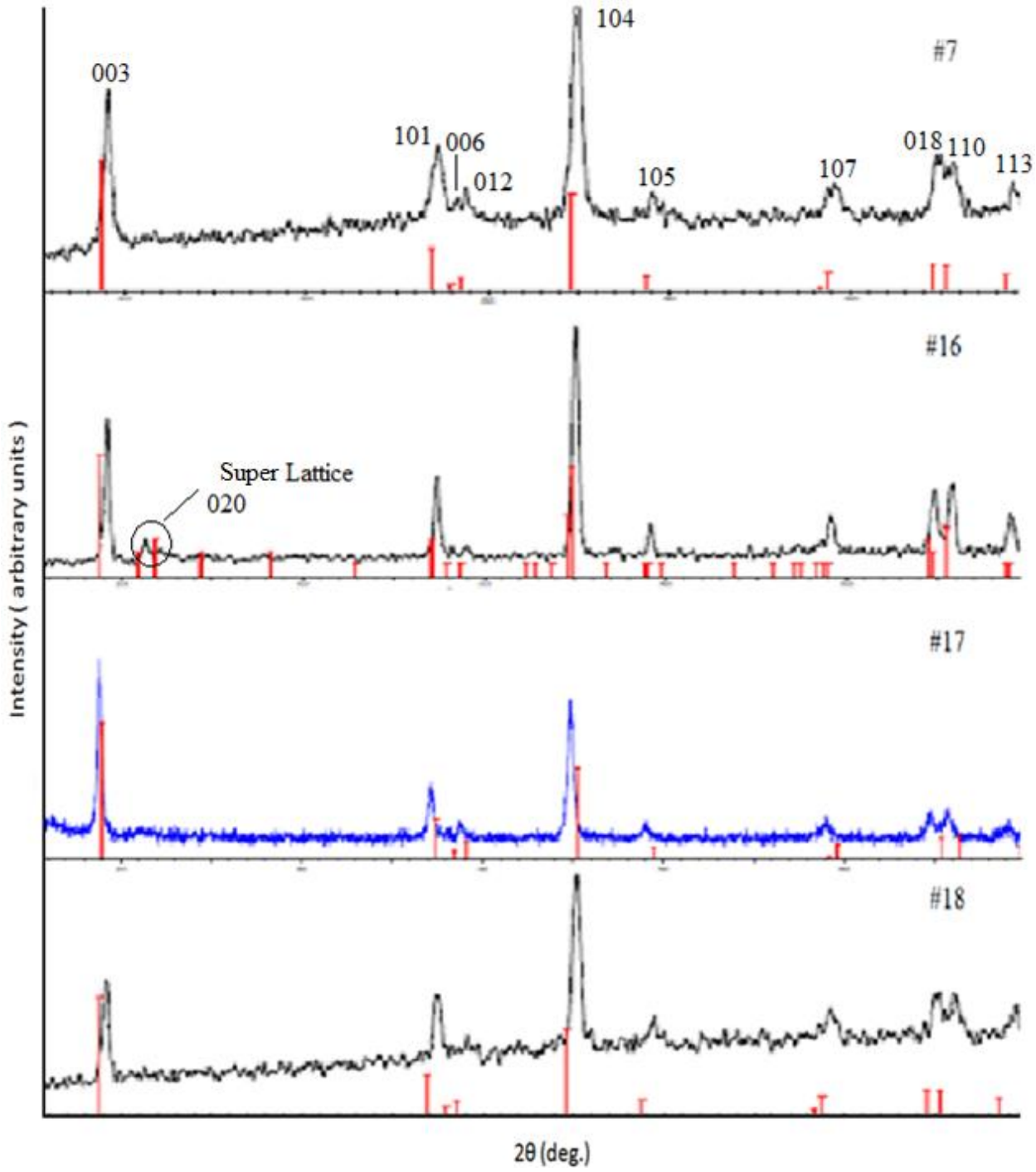

Figure 33: XRD plots for the selected samples.

The XRD results showed that all the samples established a α-$NaFeO_2$ structure with R-3m space group. The peak locations and intensities for all the samples were found to be correct.

Additionally, weak reflections corresponding to super lattice peaks were observed for samples #16 and #17 in the range of 20 - 25 º indicating the presence of Li_2MnO_3[44].

5.2.5 XPS

X- Ray photoelectron spectroscopy (XPS) experiments were conducted on the samples to determine the valence states of transition metals such as Ni, Mn and Co. Figure 34 shows the XPS scans for each element in sample #17..

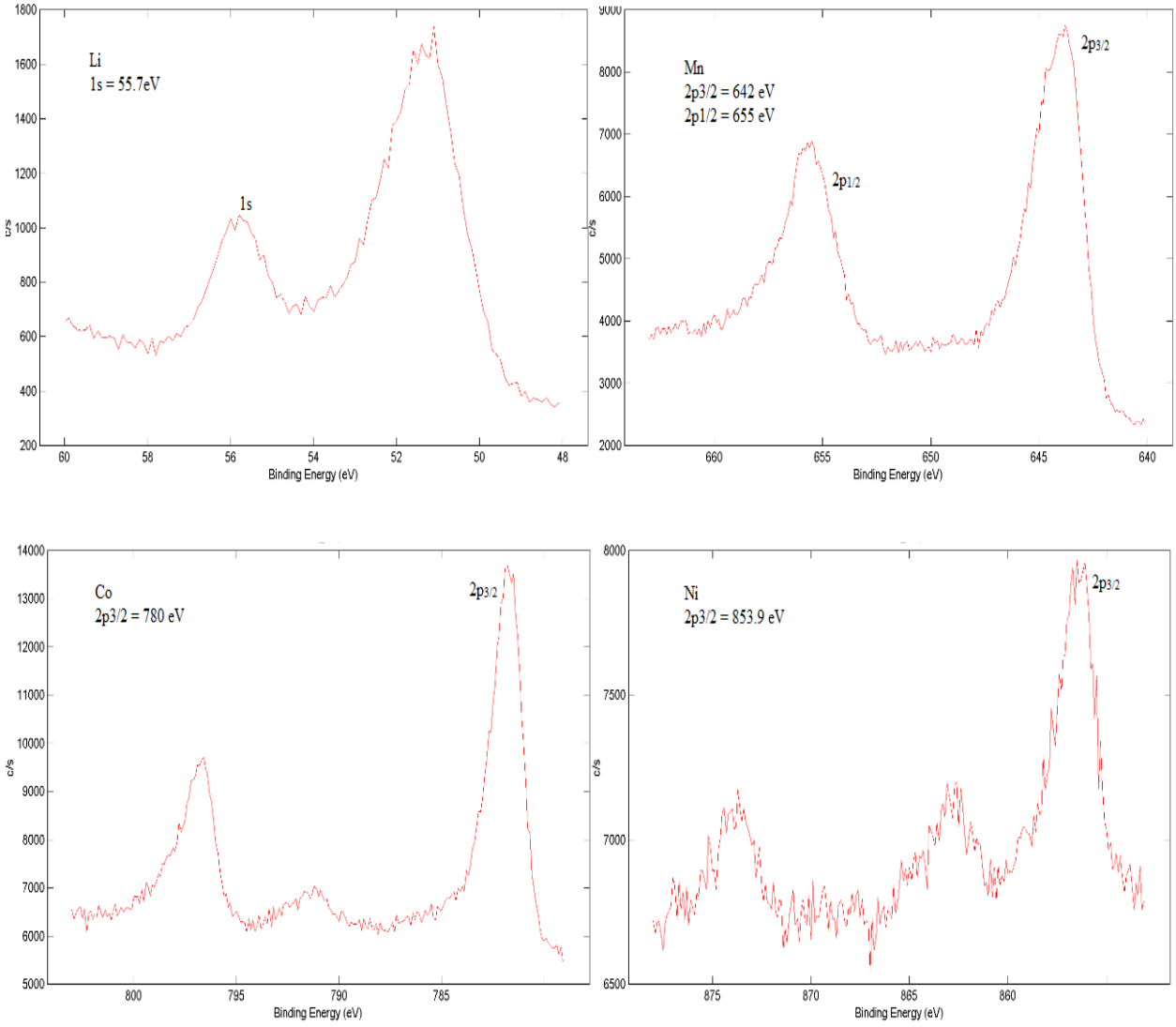

Figure 34: Individual XPS plots for sample #17.

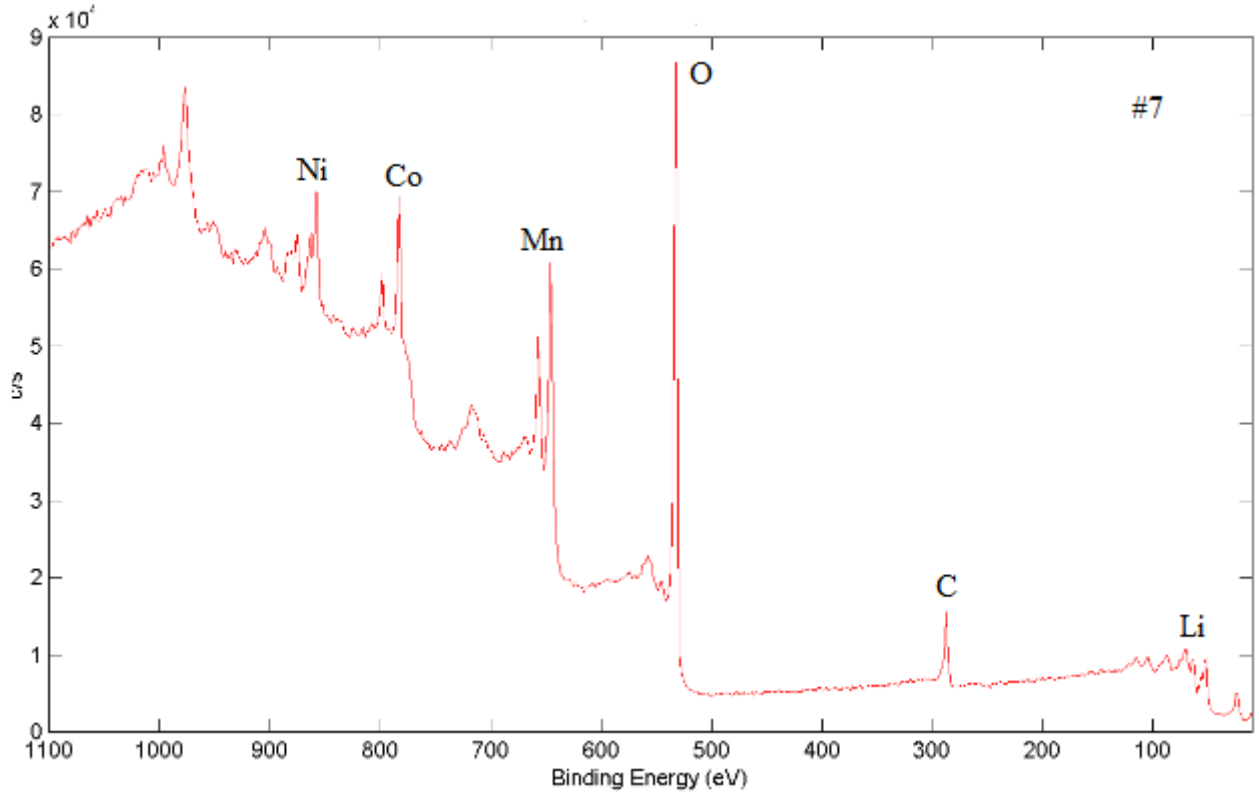
x 10^4
O
#7
Ni
Co
Mn
C
Li
c/s
Binding Energy (eV)

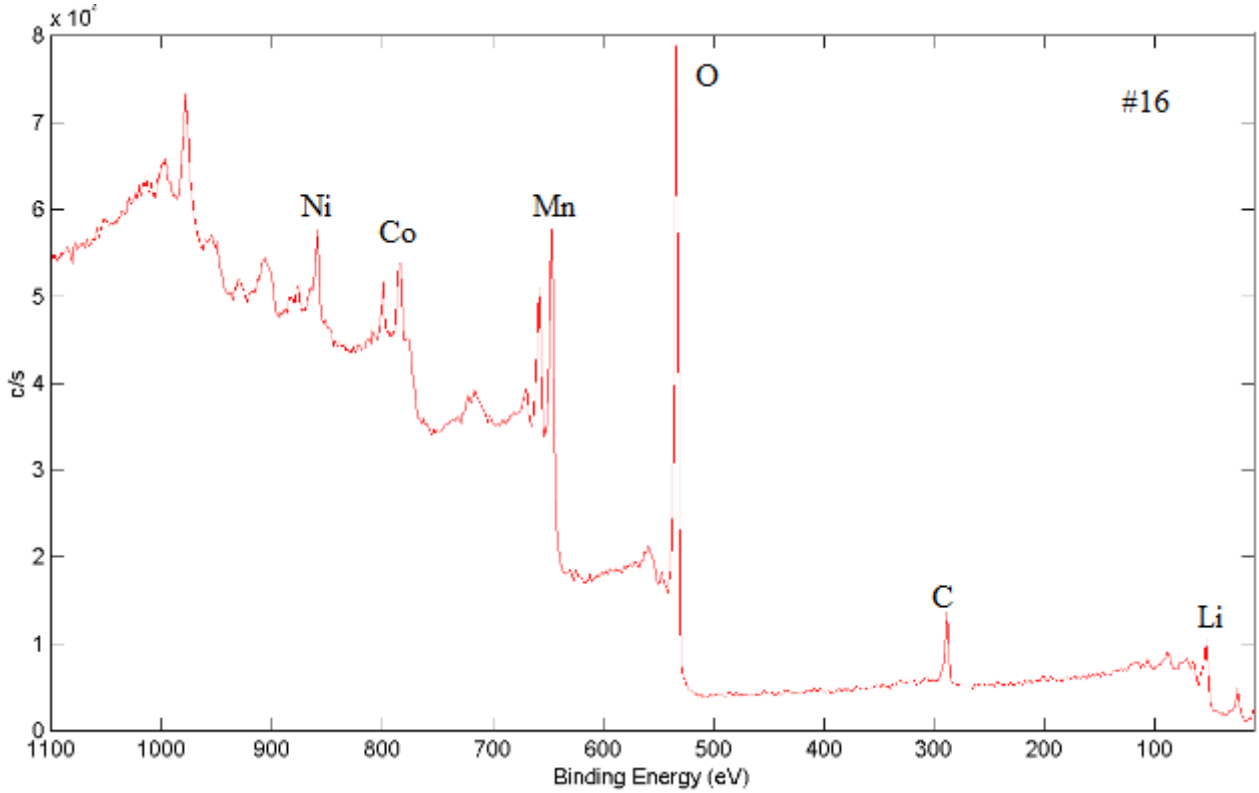
x 10^4
O
#16
Ni
Co
Mn
C
Li
c/s
Binding Energy (eV)

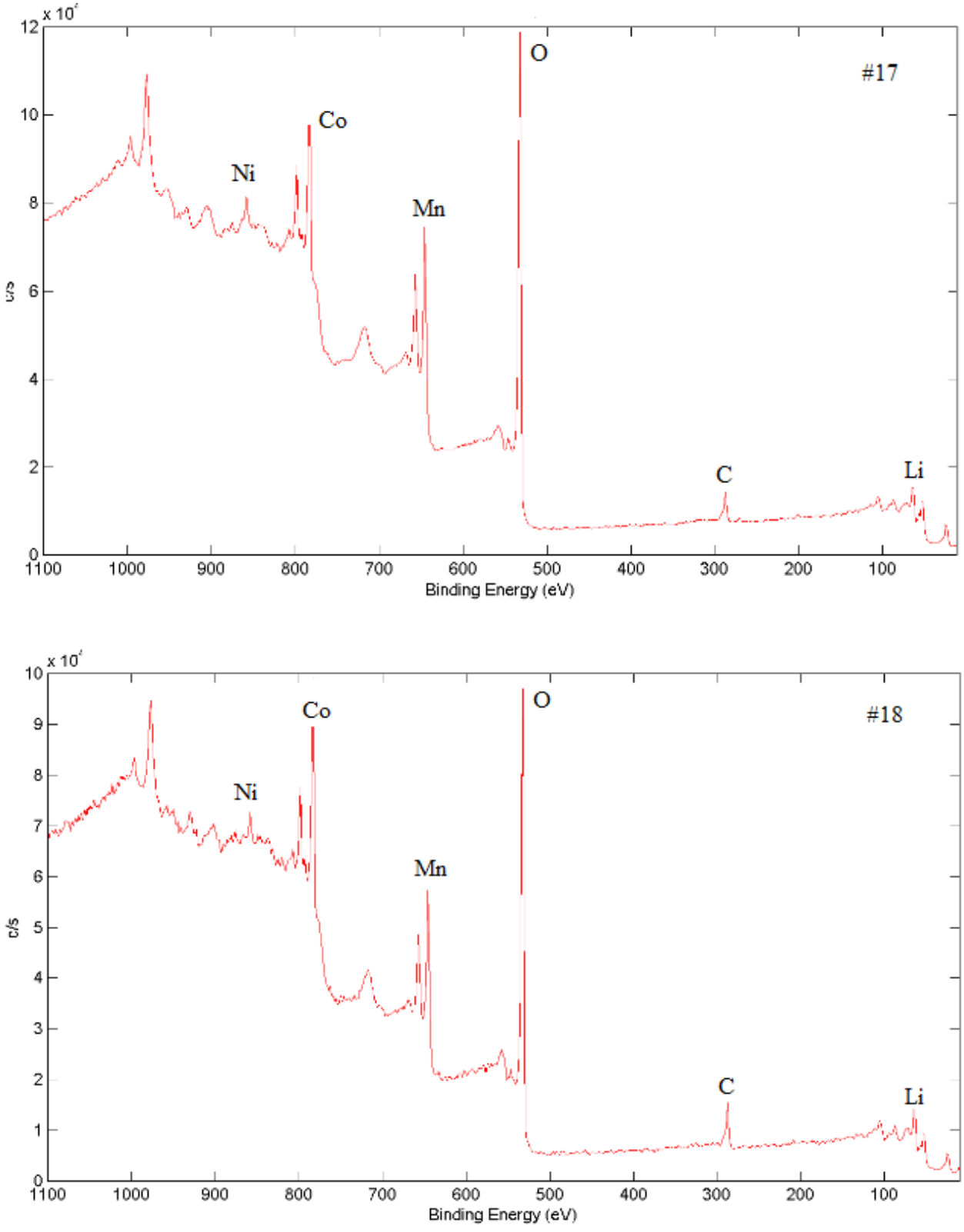

Figure 35: XPS plots for all the selected samples.

A detailed XPS analysis was performed on sample #17. For Ni the binding energy of the main peak was found to be at 854 eV corresponding to Ni 2p3/2 core level, which is indicative of Ni+2 (similar to Ni in NiO). XPS results showed the valence state of Ni synthesized in the sample #17 is +2.

Mn 2p core levels in which the 3/2 and 1/2 orbit doublet components are at 642 and 655eV, respectively. The main peak was found at 642eV which strongly suggests Mn to be present with an oxidation state of +4. While, Co 2p core levels spectra showed peaks corresponding to Cp 2p3/2 (780eV) indicative of Co^{+3} as in $LiCoO_2$ and low spin in nature.

Therefore, the predominant valence states of the transition metals are determined to be Ni^{+2}, Co^{+3} and Mn^{+4}. This result implies that the primary redox couple involved in the chemical reaction process will be Ni^{+2}/Ni^{+4}, Co^{+3}/Co^{+4} and since Mn is already present in its maximum oxidation state of +4 it does not oxidize in this voltage range. Figure shows the XPS spectra of all the remaining compositions showing the electronic transitions of different elements present.

5.2.6 Battery testing

Following figures show the results from the electrochemical testing i.e. capacity plots. These were tested under the same conditions as the initial testing.

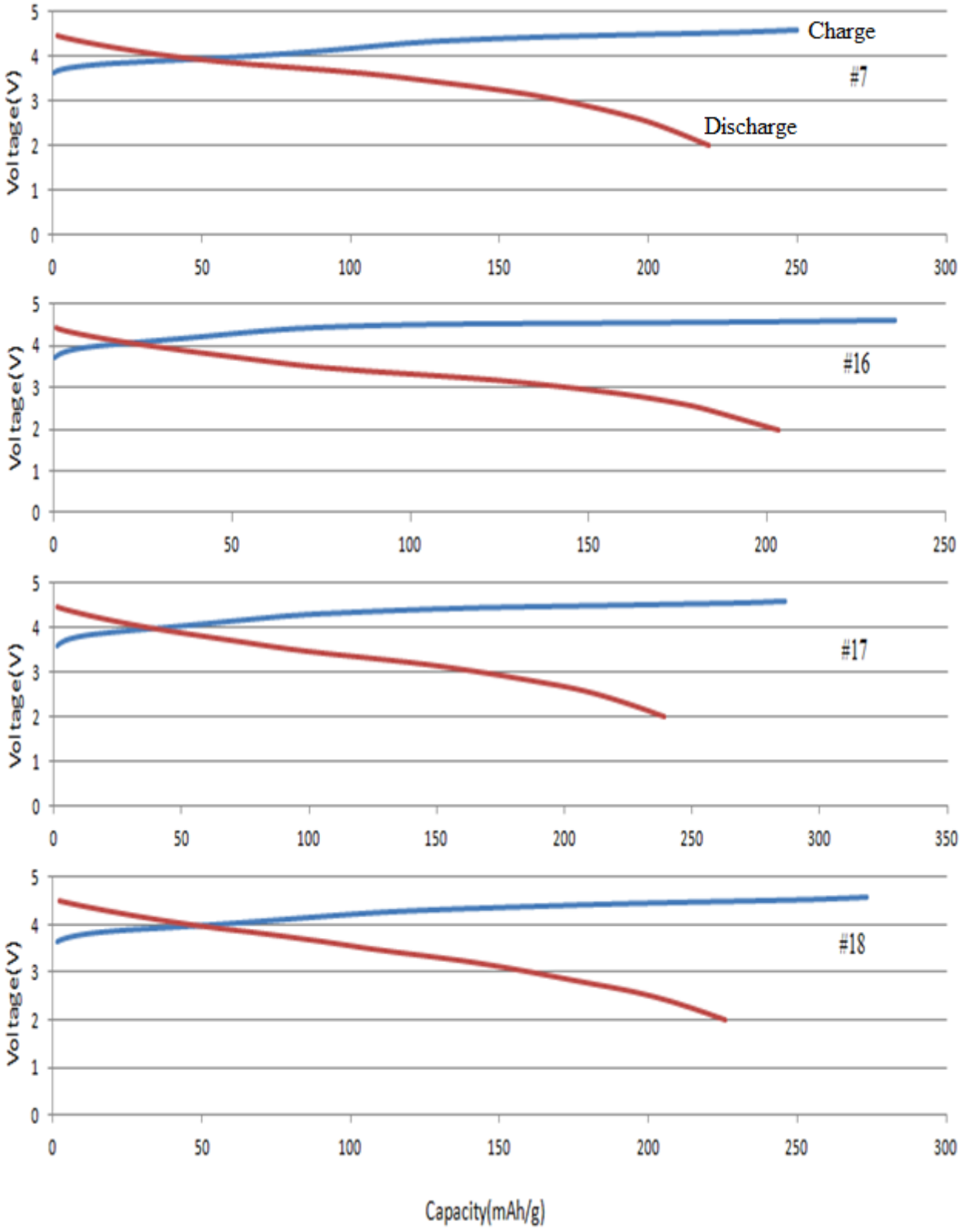

Figure 36: Capacity v. voltage plots of the repeated samples.

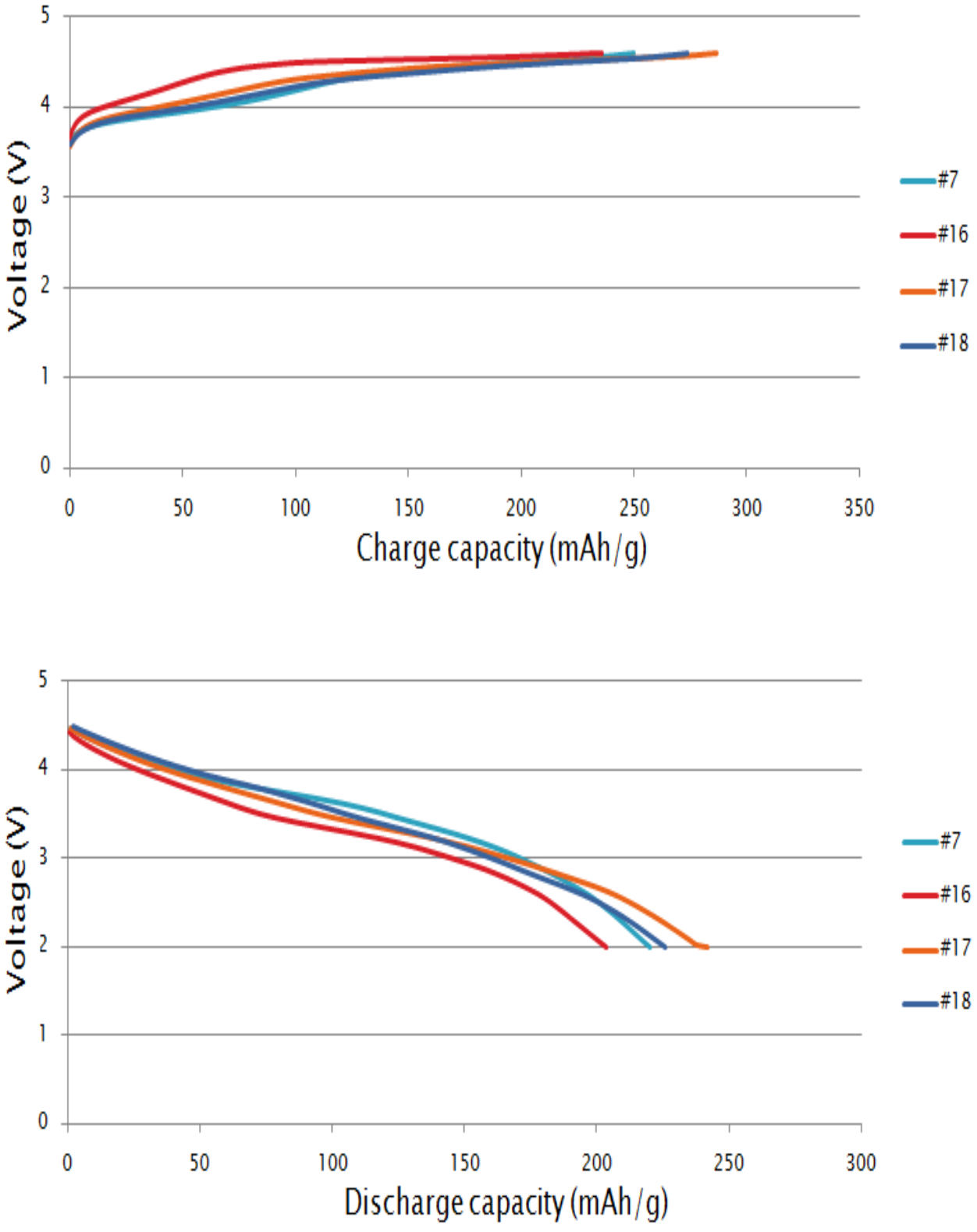

Figure 37: Comparison between charge and discharge profiles for repeated samples.

5.3 Results and Discussion

As expected, all the samples showed constant S-shaped charge and discharge curves. Overall, sample #17 exhibited the highest discharge capacity of 242 mAh/g in the voltage range from 2 – 4.6V. This sample showed an irreversible capacity loss of 35mAh/g and capacity retention of 97 % under these testing conditions. Following Table summarizes all the capacity results along with the capacity retention for the tested samples.

Table 7: Summarizes results from the electrochemical testing

No.	Sample Composition	Charge Capacity (mAh/g)	Discharge Capacity (mAh/g)	Retention (%)
7.	$Li_{1.167}Mn_{.5}Ni_{.167}Co_{.167}O_2$	250.01	220.23	95
16.	$Li_{1.278}Mn_{.611}Ni_{.056}Co_{.056}O_2$	236.98	203.40	98
17.	$Li_{1.222}Mn_{.5}Ni_{.056}Co_{.222}O_2$	277.15	242.04	97
18.	$Li_{1.167}Mn_{.389}Ni_{.056}Co_{.389}O_2$	273.52	226	96

The following table 8 shows a comparison between the capacities of the original cathodes to the repeated cathodes. Except for sample #16, there were not any drastic differences in the capacity numbers for the remaining samples.

Table 8: Comparison between capacities of original and repeated samples

No	Formula	Original		Repeated sample	
		Charge (mAh/g)	Discharge (mAh/g)	Charge (mAh/g)	Discharge (mAh/g)
7	$Li_{1.167}Mn_{.5}Ni_{.167}Co_{.167}O_2$	264.40	226.00	250.01	220.23
16	$Li_{1.278}Mn_{.611}Ni_{.056}Co_{.056}O_2$	300.04	219.00	236.98	203.40
17	$Li_{1.222}Mn_{.5}Ni_{.056}Co_{.222}O_2$	278.45	230.00	277.15	242.04
18	$Li_{1.167}Mn_{.389}Ni_{.056}Co_{.389}O_2$	277.63	227.00	273.52	226.00

Figure 37 represents the voltage profile for the charge/discharge for sample #17. For this sample, the electrochemical reaction during the charge process can be divided into two stages. This is evident since it is a known fact that the extraction of Li from Li_2MnO_3 in the form of Li_2O occurs at voltage >4.5V. Therefore, we can say that the increase in the charge capacities at voltages >4.5V is attributed to the removal of Li_2O from the structure and the later i.e. increase in the charge capacities upto 4.5V being attributed to the removal of Li from the electrode structure with the oxidation of Ni^{+2} to Ni^{+4} and Co^{+3} to Co^{+4}. During the discharge process lithium insertion takes place at 4.4V, resulting in smooth profile which corresponds to reduction of Ni^{+4} to Ni^{+2}, Co^{+4} to Co^{+3} between 4.4 – 3.5V and then into a layered MnO_2 component below 3.5V, down to 2V i.e. Mn^{+4}/Mn^{+3} redox couple. Therefore, this electrochemical reaction resulted in an extended discharge profile with a capacity of 242mAh/g.

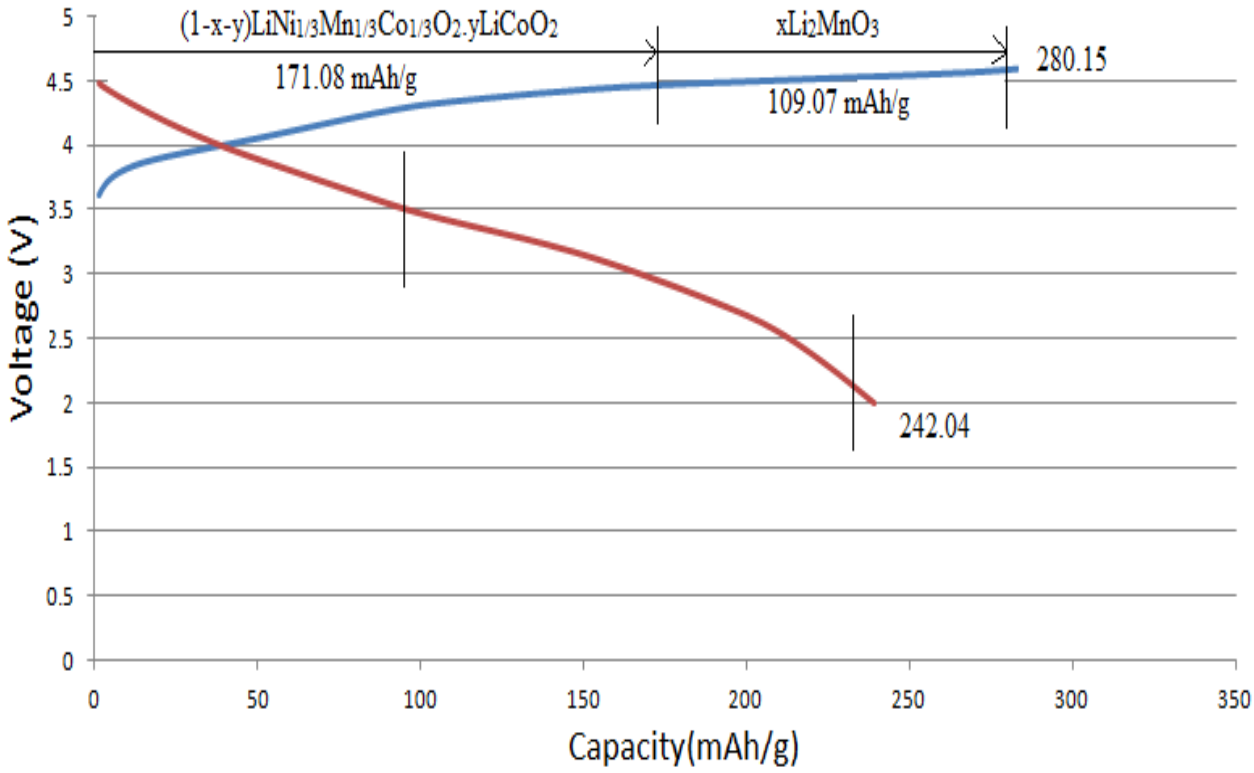

Figure 37: Initial charge/discharge profile of sample #17

The high initial discharge capacity for sample #17 at voltages >4.5V showed the effect of integrating Li_2MnO_3 component into the 2D layered compounds of $LiNi_{1/3}Mn_{1/3}Co_{1/3}O_2$ and $LiCoO_2$. Complete removal of oxygen from Li_2MnO_3 component does not take place at 4.6V, allowing some amount of lithium to be utilized during the intercalation process. This helps to maintain good cyclability of the material as we can see from the cyclability plot in figure 38, but is also companied by irreversible capacity loss.

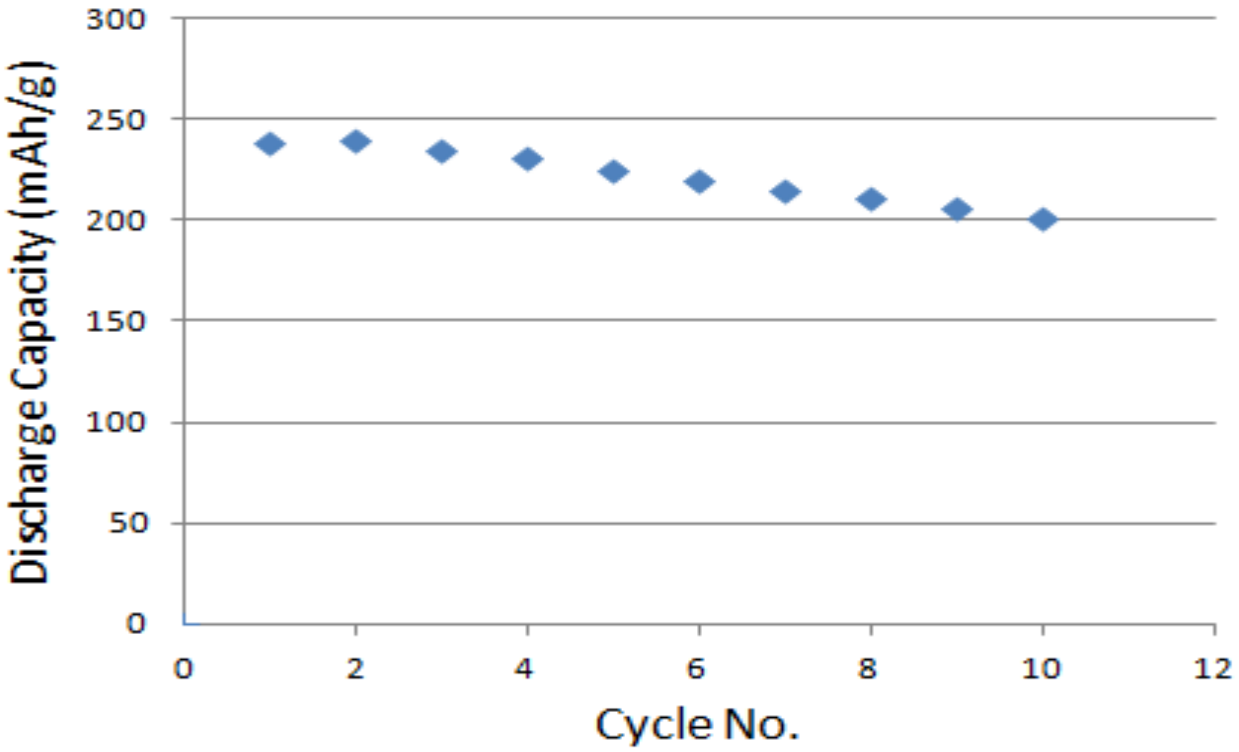

Figure 38: Plot between cycle numbers v. discharge capacity for sample #17.

The main reason for selecting these three material compositions as the components of the ternary system is that they all have the same type of layered structures and each composition offers properties the other compositions lack. For example, $LiNi_{1/3}Mn_{1/3}Co_{1/3}O_2$ is known for its high capacity and structural stability but it suffers from low cyclability. This is compensated by the presence of $LiCoO_2$ which has good cyclability and also Co prevents the migration of Ni and Mn atoms to the Li sites. Li_2MnO_3 further increases the structural stability of the samples in the system and is also safe. The only difference on all the 28 samples in the composition triangle is the content of Mn, Co and Ni transition metals. Therefore, we can say that the resulting material (sample #17) had optimum values of Mn, Co and Ni. It is also worthy to note that the resulting sample had high level of Mn content when compared to Co and Ni based materials, thereby also giving possibilities of cost reduction.

This research work was limited only to a certain section of the system compositions which showed the best possible results. There is a scope for studying the undesirable trends in capacities and cyclability for the remaining samples. This work also couldn't explain a few weird results during the original testing. For example, sample # 24 and sample #2 showed reasonably good capacities of 226mAh/g and 209mAh/g respectively but showed poor retention percentages of 85 and 91. Also, a few samples closer to the Li_2MnO_3 region showed increasing capacities with increase in number of cycles which was unexplainable. For examples, samples #22 and #23 showed retention percentages of 145 and 110 but showed lower discharge capacities.

Chapter 6 Conclusions

Several different Li-ion based cathode material compositions were developed in the system $(1-x-y)LiNi_{1/3}Mn_{1/3}Co_{1/3}O_2 \cdot xLi_2MnO_3 \cdot yLiCoO_2$. Overall, 28 different points were selected in this system conducive to a mathematical modeling. The cathode compositions in the current system comprises mainly of lithium as a base material and other transition metals such as nickel, manganese and cobalt. A simple sol-gel synthesis method was used for all the sample materials. X-ray diffraction was used to characterizing technique, all the samples showed the presence of a layered α-$NaFeO_2$ structure with an R3m space group.

The electrochemical results showed a wide range of initial discharge capacity varying from 120mAh/g to 242mAh/g for different materials compositions. The most promising materials were found in the region closer to Li_2MnO_3 component when compared to the other counterparts.

Statistical data analysis was carried out to find variations in capacities and cyclability results across the composition triangle. From this analysis, 4 samples were selected and ICP was conducted which confirmed the formation of optimum compositions. These samples were synthesized and tested again to confirm consistency.

The best possible results in the system $(1-x-y)LiNi_{1/3}Mn_{1/3}Co_{1/3}O_2 \cdot xLi_2MnO_3 \cdot yLiCoO_2$ was showed by $Li_{1.222}Mn_{0.5}Ni_{.056}Co_{0.222}O_2$ material composition. This material showed an initial discharge capacity of 242.04mAh/g in the voltage range of 2-4.6V at a rate of C/15 and a capacity retention of 97% for 10 cycles.

XPS tests were carried out on the samples which showed that Mn, Ni and Co were present in +4, +2 and +3 oxidation states. The presence of Li_2MnO_3 component in sample #17 was confirmed by the super lattice peaks present at 20-23° in the XRD scans. Therefore, we can state that the high capacity attained for sample #17 is because of Ni^{+2}/Ni^{+4} and Co^{+3}/Co^{+4} red-ox couple and the Li-ion extraction form Li_2MnO_3 at a voltage >4.5V which resulted in an extended discharge profile.

Future work in this research would be in performing a detailed structural study by using Reitveld analysis which will give a better idea about the location of different elements inside the structure. Also to use alternative synthesis methods such as solid state method and co-precipitation method and check for performance of the resulting composition.

Additionally, there was nothing in this work which showed about the safety of this material composition; therefore performing DSC would also be necessary. Surface treatments, such as coating the material with metal oxides such as Al_2O_3 which has proved to reduce the irreversible capacity loss, can also be explored.

REFERENCES

1. Scrosati, B. and J. Garche, *Lithium batteries: Status, prospects and future.* Journal of Power Sources, 2010. 195(9): p. 2419-2430.
2. M.Armand, J.M.T.a., *Issue and challenges facing rechargeable lithium batteries.* Nature, 2001. 414(6861): p. 359-367
3. G.N.Lewis, *The potential of lithium electrode* Journal of the American Chemical Society, 1913. 192: p. 1126-1127.
4. M.S.Whittingham, *Electrical Energy Storage and Intercalation Chemistry.* Science, 1976. 192(4244): p. 1126-1127.
5. P Touzain, R.Y., *Insertion compounds of graphite with improved performances and electrochemical applications of those compounds*, 1986: US.
6. H. H. Lee, C.C.W., Y. Y. Wang, Journal of power sources with press, 2003: p. 1-7.
7. K.Mizushima, *Li_xCoO_2(0<x<1): A new cathode material for batteries of high enery density.* Materials Research Bulletin, 1980. 15: p. 783-789.
8. K.Tozawa, T.N.a., *Lithium Ion Rechargeble battery.* Progress in batteries and solar cells, 1990. 9: p. 209-217.
9. K.Ozawa, *Lithium-ion rechargeable batteries with $LiCoO_2$ and carbon electrodes: the $LiCoO_2$/C system.* Solid State Ionics, 1994. 69(3): p. 212-221.
10. Ehrlich, G.M., *Lithium-ion batteries*. 2002.
11. Shimadzu, *Rechargeable Lithium-Ion Battery Evaluation*.
12. Shaju, K.M., G.V. Subba Rao, and B.V.R. Chowdari, *Performance of layered $Li(Ni_{1/3}Co_{1/3}Mn_{1/3})O_2$ as cathode for Li-ion batteries.* Electrochimica Acta, 2002. 48(2): p. 145-151.
13. Akimoto, J., Y. Gotoh, and Y. Oosawa, *Synthesis and Structure Refinement of LiCoO2Single Crystals.* Journal of Solid State Chemistry, 1998. 141(1): p. 298-302.
14. Madhu, C., J. Garrett, and V. Manivannan, *Synthesis and characterization of oxide cathode materials of the system (1-x-y)LiNiO₂·xLi₂MnO₃·yLiCoO<sub>2</sub&gt.* Ionics, 2010. 16(7): p. 591-602.
15. Sun, Y., et al., *The preparation and electrochemical performance of solid solutions $LiCoO_2$–Li_2MnO_3 as cathode materials for lithium ion batteries.* Journal of Power Sources, 2006. 159(2): p. 1353-1359.
16. Jiang, J., et al., *Structure, Electrochemical Properties, and Thermal Stability Studies of Cathode Materials in the xLi[Mn[sub 1/2]Ni[sub 1/2]]O[sub 2][bold [center-dot]]yLiCoO[sub 2][bold [center-dot]]zLi[Li[sub 1/3]Mn[sub 2/3]]O[sub 2] Pseudoternary System (x + y + z = 1).* Journal of The Electrochemical Society, 2005. 152(9): p. A1879-A1889.
17. Zhong, Q., et al., *Synthesis and Electrochemistry of LiNi[sub x]Mn[sub 2 - x]O[sub 4].* Journal of The Electrochemical Society, 1997. 144(1): p. 205-213.
18. Zhong, S.-w., et al., *Characteristics and electrochemical performance of cathode material Co-coated $LiNiO_2$ for Li-ion batteries.* Transactions of Nonferrous Metals Society of China, 2006. 16(1): p. 137-141.
19. Makimura, Y. and T. Ohzuku, *Lithium insertion material of $LiNi_{1/2}Mn_{1/2}O_2$ for advanced lithium-ion batteries.* Journal of Power Sources, 2003. 119–121(0): p. 156-160.
20. Ohzuku, T. and Y. Makimura, *Layered Lithium Insertion Material of $LiNi_{1/2}Mn_{1/2}O_2$: A Possible Alternative to $LiCoO_2$ for Advanced Lithium-Ion Batteries.* Chemistry Letters, 2001. 30(8): p. 744-745.

21. Rossen, E., C.D.W. Jones, and J.R. Dahn, *Structure and electrochemistry of $Li_xMn_yNi_{1-y}O_2$.* Solid State Ionics, 1992. 57(3–4): p. 311-318.
22. Spahr, M.E., et al., *Characterization of Layered Lithium Nickel Manganese Oxides Synthesized by a Novel Oxidative Coprecipitation Method and Their Electrochemical Performance as Lithium Insertion Electrode Materials.* Journal of The Electrochemical Society, 1998. 145(4): p. 1113-1121.
23. Yang, X.-Q., et al., *Crystal structure changes of $LiMn_{0.5}Ni_{0.5}O_2$ cathode materials during charge and discharge studied by synchrotron based in situ XRD.* Electrochemistry Communications, 2002. 4(8): p. 649-654.
24. Lu, Z., D.D. MacNeil, and J.R. Dahn, *Layered Cathode Materials Li[Ni[sub x]Li[sub (1/3 - 2x/3)]Mn[sub (2/3 - x/3)]]O[sub 2] for Lithium-Ion Batteries.* Electrochemical and Solid-State Letters, 2001. 4(11): p. A191-A194.
25. Neudecker, B.J., et al., *Lithium Manganese Nickel Oxides Li[sub x](Mn[sub y]Ni[sub 1 - y])[sub 2 - x]O[sub 2].* Journal of The Electrochemical Society, 1998. 145(12): p. 4148-4159.
26. Ohzuku, T., et al., *A 3-Volt Lithium-Ion Cell with $Li[Ni_{1/2}Mn_{3/2}]O_4$ and $Li[Li_{1/3}Ti_{5/3}]O_4$: A Method to Prepare Stable Positive-Electrode Material of Highly Crystallized $Li[Ni_{1/2}Mn_{3/2}]O_4$.* Chemistry Letters, 2001. 30(12): p. 1270-1271.
27. Kim, J.-S., et al., *Electrochemical and Structural Properties of $xLi_2M'O_3 \cdot (1-x)LiMn_{0.5}Ni_{0.5}O_2$ Electrodes for Lithium Batteries (M' = Ti, Mn, Zr; $0 \le x \leqslant 0.3$).* Chemistry of Materials, 2004. 16(10): p. 1996-2006.
28. Liu, Z., A. Yu, and J.Y. Lee, *Synthesis and characterization of $LiNi_{1-x-y}Co_xMn_yO_2$ as the cathode materials of secondary lithium batteries.* Journal of Power Sources, 1999. 81–82(0): p. 416-419.
29. Yoshio, M., et al., *Preparation and properties of $LiCoyMnxNi_{1-x-y}O_2$ as a cathode for lithium ion batteries.* Journal of Power Sources, 2000. 90(2): p. 176-181.
30. Ohzuku, T. and Y. Makimura, *Layered Lithium Insertion Material of $LiCo_{1/3}Ni_{1/3}Mn_{1/3}O_2$ for Lithium-Ion Batteries.* Chemistry Letters, 2001. 30(7): p. 642-643.
31. Yabuuchi, N. and T. Ohzuku, *Novel lithium insertion material of $LiCo_{1/3}Ni_{1/3}Mn_{1/3}O_2$ for advanced lithium-ion batteries.* Journal of Power Sources, 2003. 119–121(0): p. 171-174.
32. Lu, Z., D.D. MacNeil, and J.R. Dahn, *Layered Li[Ni[sub x]Co[sub 1 - 2x]Mn[sub x]]O[sub 2] Cathode Materials for Lithium-Ion Batteries.* Electrochemical and Solid-State Letters, 2001. 4(12): p. A200-A203.
33. Ngala, J.K., et al., *The synthesis, characterization and electrochemical behavior of the layered $LiNi_{0.4}Mn_{0.4}Co_{0.2}O_2$ compound.* Journal of Materials Chemistry, 2004. 14(2): p. 214-220.
34. Belharouak, I., et al., *$Li(Ni_{1/3}Co_{1/3}Mn_{1/3})O_2$ as a suitable cathode for high power applications.* Journal of Power Sources, 2003. 123(2): p. 247-252.
35. Yoon, W.-S., et al., *A comparative study on structural changes of $LiCo_{1/3}Ni_{1/3}Mn_{1/3}O_2$ and $LiNi_{0.8}Co_{0.15}Al_{0.05}O_2$ during first charge using in situ XRD.* Electrochemistry Communications, 2006. 8(8): p. 1257-1262.
36. Choi, J. and A. Manthiram, *Role of Chemical and Structural Stabilities on the Electrochemical Properties of Layered LiNi[sub 1/3]Mn[sub 1/3]Co[sub 1/3]O[sub 2] Cathodes.* Journal of The Electrochemical Society, 2005. 152(9): p. A1714-A1718.
37. Chen, R. and M.S. Whittingham, *Cathodic Behavior of Alkali Manganese Oxides from Permanganate.* Journal of The Electrochemical Society, 1997. 144(4): p. L64-L67.
38. Armstrong, A.R. and P.G. Bruce, *Synthesis of layered $LiMnO_2$ as an electrode for rechargeable lithium batteries.* Nature, 1996. 381(6582): p. 499-500.
39. Thackeray, M.M., *Structural Considerations of Layered and Spinel Lithiated Oxides for Lithium Ion Batteries.* Journal of The Electrochemical Society, 1995. 142(8): p. 2558-2563.

40. Amatucci, G., et al., *The elevated temperature performance of the $LiMn_2O_4$/C system: failure and solutions.* Electrochimica Acta, 1999. 45(1–2): p. 255-271.
41. Shao-Horn, Y. and R.L. Middaugh, *Redox reactions of cobalt, aluminum and titanium substituted lithium manganese spinel compounds in lithium cells.* Solid State Ionics, 2001. 139(1–2): p. 13-25.
42. Gummow, R.J., A. de Kock, and M.M. Thackeray, *Improved capacity retention in rechargeable 4 V lithium/lithium-manganese oxide (spinel) cells.* Solid State Ionics, 1994. 69(1): p. 59-67.
43. Krins, N., et al., *$LiMn_{2-x}Ti_xO_4$ spinel-type compounds (x ≤ 1): Structural, electrical and magnetic properties.* Solid State Ionics, 2006. 177(11–12): p. 1033-1040.
44. Johnson, C.S., et al., *The significance of the Li_2MnO_3 component in 'composite' xLi2MnO3 · (1 − x)$LiMn_{0.5}Ni_{0.5}O_2$ electrodes.* Electrochemistry Communications, 2004. 6(10): p. 1085-1091.
45. Lu, Z., Z. Chen, and J.R. Dahn, *Lack of Cation Clustering in $Li[Ni_xLi_{1/3-2x/3}Mn_{2/3-x/3}]O_2$ ($0 < x \leq 1/2$) and $Li[Cr_xLi_{(1-x)/3}Mn_{(2-2x)/3}]O_2$ ($0 < x < 1$).* Chemistry of Materials, 2003. 15(16): p. 3214-3220.
46. Kang, S.H. and K. Amine, *Synthesis and electrochemical properties of layer-structured $0.5Li(Ni_{0.5}Mn_{0.5})O_2$–$0.5Li(Li_{1/3}Mn_{2/3})O_2$ solid mixture.* Journal of Power Sources, 2003. 124(2): p. 533-537.
47. Park, Y.J., et al., *Structural investigation and electrochemical behaviour of $Li[Ni_xLi_{(1/3-2x/3)}Mn_{(2/3-x/3)}]O_2$ compounds by a simple combustion method.* Journal of Power Sources, 2004. 129(2): p. 288-295.
48. Kang, S.H., Y.K. Sun, and K. Amine, *Electrochemical and Ex Situ X-Ray Study of Li(Li[sub 0.2]Ni[sub 0.2]Mn[sub 0.6])O[sub 2] Cathode Material for Li Secondary Batteries.* Electrochemical and Solid-State Letters, 2003. 6(9): p. A183-A186.
49. Lu, Z., et al., *Synthesis, Structure, and Electrochemical Behavior of Li[Ni[sub x]Li[sub 1/3 - 2x/3]Mn[sub 2/3 - x/3]]O[sub 2].* Journal of The Electrochemical Society, 2002. 149(6): p. A778-A791.
50. Barkhouse, D.A.R. and J.R. Dahn, *A Novel Fabrication Technique for Producing Dense Li[Ni[sub x]Li[sub (1/3--2x/3)]Mn[sub (2/3 - x/3)]]O[sub 2], 0 <= x <= 1/2.* Journal of The Electrochemical Society, 2005. 152(4): p. A746-A751.
51. Ammundsen, B., et al., *Local Structure and First Cycle Redox Mechanism of Layered Li[sub 1.2]Cr[sub 0.4]Mn[sub 0.4]O[sub 2] Cathode Material.* Journal of The Electrochemical Society, 2002. 149(4): p. A431-A436.
52. Thackeray, M.M., et al., *Advances in manganese-oxide 'composite' electrodes for lithium-ion batteries.* Journal of Materials Chemistry, 2005. 15(23): p. 2257-2267.
53. Johnson, C.S., et al., *Structural and electrochemical analysis of layered compounds from Li_2MnO_3.* Journal of Power Sources, 1999. 81–82(0): p. 491-495.
54. Sun, Y., et al., *Effect of Co Content on Rate Performance of LiMn[sub 0.5 - x]Co[sub 2x]Ni[sub 0.5 - x]O[sub 2] Cathode Materials for Lithium-Ion Batteries.* Journal of The Electrochemical Society, 2004. 151(4): p. A504-A508.
55. Zhang, L., H. Noguchi, and M. Yoshio, *Synthesis and electrochemical properties of layered Li–Ni–Mn–O compounds.* Journal of Power Sources, 2002. 110(1): p. 57-64.
56. Shin, S.S., Y.K. Sun, and K. Amine, *Synthesis and electrochemical properties of $Li[Li_{(1-2x)/3}Ni_xMn_{(2-x)/3}]O_2$ as cathode materials for lithium secondary batteries.* Journal of Power Sources, 2002. 112(2): p. 634-638.
57. Numata, K., C. Sakaki, and S. Yamanaka, *Synthesis and characterization of layer structured solid solutions in the system of $LiCoO_2$–Li_2MnO_3.* Solid State Ionics, 1999. 117(3–4): p. 257-263.

58. Kim, J.S., C.S. Johnson, and M.M. Thackeray, *Layered $xLiMO_2 \cdot (1-x)Li_2M'O_3$ electrodes for lithium batteries: a study of $0.95LiMn_{0.5}Ni_{0.5}O_2 \cdot 0.05Li_2TiO_3$.* Electrochemistry Communications, 2002. 4(3): p. 205-209.
59. Johnson, C.S., et al., *The role of Li_2MO_2 structures (M=metal ion) in the electrochemistry of $(x)LiMn_{0.5}Ni_{0.5}O_2 \cdot (1-x)Li_2TiO_3$ electrodes for lithium-ion batteries.* Electrochemistry Communications, 2002. 4(6): p. 492-498.
60. Zhang, L. and H. Noguchi, *Novel layered Li–Cr–Ti–O cathode materials for lithium rechargeable batteries.* Electrochemistry Communications, 2002. 4(7): p. 560-564.
61. Zhang, L. and H. Noguchi, *Novel Layered Li-Cr-Ti-O Cathode Materials Related to the LiCrO[sub 2]-Li[sub 2]TiO[sub 3] Solid Solution.* Journal of The Electrochemical Society, 2003. 150(5): p. A601-A607.
62. Zhang, L., et al., *Peculiar electrochemical behaviors of $(1-x)LiNiO_2 \cdot xLi_2TiO_3$ cathode materials prepared by spray drying.* Journal of Power Sources, 2003. 117(1–2): p. 137-142.
63. Zhang, L., et al., *Electrochemical and ex situ XRD investigations on $(1-x)LiNiO_2 \cdot xLi_2TiO_3$ $(0.05 \le x \le 0.5)$.* Electrochimica Acta, 2004. 49(20): p. 3305-3311.
64. Tabuchi, M., et al., *Preparation of lithium manganese oxides containing iron.* Journal of Power Sources, 2001. 97–98(0): p. 415-419.
65. Tabuchi, M., et al., *Synthesis, Cation Distribution, and Electrochemical Properties of Fe-Substituted Li[sub 2]MnO[sub 3] as a Novel 4 V Positive Electrode Material.* Journal of The Electrochemical Society, 2002. 149(5): p. A509-A524.
66. Lim, J.-H., et al., *Electrochemical characterization of Li_2MnO_3–$Li[Ni_{1/3}Co_{1/3}Mn_{1/3}]O_2$–$LiNiO_2$ cathode synthesized via co-precipitation for lithium secondary batteries.* Journal of Power Sources, 2009. 189(1): p. 571-575.
67. Wu, Y. and A. Manthiram, *High Capacity, Surface-Modified Layered Li[Li[sub (1 - x)/3]Mn[sub (2 - x)/3]Ni[sub x/3]Co[sub x/3]]O[sub 2] Cathodes with Low Irreversible Capacity Loss.* Electrochemical and Solid-State Letters, 2006. 9(5): p. A221-A224.
68. Liu, J. and A. Manthiram, *Functional surface modifications of a high capacity layered $Li[Li_{0.2}Mn_{0.54}Ni_{0.13}Co_{0.13}]O_2$ cathode.* Journal of Materials Chemistry, 2010. 20(19): p. 3961-3967.
69. Zhang, L., et al., *Layered (1 - x - y)LiNi[sub 1/2]Mn[sub 1/2]O[sub 2] [center-dot] xLi[Li[sub 1/3]Mn[sub 2/3]] O[sub 2] [center-dot] yLiCoO[sub 2] (0 <= x = y <= 0.3 and x + y = 0.5) Cathode Materials.* Journal of The Electrochemical Society, 2005. 152(1): p. A171-A178.